SYNTHESIS AND CHARACTERIZATION OF MEMBRANE SUPPORTED METAL NANOPARTICLES

By

Rakesh Kumar
(CHEM 01 2006 04 013)

Bhabha Atomic Research Centre, Mumbai

A thesis submitted to the

Board of Studies in Chemical Sciences

In partial fulfillment of requirements

for the Degree of

DOCTOR OF PHILOSOPHY

of

HOMI BHABHA NATIONAL INSTITUTE

Aug, 2013

HOMI BHABHA NATIONAL INSTITUTE

Recommendations of the Viva Voce Board

As members of the Viva Voce Board, we certify that we have read the dissertation prepared by **Shri Rakesh Kumar** entitled "**Synthesis and Characterization of Membrane Supported Metal Nanoparticles**" and recommend that it may be accepted as fulfilling the dissertation requirement for the Degree of Doctor of Philosophy.

24.02.14 Date:

Chairman - Prof. A.V. R. Reddy

Goswami 24.2.2014 Date:

Guide / Convener - Prof. A. Goswami

24/02/2014 Date:

External Examiner- Prof. Tarasankar Pal

24/2/2014 Date:

Member 1 - Prof. B.S. Tomar

24/2/2014 Date:

Member 2 - Prof. P.K. Pujari

Final approval and acceptance of this dissertation is contingent upon the candidate's submission of the final copies of the dissertation to HBNI.

I hereby certify that I have read this dissertation prepared under my direction and recommend that it may be accepted as fulfilling the dissertation requirement.

Date: 24/02/2014

Place: Mumbai.

Goswami

(Guide)

STATEMENT BY AUTHOR

This dissertation has been submitted in partial fulfillment of requirements for an advanced degree at Homi Bhabha National Institute (HBNI) and is deposited in the Library to be made available to borrowers under rules of the HBNI.

Brief quotations from this dissertation are allowable without special permission, provided that accurate acknowledgement of source is made. Requests for permission for extended quotation from or reproduction of this manuscript in whole or in part may be granted by the Competent Authority of HBNI when in his or her judgment the proposed use of the material is in the interests of scholarship. In all other instances, however, permission must be obtained from the author.

Rakesh Kumar

Rakesh Kumar

DECLARATION

I, hereby, declare that the investigation presented in the thesis has been carried out by me. The work is original and has not been submitted earlier as a whole or in part for a degree / diploma at this or any other Institution / University.

Rakesh Kumar

Rakesh Kumar

Dedicated
To
My Father

ACKNOWLEDGEMENTS

First and foremost, I would like to express my sincere gratitude to my research guide ***Dr. A. Goswami*** for the continuous support of my Ph.D. study and research, for his patience, motivation, enthusiasm, and immense knowledge. His guidance from the initial to the final level enabled me to develop an understanding of the subject. I could not have imagined having a better guide and mentor for my Ph.D. study. I am highly indebted to ***Dr. A.K. Pandey***, Radiochemistry Division, for his wholehearted encouragement and support, without whom it would have been impossible to carry out the work.

I am grateful to the ***Shri H. Bose*** for permitting me to register for my Ph.D. and his constant support. I express my gratitude towards ***Shri. V.K. Raina***, Ex. Director, Reactor Group, and ***Shri. R. C. Sharma***, Associate Director, Reactor Group, for their support. I am also grateful to ***Dr. A.V.R. Reddy***, Head Analytical Chemistry Division and Chairman of my Ph.D. doctoral committee, for his support throughout the work. I would also like to thank the members of my Ph.D. doctoral committee: ***Dr. B.S.Tomar*** and ***Dr. P.K.Pujari*** for their time, insightful comments and suggestions.

I am thankful to my collaborators ***Prof. J. Bellare, Dr. A. K. Tyagi, Dr. N.L. Mishra, Dr. L.V. Panicker, Dr. S. Dhara, Mr. R. K. Shukla, and Dr. M. K. Sharma*** for their support.

I am indebted to many of my fellow lab mates, particularly ***Dr. (Smt) Suparna Sodaye, Dr. Sadananda Das, Dr. T. Vasudevan, Dr (Smt) Chhavi Agarwal, Sanhita Chaudhury**, **Amol Mhatre**,* and ***Vivek Chavan*** for all the precious help and cooperation that they lent to me during my research work. I am heartily thankful to ***Dr. Jitendra Kumar, V.S.Tripathi, Ashish Thakur, C.L. Prajapat, H. Poswal, D.K.Dixit, Dr. (Smt) Neetika Rawat, Dr. Arunasis Bhattacharya, Dr. Sumit Kumar,*** and ***Dr. Seraj Ansari*** for sharing their knowledge and to help me on day to day basis. I, also, thanks to all my friends and colleagues of Reactor Chemistry Section for their love and support.

My deepest gratitude goes to my ***family*** for their unflagging love, support and encouragement throughout my life. My ***parent*** deserves special mention for their support in all my pursuits and their persistent confidence in me. I owe my every achievement to them. I also thank my siblings for their love and support at times I tend to give away. Words fail to express my appreciation to my wife ***Archana*** *and daughter* ***Arni*** for their unconditional love, relentless support and endless patience, especially during the final stages of this Ph.D. I am privileged to have them around me.

Last but not least, I would like to thank everyone, whose contributions were important for the successful realization of this thesis, but I could not mention them personally.

Rakesh Kumar

CONTENTS

Synopsis

There has been an ever increasing need for novel functional materials with special combination of properties (e.g., magnetic–transparent, conductive–transparent, catalytic–magnetic, etc.). Materials based on metals nanoparticles (nps) have special characteristics that can be exploited for these advanced functional applications. The metal nanoparticles, having size less than 100 nm, show interesting mechanical [1], chemical [2,3], electrical [4], optical [5-7], magnetic [8,9], electro-optical [10,11], and magneto-optical [12] properties which are substantially different from those observed for the corresponding bulk materials. The reasons for these properties can be attributed to high surface area and quantum size effect, which is caused by the reduced size in three dimensions [13-16]. As for example, small nanoparticles could be a very bad conductor, although they are tiny silhouettes of the conducting bulk. Like- wise, a tiny nanoparticle of a ferromagnet can be paramagnetic in nature. However, the difficulty in the handling of these metal nanoparticles has represented a strong limitation to their use. They can aggregate because of the high surface free energy and can be oxidized or contaminated by air, moisture, etc.

The embedding of metal nanoparticles into dielectric matrices can be potential solution to the manipulation and stabilization problems [17]. Membranes are particularly interesting as an embedding matrix, since they have a variety of desirable characteristics. The membrane can be an electrical and thermal insulator or conductor, may have a hydrophobic or hydrophilic nature, can be mechanically hard or plastic or rubbery, and so on [18]. Many of the unique chemical–physical characteristics of nano-sized metals leave unmodified after embedding in the membrane (e.g., optical [19], magnetic [20], and photoluminescence [21]), and therefore they can be used to provide special functionalities to the membrane.

The expanding availability and diversity of nanoparticles with unique physicochemical properties and possibility of chemically functionalizing the nanoparticles opens up new possibilities for the fabrication of nanocomposite membranes. Membrane with silver nanoparticles can controllably release bactericidal silver ions directly into the membrane feed stream and thus prevent the formation of biofilm on the membrane surface [22]. Inclusion of metal nanoparticles increases the hydrophilicity of the membrane, which reduces membrane fouling due to deposition of organic matter on the membrane surface [23,24]. A membrane with magnetic nanoparticles is raising considerable attention towards various applications including "smart" actuators [25], dampers, and artificial muscles. The magnetic nanoparticles can be used for micro mixing in the membrane phase that enhances its transport properties [26].

Many methods have been developed for incorporation of nanoparticles in the membrane. In general, these methods can be classified as *in situ* and *ex situ* methods. In the *in situ* methods, precursor metal ions are introduced in the membrane matrix and then they are reduced chemically [27], thermally [28], by gamma/UV irradiation [29,30] etc. It is possible to control size distribution of the particles by appropriate manipulation of concentration of metal ions. Metal nanoparticles are expected to form in the micro domain in membrane. In *ex situ* processes, the metal nanoparticles are chemically synthesized and their surface is organically passivated. The derivatized nanoparticles are dispersed into a membrane forming polymer solution.

In the present thesis, the possibility of controlled formation of metal nanoparticles in different membranes has been explored using two steps involving ion-exchange and subsequent *in situ* reduction. The experimental parameters controlling the size, shape, and spatial distribution in the membrane matrix have been investigated. The formation of metal nanoparticles by galvanic reaction of Ag nanoparticles with precursor ions, which cannot be loaded in the membrane matrix by ion-exchange, has also been studied. The studies carried out in this thesis are organized into six chapters.

CHAPTER I

This chapter provides appropriate background to the studies carried in the present thesis. The brief introduction of membranes, nanoparticles, and nonocomposite membranes are given in this chapter. This chapter also deals with the methods and concepts used in the present studies. A brief overview of different experimental and characterization technique such as radiotracer, transmission electron microscopy (TEM), energy dispersive X-ray fluorescence (EDXRF), X-ray powder diffraction (XRD), optical spectroscopy (UV–Vis), etc. have been discussed. Finally, the scope and motivation for the present work have been discussed.

CHAPTER II

This chapter deals with formation and characterization of silver and rhodium nanoparticles in the cation-exchange membrane. The choice of poly(perfluorosulfonic) acid membrane (Nafion-117) as a membrane host has been based on the fact that it is used for a variety of applications ranging from fuel cell to sensor and actuator [31]. Apart from this, this membrane has superior chemical stability and high optical quality. Silver nanoparticles (Ag nanoparticles) in the Nafion were prepared by first transferring silver ion in membrane by ion-exchange process followed by *in situ* reduction of the Ag^+ ions with ionic (sodium Borohydride (BH)) and non-ionic (dimethyl formamide (DMF) and formamide (FA)) reagents at different temperatures [32]. Analyses with the radiotracer Ag^{110m} were carried to monitor the formation of Ag nanoparticles in the membrane matrix. The ion-exchange capacity of the membrane did not change significantly after reduction of Ag^+ ions in the membrane indicating that the formation of nanoparticles did not hinder accessibility of the ion-exchange sites in the membrane.

The rate of formation of Ag nanoparticles in the membrane was quite slow, when it was reduced with DMF and FA while, it was quite fast with BH at room temperature. Reduction rates as well as amount of Ag nanoparticles in the membrane were increased when Ag^+-

loaded membrane samples were reduced by FA at 65 °C. The size and spatial distributions of Ag nanoparticles were studied by TEM of ultra-thin cross-section of the membrane samples reduced with BH and DMF at room temperature, and with FA at 65°C. The shapes of Ag nanoparticles were nearly spherical in all the cases. Ag nanoparticles, with the average size of 9 nm, were formed uniformly throughout the membrane sample reduced with FA at 65°C. In the case of DMF reduced sample at room temperature, a bimodal size distribution of silver nanoparticles were observed. It occurred due to swelling of Nafion in DMF and Ostwald ripping during slow reduction process. It was observed that BH_4^- ions reduced Ag^+ ions preferentially just below surface of the membrane due to Donnan exclusion of co-ion in the cation-exchange matrix.

The self-diffusion coefficients of Na^+, Cs^+, and Eu^{3+} counterions in the Ag nanoparticles embedded membrane samples were measured by the isotopic-exchange method [33-35]. It was observed that the presence of mono-dispersed Ag nanoparticles in the membrane enhanced diffusion mobility of slow moving Cs^+ and Eu^{3+} counterions ions by 2 and 5 times, respectively. The inclusion of Ag nanoparticles in the membrane led to the higher water content than the corresponding ionic form of the nascent Nafion-117 membrane. This leads to higher diffusion mobility of less hydrated ions.

The Rh^{3+}-loaded nafion membrane sample was reduced with formamide at 65 °C. Formations of fractals in the membrane were observed by TEM analyses [36]. The self-diffusion mobility of the trivalent counterions in the Nafion-117 membrane is quite slow. It lead to diffusion limited aggregation and formation of fractals of Rh nanoparticles. The fractal dimension of the two dimensional cluster was calculated by the power law relationship and was found to be 1.8.

CHAPTER III

In this chapter, an interesting possibility of synthesizing metal nanoparticles and their alloys by using the galvanic reaction was studied [37]. Ag nanoparticles embedded in Nafion membrane were used as templates and with the metal ions whose redox potential is more positive than the Ag^+/Ag pair were used for galvanic reaction. The standard redox potentials of the systems Hg^{2+}/Hg (+0.85 V) is higher than that of Ag^+/Ag (+0.80 V). Ag nanoparticles were prepared in the membrane sample by reduction with formamide (at 65 ^oC) and used as templates for following reaction

$$Ag_m^0 + (m/2)Hg^{2+} \rightarrow mAg^+ + (m/2)\,Hg^0$$

Radiotracer and energy dispersive x-ray fluorescence studies showed that the above galvanic reaction in the membrane matrix proceeded quantitatively in the presence of excess of Hg^{2+} ions in equilibrating aqueous solution. It was observed in UV-Vis spectra of the membrane sample that the intensity of surface plasmon band (SPB) of Ag nanoparticles($\lambda_{max} \approx 400$ nm) decreased initially and blue shifted to ≈ 375 nm with decrease in the intensity as a function of equilibration time in aqueous solution containing Hg^{2+} ions afterwards. This blue shift and absence of amalgam formation, shown by XRD experiment, indicated the formation of core shell structure in the intermediate of reaction. The above observation was also supported by TEM analyses of membrane samples at 50 % reactions and completion of the reaction [36].

The galvanic replacement of Ag nanoparticles with Rh^{3+} in the membrane was found to be nearly complete as indicated by EDXRF spectra. Rh nanoparticles with an average size of 2 nm were formed uniformly dispersed throughout the matrix of membrane. It appeared that Rh nanoparticles grown independently during galvanic reaction of Rh^{3+} ions with Ag nanoparticles.

The galvanic reaction of $AuCl_4^-$ anions with Ag nanoparticles were studied using BH_4^- ions reduced membrane samples that produce Ag nanoparticles at surface of the cation-exchange membrane. The radiotracer and EDXRF studies showed that 95 % of Ag^0 was replaced by galvanic reaction with $AuCl_4^-$ ions. Au nanostructures with a very high concentration at both surfaces of the membrane were formed. In case of formamide reduced samples having Ag nanoparticles dispersed throughout the matrix, only 70% of Ag^0 was replaced during galvanic reaction with $AuCl_4^-$ ions. Au nanoparticles of sizes ranging from 3 nm to 18 nm and average size 10 nm were formed uniformly dispersed in the membrane matrix.

CHAPTER IV

Preparation and characterization of tunable nanoparticles host membrane have been described in this chapter. These host membrane was prepared by physical immobilization of the carrier in the matrix formed by plasticized cellulose triacetate (CTA). The host membrane thus prepared can work as cation-exchange or anion exchange membrane based on the properties of the carrier.

To study simple tunable host membrane, a plasticized anion-exchange membrane was prepared by physical immobilization of a liquid anion exchanger trioctylmethylammonium chloride (Aliquat-336) in the matrix formed by plasticized cellulose triacetate (CTA). These types of membranes are called polymer inclusion membrane (PIM) [38]. Three plasticizers, 2-nitrophenyl octyl ether (NPOE), dioctyl phthalate (DOP), and tri-(2-ethylhexyl) phosphate (TEHP), having different dielectric constant and viscosity were used to vary the local environment of the membrane matrix. Various membrane samples were prepared by systematically varying the amount of carrier, trioctylmethylammonium chloride (Aliquat-336), amount of base polymer, cellulose triacetate (CTA) and amount of different plasticizers in the membrane. Surface morphology of these membranes was studied using Atomic Force Microscopy (AFM) in non-contact mode. Radiotracer study of membrane samples suggested that addition of plasticizer slightly improved the ion-exchange capacity of the PIM from 85 %

to 90% of the expected ion-exchange capacity. DSC thermograms were studied to understand the thermal transition temperature (T_g) of membrane samples.

Plasticizer in the PIM also acts as a solvent for the carrier Aliquat-336. Therefore, the nature and amount of the plasticizer is expected to influence intrinsic diffusion property of the PIM. The self-diffusion coefficients of I^- ions and water were measured in the PIM samples having fixed proportion of different plasticizers. Self-diffusion coefficient D (I^-) of I^- ions was highest in the sample made up of the plasticizer (NPOE) having higher ε_r and lower viscosity. The self-diffusion coefficients of I^- ions in the membrane samples having constant proportion of CTA and NPOE (1:1) and varying concentration of Aliquat-336 were obtained. It was observed that a threshold concentration of Aliquat-336 was required to influence the self-diffusion mobility of counterions. Thereafter, self-diffusion coefficients of I^- ions increased linearly with Aliquat-336 concentration. It suggested the 'fixed-site hopping' mechanism for the transport processes[39]. The Electrochemical Impedance Spectroscopic and counterions-exchange kinetics studies indicated the variation of self-diffusion mobility of anions in order: $NO_3^- > Cl^- \approx I^- \approx ClO_4^- > SO_4^{2-}$.

CHAPTER V

This chapter deals with *in situ* synthesis of nanoparticles in polymeric inclusion membrane (PIM). The host membranes were prepared as described in the previous chapter. The plasticizers used in the present work were dioctyl phthalate (DOP), tris-(2-ethylhexyl)phosphate (TEHP), and 2-nitrophenyl octyl ether (NPOE). Gold nanoparticles were prepared by equilibrating membrane samples with aqueous solutions containing $AuCl_4^-$ anions, and subsequent reduction of $AuCl_4^-$-loaded membrane samples with BH_4^- anions. Membrane showed the characteristics colour of gold nanoparticles with $\lambda_{max} \approx 530$ nm [40]. Gold nanoparticles contents in the membrane samples were increased by subjecting membrane samples with repeated sequential cycles of loading and reduction of $AuCl_4^-$ ions in the membrane matrix. The average size of Au nanoparticles after first cycle of synthesis was found to be 10 nm by TEM analyses which was in close agreement with the size obtained from the analysis of broadening of the X-ray diffraction peak width. The size distribution of Au nanoparticles broadened after the second cycle of synthesis. Bulk of Au remained as the spherical nanoparticles with 10 nm size, but size distribution was broadened from 5 nm to 20 nm. A few nanostructures like prism, rod, bipyramid and cuboid were also observed [41].

In order to study the effects of Au nanoparticles on the diffusion mobility of the anions, the self-diffusion coefficients of I^- ions were measured using a radiotracer method. Self-diffusion mobility of iodide ions increased significantly after formation of the Au nanoparticles in membrane matrix. After second cycle of Au synthesis, the self-diffusion coefficient of I^- ions was increased 2 times of that in the membrane without nanoparticles. The higher diffusion mobility of I^- ions seems to indicate that tortuosity of the membrane diffusion channels might be reduced after formation of the Au nanoparticles, which would decrease the effective diffusion path length of the anions.

CHAPTER VI

In this chapter, the summary and conclusions of the work carried in this thesis have been given. The future studies required to explore the applications of the present work were also discussed.

Different routes for synthesis of metal nanoparticles in the matrix of functionalized membranes have been developed in the present work. One of the routes is to load desirable metal ions in the membrane matrix by ion-exchange mechanism and reduce them in the matrix using ionic (BH_4^-) or non-ionic (formamide and dimethyl formamide) reductant. Ionic reductants that can enter in the membrane as a counterions produce metal nanoparticles uniformly throughout the matrix. If it has same charge as that of fixed charge, the metal nanoparticles are formed preferentially at the surface of the membrane. However, non-ionic reductant produces nanoparticles uniformly distributed in the membrane. The TEM analyses showed that the spatial distributions of Ag nanoparticles in the ion-exchange membrane could be controlled by using ionic or non-ionic reducing agents.

Another method involving the galvanic reactions of precursor ions with preformed Ag nanoparticles was developed for synthesis of metal nanoparticles in the Nafion-117 membrane. The radiotracer tagged nanoparticles has been used to study the galvanic reactions of Ag nanoparticles with Hg^{2+}, Rh^{3+}, and $AuCl_4^-$ ions in the membrane matrix. The TEM analyses showed that the spatial distributions of Ag nanoparticles in the ion-exchange membrane could be controlled by using ionic or non-ionic reducing agents. It was also observed that shape of nanoparticles in the membrane is also dependent on the nature of precursor ions. For example, the clusters are formed with Rh^{3+} ions and non-spherical nanoparticles are formed with $AuCl_4^-$ ions in the Nafion-117 membrane. These metal nanoparticles embedded membranes can be utilized for modifying the transport properties of the membrane and as a base material for developing the membrane based chemical sensors. For example, a chemical sensor for Hg^{2+} ions can be developed using their galvanic reaction with Ag nanoparticles in the matrix of cation-exchange membrane. The blue shift and decrease in the intensity of surface plasmon absorption band (SPB) of Ag nanoparticles can be used for generating the response signal for detection and quantification of Hg^{2+} ions by the using galvanic reaction. Finally, a home-made polymer inclusion membrane was developed which was exploited as a tunable host for a variety of nanoparticles. This class of membranes would find many futuristic applications to utilize the amazing properties of nanoparticles.

.

List of Figures

Page No.

Fig. No

Fig. No **Page No.**

Fig. No **Page No.**

List of tables

Page No.

Table No

Chapter -1

Introduction

1.1. Introduction

An emerging field of materials engineering with promising applications is that focused on the development of the advanced functional materials that contains two or more components, wherein at least one of the components has nanoscale dimensions. Polymer membranes embedded with nanoparticles are potentially useful for a number of technological applications [42-45].

Because of quantum-size effects and high surface energy, metals nanoparticles show a set of properties completely different from that of bulk. Size-dependent ferromagnetism, superparamagnetism characterizing all metals, the chromatism observed with silver, gold, and copper metals due to plasmon absorption, the photo- and thermoluminescence, and the supercatalytic effects are particularly important properties that have many potential applications. In addition, because of the band-structure disappearance, metals become thermally and electrically insulators at very small sizes. They are highly chemically reactive, super absorbent, and show completely different thermodynamic parameters. For example, they melt at much lower temperatures. Many of these unique physicochemical characteristics (like optical, magnetic, dielectric, and thermal transport properties) of nano-sized metals remain unaltered in membranes matrix, and therefore they can be used to provide special functionalities to membranes. The expanding availability and diversity of nanoparticles offers new possibilities for the manufacture of a new generation of membranes for specific application. Examples the bottom-up design of nanoparticle containing membranes capable of performing multiple tasks or the incorporation of nanoparticles within the membrane structure to obtain membranes with improved mechanical and separation properties. An example of such membranes is that of membrane-based sensors [46,47], which couple the separation and pre-concentration functions with additional sensing features, allowing for the detection, identification, and quantification of targeted compounds. Another example of such membranes is the membrane with silver nanoparticles that can controllably release bactericidal silver ions directly into the membrane feed stream and thus prevent the formation of biofilm on the membrane surface [48].

Since integration of nanoparticles in the polymeric membrane modifies the physico-chemical properties of the host polymer membrane, it is important to understand the effect of nanoparticles shape, size, and inclusion methodology (namely loading concentration and synthetic incorporation route); on the structure of the nanoparticle containing membranes. Studies have shown the effect of incorporated particles on the hydrophilicity of resulting nanocomposite membranes. Increasing the amount of alumina (Al_2O_3) nanoparticles in phase inversion PVDF membranes were correlated with an increase in hydrophilicity of the modified membranes [49]. As the surface area of nanoparticles is related to the nanoparticle size, higher hydrophilic enhancements of modified membranes could be attained with lower loadings of smaller sized nanoparticles.

Aspect ratio of the nanoparticle is expected to play a significant role in the development of new generation of modified membrane. Mechanical properties Such as glass transition temperature, Young's modulus, and elastic and viscous moduli can also be changed by incorporating nanoparticles. Camponeschi et al. [50] showed that the mechanical properties of carbon nanotube doped epoxy composites could be altered upon exposure to an external magnetic field.

The above findings opens up new research opportunities involving the development of membranes containing nanoparticles and stress the importance of studying the interplay between nanoparticle loading, inclusion methodology, nanoparticle size, morphology of the membrane, and the performance of nanoparticle-filled membranes.

1.2. Nanoparticles (nps)

On 29th December, 1959, Nobel Laureate Richard P. Feynman gave a talk at the annual meeting of the American Physical Society that has become one of the twentieth century's classic science lectures, titled "There's Plenty of Room at the Bottom" [51]. Extrapolating from known physical laws, Feynman envisioned a technology using the ultimate toolbox of nature of building nanoobjects atom by atom or molecule by molecule. Nature has many objects and processes that function on a micro- to nanoscale. The flagella, a type of bacteria, is an example of a biological molecular machine [52]. The flagella motor is driven by the proton flow caused by the electrochemical potential differences across the membrane. The diameter of the bearing is about 20–30 nm, with an estimated clearance of about 1 nm.

It is not clear when humans first began to take advantage of nanosized materials. Gold nanoparticles have a long and storied history dating back for millennia. An artifact of 4th century AD called Lycurgus Cup, containing gold and silver nanoparticles, resides in the British Museum in London. In the Middle Ages, colloidal gold was used for a diverse assortment of purposes including as a colorant in stained glass windows and as a purported curative for a wide variety of diseases [53]. Probably the earliest scientific investigation into the synthesis of colloidal gold was carried out by Michael Faraday, who in 1857, reported a method for preparing colloidal gold by electrochemical reduction of aqueous tetrachloroaurate ions, $AuCl_4^-$.

Nanoparticles are defined as particles composed of a few hundred to a few thousand atoms and are, characteristically, of nanometer dimension with size in the range of 1 to 100 nm. When the size of particles is reduced to nanometer scale, the number of atoms at the surfaces or grain boundaries of the crystalline regions is comparable to the number of those that are in the crystalline lattice itself. Because of this, they have a high proportion of atoms on the surface and thus possess an immense surface area per unit volume. The finite size of the particle confines the spatial distribution of the electrons leading to the quantized energy level and thus exhibit quantum effects due to size. The chemical nature and the size of the nanoparticle control the ionic potential or the electron affinity and thereby the electron transport properties. The resulting unique properties of nanoparticles cannot be anticipated from a simple extrapolation of the properties of bulk materials as well as from those of isolated atoms and molecules. For example, some metals and metal oxides exhibit change in the magnetic behavior with the decrease of the particle size. Individual metallic magnetic nanoparticles can exhibit superparamagnetic behavior. Nanoparticles can be made of materials of diverse chemical nature, the most common being metals, metal oxides, silicates, non-oxide ceramics, polymers, organics, carbon, and biomolecules. They also exhibit great morphological diversity with shapes such as spheres, cylinders, disks, platelets, hollow spheres and tubes, etc. Since the properties of the nanoparticles follow from the confinement of the electrons to the physical dimensions of the nanoparticles, it would be interesting to vary the shape of the nanoparticles and study the effect of confinement of electrons in such artificial shapes. For example, it is predicted that light emitted from a nanorod would be linearly polarized along the growth axis.

Metal nanoparticles have very interesting extraordinary size-dependent mechanical [1], chemical [2,3,15], electronic [54], optical [5-7], electro-optical [10,11], magnetic [8,9], and catalytic [55-57] properties that are significantly different from those of the corresponding bulk materials and have, consequently, been the subject of intense research during the past two decade. Noble metal nanostructures attract much interest because of their unique properties, including large optical field enhancements resulting in the strong scattering and absorption of light. Noble metals nanoparticles have attracted steadily growing attention due to their interesting optical [58], electrochemical [59], electronic, [60] and photo-electrochemical properties [61,62]. For example, gold nanoparticles deposited on solid supports show useful catalytic and electro-catalytic properties that are dependent upon their size [63,64]. Silver and gold metal sols possess fascinating colors and have long been used as dyes and catalysts. In the presence of the oscillating electromagnetic field of the light, the free electrons of the metal nanoparticle undergo a collective coherent oscillation with respect to the positive metallic lattice. This process is resonant at a particular frequency of the light and is termed the surface plasmon resonance (SPR) oscillation. It leads to the enhancement in the optical and photothermal properties of noble metal nanoparticles The plasmon resonance can either radiate light (Mie scattering), a process that finds great utility in optical and imaging fields, or be rapidly converted to heat (absorption) [65]; the latter mechanism of dissipation has opened up applications in several new areas. These intrinsic properties strongly depend on composition, size, and shape. As for example, nonspherical nanostructures exhibit more surface plasmon-resonance modes than nanospheres due to dipolar and multipolar electron oscillations along different directions. Nanorods have transverse and longitudinal plasmon modes, resulting in two extinction peaks from the visible to the near infrared spectral region [66]. Noble metal nanoparticles are promising candidates for applications in various fields such as photothermal therapy [67], bioimaging [68], biosensors [69,70], surface-enhanced Raman scattering (SERS) [71], opticalsensors [72-74], electrochemical nanoprobes, [75,76] and catalysis [77-79]. Specifically, gold and silver nanoparticles have been of increasing interest in applications to biological and chemical nanosensors. In recent years, optical [72-74] and electrochemical [75,76] nanoprobes have been developed by modifying the surface of metal nanoparticles with various functional molecules. The ability to integrate metal nanoparticles into biological systems has had greatest impact in biology and biomedicine.

1.3. Membrane as host for nanoparticles

Nanoparticles can be synthesized from a variety of materials with controllable sizes, shapes, and structures. The successful synthesis of nanoparticles involves three steps: nucleation, growth, and termination by the capping agent or ligand [80,81]. Though the reaction temperature and reagent concentrations provide a primary control of the three steps, it is often impossible to independently control them and so the obtained nanoparticles usually exhibit a distribution in size. Due to their high specific surface area, nanoparticles are not stable in ambient condition. Hence, they must be incorporated in certain kinds of materials or capped with capping agent or ligand. Materials such as surfactants [82], glass [83], silica [84], zeolites [85], dendrimers [86], and polymers [45,87-89] have been used as the substrate to prepare materials containing nanoparticles. The capping agents employed also play a role in determining the property of the nanoparticles. Hence, it is necessary to tailor its surface with the right capping agent. Polymer membrane assisted fabrication of nanoparticles is probably one of the most efficient ways to overcome the stability problem of metal nanoparticles and to save their properties. Metal nanoparticles synthesized by this approach exhibit long-time stability against aggregation and oxidation.

A membrane is an interphase between two adjacent phases, acting as a selective barrier, regulating the transport of solute/solvent between the two compartments. It can selectively separate compounds over a wide range of particle sizes and molecular weights, from macro molecular materials such as protein to monovalent ions. Membranes have applications in water purification, health care, water treatment, separation science, fuel cell, chemical sensor, electro dialysis etc. [18,90].

J Abbe Nollet, in 1748, discovered the phenomenon of osmosis. He observed that water diffuses from a dilute solution to a more concentrated one, when separated by a pig's bladder [91]. During the following century, osmosis was of special interest and experiments were conducted primarily with membrane of animal and plant origin. *Schoenbein*, in 1845, invented the nitrocellulose [92], which has paved the way for preparation of the synthetic membranes. *Thomas Graham*, who may be regarded as the father of membrane science, performed the first recorded experiments on transport of gases and vapours across the polymeric membranes. In 1961, *Graham* reported his first dialysis experiment using synthetic membrane [93,94]. The theoretical treatments and much of the interpretation of osmotic phenomena and mass transport through membranes were based on the studies of *Fick,* who interpreted diffusion in liquids as a function of concentration gradient [95]. Van't Hoff, in 1887, used the measurements of solution osmotic pressure made with membranes to develop his limit law, which gives a thermodynamic explanation for the osmotic pressure of dilute solutions [96]. Later, *Nernst and Plank* introduced the flux equation for electrolytes under the driving force of a concentration or electrical potential gradient [97,98]. The classical publications of *Donnan* explained and interpreted the theory of membrane equilibrium and so-called "Donnan exclusion potential" in the presence of electrolytes [99].

With the beginning of the twentieth century, the membrane science and technology has entered a new phase with the development of synthetic membrane. In the early days, the membranes had been mainly a subject of scientific interest with only very few practical applications. Afterwards, when the practical use of membranes in technically relevant applications became the main focus of interest then a significant number of membrane-based industries developed rapidly. Today, membranes are used on a large scale to produce potable water from the sea by reverse osmosis, to clean industrial effluents and recover valuable constituents by electro dialysis, to fractionate macromolecular solutions in the food and drug industry by ultrafiltration, to remove urea and other toxins from the blood stream by dialysis in an artificial kidney, and to release drugs such as scopolamin, nitroglycerin, etc. at a predetermined rate in medical treatment.

A membrane can be homogeneous or heterogeneous, symmetric or asymmetric in structure; solid or liquid; it may be neutral or may carry positive or negative charges or may be bipolar. Depending upon the chemical compositions, the membranes can be classified into three groups: (i) neutral membranes, (ii) ion-exchange membranes, and (iii) functionalized membranes.

Since, in present thesis, ion exchange membranes were used for hosting metal nanoparticles. A brief account of ion exchange membrane is given below.

1.3.1. Ion exchange membrane

H.P. Thompson and J.T. Way, in 1850, found ion exchange phenomenon when they noted the adsorption of ammonium sulfate on soil [100,101]. However, the actual studies related to ion exchange membranes begun in 1925 and carried out by Michaelis and Fujita with the homogeneous, weak acid collodium membranes [102]. First ion exchange membrane was reported in 1950, which was prepared using finely powdered ion exchange resin and binding polymer [103,104].

Ion exchange membranes are, in general, finely microporous, with the pore walls carrying fixed positive or negative charges [18,105]. The characteristic of these membranes are i) ion conductivity, ii) hydrophilicity, and iii) the existence of fixed carrier (ion exchange group). There are five types of ion exchange membranes based on composition of the fixed charged groups: cation, anion, combined cation/anion exchange (bipolar), amphoteric (without mobile counterions), and mosaic ion-exchange membranes. Cation exchange membranes contain negatively charged groups, such as $–SO_3^-$, $–COO^-$, $–PO_3^{2-}$,$–PO_3H^-$, $–C_6H_4O^-$, etc., fixed to the membrane backbone and allow the passage of cations but reject anions. While anion exchange membranes contains positively charged groups, such as $–NH_3^+$, $–NRH_2^+$, $–NR_2H^+$, $–NR_3^+$, $–PR_3^+$, $–SR_2^+$, etc., fixed to the membrane backbone and allow the passage of anions but reject cations. In amphoteric ion-exchange membrane, fixed ionic group can behave as cation or anion exchange sites. While, mosaic ion-exchange membranes are composed of macroscopic domains of polymers with negatively fixed ions and positively fixed ions randomly distributed in a neutral polymer matrix. Ion exchange membranes are semi-permeable, i.e., they allow only the counter ion to pass through them, excluding the co-ions. In ion exchange membranes the counterions interact with the fixed charged functional groups in the membrane electrostatically. Separation techniques based on ion exchange membranes are increasingly gaining importance as relatively clean separations with high separation factors are achievable and also they are cost effective [105]. The key parameters for specific applications of ion exchange membranes are: (i) selective partitioning of target species from solution to membrane phase, (ii) diffusion of the species in the membrane matrix, and (iii) release of the target species into the receiver phase. Therefore, the interactions of the target species with the functional groups as well as physical and chemical architecture of the membrane matrix play an important role in designing target specific membranes. There are fundamental principles that govern the transport of counter ions across the ion-exchange membranes. These are given below:

a) Fixed charge has mobile counter ions that can be exchanged.
b) Co-ions having same charge as that of fixed sites are rejected (*Donnan exclusion*).
c) Electrical neutrality at feed side and receiver side is maintained (coupled diffusion).
d) Salt leaks across the membrane, if fixed charge density in the membrane is less than salt concentration in the feed.
e) H^+ ions can leak by hopping in water channels (*Grothus Mechanism*) across the anion-exchange membrane.
f) *Donnan equilibrium* in the feed and receiver compartment is attained

In recent time, ion-exchange membrane are used in large variety of applications such as water desalination, production of acids and bases by electrodialysis, Donnan and diffusion dialysis, chlorine-alkaline electrolysis, hydrogen and oxygen production, fuel cells, batteries etc. [106].

1.3.2. Nafion

Nafion membrane has been the most used synthetic polymer cation-exchange membrane for a variety of applications [31,105-108]. Nafion was discovered in the late 1960s by Dr. Walther Gustav Grot of DuPont de Nemours. It is a tetrafluoroethylene copolymer with a pendent side chain of perfluoroinated vinyl ether terminated by sulfonic acid group. This is the first of a class of synthetic polymers, perfluorosulfonic acid (PFSA), with ionic properties called ionomers. Perfluorosulfonic acid is made by copolymerization of tetrafluoroethylene and a perfluorovinyl ether terminated with a sulfonyl fluoride [31]. After polymerization the sulfonyl fluoride is hydrolyzed and ion exchanged to produce the perfluorosulfonic acid. The hydrophobic fluorinated backbone of the polymer is polytetrafluoroethylene (PTFE) or Teflon, which maintains the structural integrity in most solvent environments and gives it superior chemical and thermal stability. The regularly spaced long perfluorovinyl ether with pendant side chain terminated by a sulphonate ionic group gives ionic properties. The chemical structure of Nafion is shown Fig. 1.1.

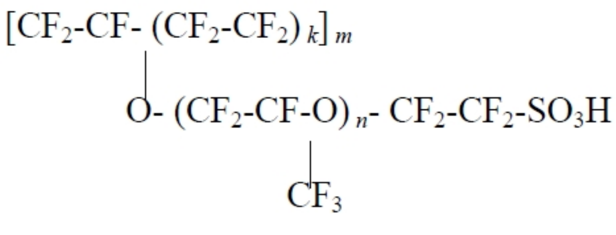

$$[CF_2\text{-}CF\text{-}\ (CF_2\text{-}CF_2)_k]_m$$
$$O\text{-}\ (CF_2\text{-}CF\text{-}O)_n\text{-}\ CF_2\text{-}CF_2\text{-}SO_3H$$
$$CF_3$$

Fig. 1.1 *Chemical structure of Nafion*

Physical properties of Nafion, such as permeability and ion transport, are linked to its microstructure. The microstructure of Nafion consists of three regions, the hydrophobic fluorocarbon backbone, hydrophilic ionic clusters of sulfonic acid groups, and an interfacial region [109]. The absence of chemical cross-linking between polymer chains in the Nafion is responsible for its phase segregation into hydrophilic and hydrophobic domains [110,111]. In hydrated Nafion membranes, the hydrophobic domains are responsible for the mechanical stability, whereas the hydrated, hydrophilic domains are responsible for proton transfer and water transport. Many morphological models were employed to explain Nafion properties:

a) cluster-network model proposed by Gierke et al. [109,112,113];
b) fibrillar or polymeric bundle model proposed by Gebel et al.[114,115], consisting of fluorocarbon chains surrounded by ionic groups and water,
c) core –shell model proposed by Fujimura et al.[116,117] which shows ion rich core which is surrounded by an ion poor shell;
d) sandwich model proposed by Haubold et al.,[118] illustrating the polymer structure which composed of two layers whose sulfonic group attract across an aqueous layer where transport occurs;
e) rod model proposed by Rubatat et al.[115] includes the sulfonic groups arrange into crystal –like rods;
f) lamellar model proposed by Litt[119].

The Geirke model, known as the cluster-network model (Fig. 1.2), is widely accepted model describes the structure of Nafion. It assumes that the sulfonate groups form spherical clusters of ~40Å diameter that resemble reverse micelle. These clusters are arranged on a regular lattice of ~50Å and interconnected with each other by narrow water channels of 10 Å diameters. Cluster size and no of water channels are dependent on water content and will change during absorption and desorption process and its method of water immersion and water vapor [120-122]. The biggest problem in this model is the presence of water channel which has never been experimentally observed either by microscopic or by small angle scattering experiment. Recently some models have suggested in which water clusters themselves join each other forming continuous self-assembled cylindrical channels [123-125].

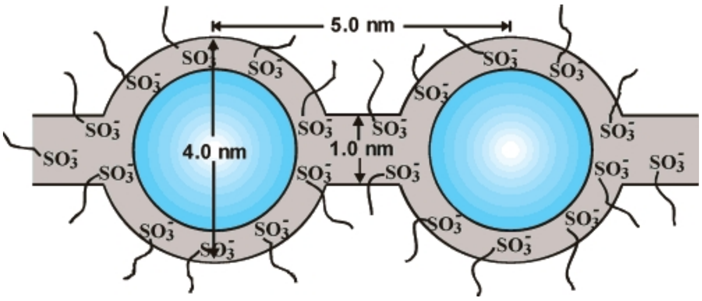

Fig. 1.2 *The cluster-network model of the structure of Nafion*

A swelling mechanism (Fig.1.3) was suggested by Gebel showed structural reorganization, which was analysed by a cluster number decrease and an intercluster distance increase [126-128]. In this mechanism, the dry membrane is considered to contain isolated, spherical ionic clusters with diameters of ~1.5 nm and a center-to-center separation distance of ~2.7 nm. With the absorption of water, the clusters swell to hold pools of water surrounded by ionic groups at the polymer-water interface in order to minimize the interfacial energy.

As the water content increases to between $\varphi_w = 0.3$ and 0.5, structural reorganization occurs to keep the specific surface area constant, and the onset of percolation is achieved by the formation of connecting channels of water between the swollen spherical clusters. At φ_w values greater than 0.5, an inversion of the structure occurs such that the structure resembles a connected network of rods. Finally, as the membrane “dissolves” into solution, the rod like structures separate to yield a colloidal dispersion of isolated rods.

Several versions of Nafion membranes are available that differ by membrane thickness, density of sulfonic acid groups and the capping groups on the ends of the polymer chains. The number of grams of dry polymer per mole of sulfonic acid groups of the material is referred to as equivalent weight (EW). For a given equivalent weight, the cluster diameter, the exchange sites per cluster, and the number of water molecules per exchange site increased

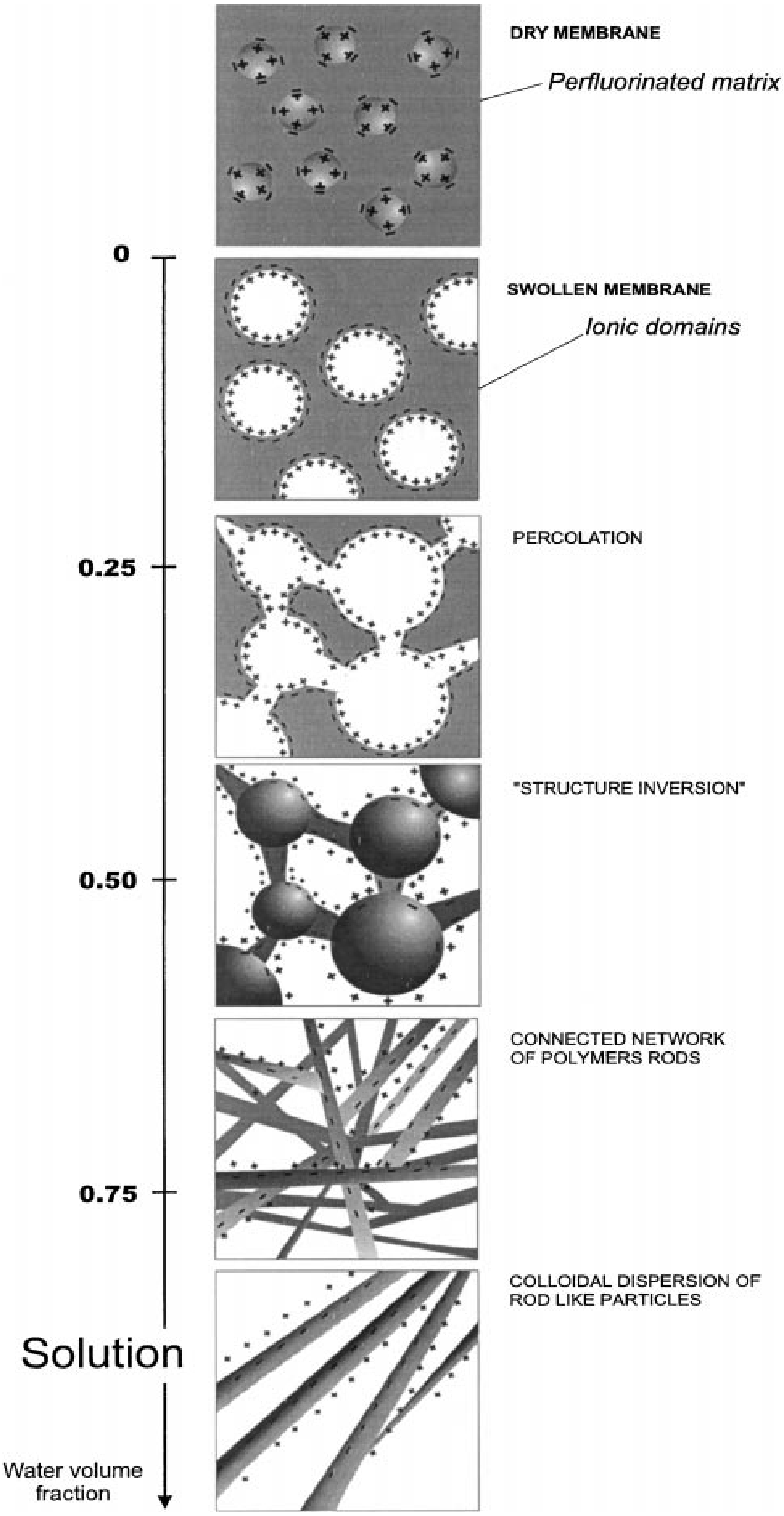

Fig. 1.3 *changes in the physical structure of nafion with hydration.*

linearly with water content. Nafion is denoted by a system of numbers. The first two numbers denote equivalent weight (EW) while the third denotes dry membrane thickness in thousandths of an inch. For Example, Nafion N117 refers to a film having 1100 EW and a nominal thickness of 0.007 in. Generally for the Nafion 117 membrane $n = 1$, $k = 6.5$ and $100<m<1000$. (Fig 1.1)

1.3.3. Polymer inclusion membranes

Functionalized membranes are the new entrant in the field of membrane processes. Permeation selectivity or perm-selectivity of the membrane towards competing ions is an important factor for selective preconcentration of the target ions from the multicomponent aqueous feed. Generally, the perm-selectivity is achieved by anchoring the target ions specific functional groups (receptors) in the membrane. These membranes are termed as the functionalized membranes. The functionalized membranes are prepared by either physical containment or covalent attachment of the functional groups in a suitable organic or inorganic-organic hybrid matrix [129-132]. One of the simplest example of functionalized membrane system is the bulk liquid membrane (BLM) formed by the organic liquid having ion-selective reagent [133]. The improved version of BLM is the supported liquid membranes (SLMs) [134-138]. SLMs are formed by physical immobilization of the organic phase containing an extractant in pores of the microporous host membrane. The capillary force stabilizes the organic phase in the membrane matrix. This class of membranes has been found to be useful for small scale applications in the analytical chemistry [139-141]. However, a major drawback associated with SLMs is their poor stability for long term applications [142-146]. The membrane can be made highly stable by linking functional groups covalently with the polymer chains. This type of the functionalized membranes are synthesized by grafting the monomer containing precursor chemical groups on the poly(propylene) chains and required functional groups are generated by subsequent chemical modification of the precursor chemical groups [147]. This class of membranes is termed as a fixed-site membrane. However, these membranes have not been successful for the facilitated transport of ions due to slow transport rate across the membrane and also due to complicated synthetic chemistry involved in the formation of the target specific receptors in the membrane [148-151]. The intermediate of SLMs and fixed-site membranes is the polymer inclusion membrane (PIM), which is also known in chemical sensors as the solvent polymeric membrane [152-156]. These membranes are analogous to SLM but show better stability [157-159].

Polymer inclusion membranes (PIMs) were first introduced by *Sugiura et.al* [73]. PIMs have been developed for variety of applications in the separation science and chemical sensors [152-156,160-164]. They are prepared by the physical immobilization of a selective extractant into a plasticized polymer matrix. Two of the commonly used polymer matrices are poly (vinyl chloride) (PVC) and cellulose triacetate (CTA) [165,166]. They are inert and highly hydrophobic polymers The base polymer form skeleton of the PIM to provide mechanical strength. The chemical structure of the base polymer also plays an important role in transport of ions across the PIMs.

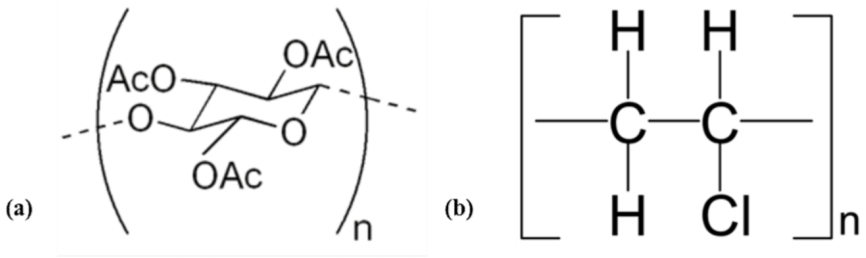

Fig. 1.4 *Chemical structure of matrix forming polymer (a) cellulose triacetate (CTA) and (b) poly (vinyl chloride) (PVC).*

These matrix forming polymers can be plasticized upto 70 – 80% by weight with a variety of plasticizers like 2-nitrophenyl octyl ether (NPOE), dioctyl phthalate (DOP), bis(2-ethyhexyl) terephthalate (DOTP), dioctyl sebacate (DOS), and tri-(2-ethylhexyl) phosphate (T2EHP).

The network of overlapping chains of the polymer provides mechanical support to the PIMs. The solvent (plasticizer) used in these membranes plays the role of (i) plasticizing, thereby increasing the softness, flexibility, and mechanical strength of the membrane [152,167] (ii) solubilising and holding the extractant into the membrane matrix and (iii) solvent for the extractant in the membrane matrix. The transfer of analyte into the membrane phase occurs only if the plasticizer in the membrane is free to solvate the extractant like in liquid-liquid solvent extraction. The gel network of the polymer matrix materials with the solvent is expected to increase the viscosity and prevent the carrier (extractant) from leaching out. The plasticizer, acting as solvent, is expected to influence the mobility of carrier-analyte complex significantly in the membrane. Thus the nature and amount of plasticizer in the PIM is crucial for controlling the ion diffusion kinetics.

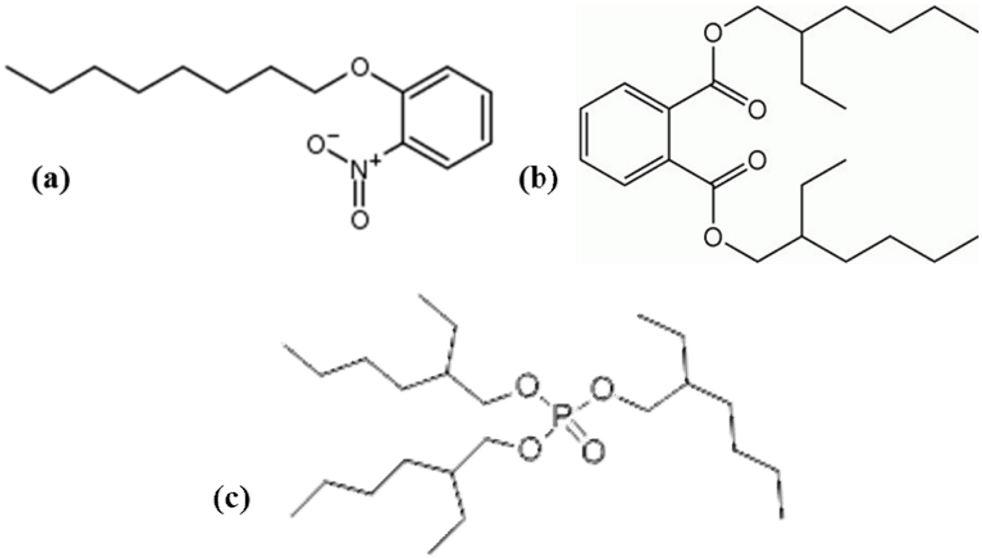

Fig. 1.4 *Chemeical structure of plasticiser (a) 2-nitrophenyl octyl ether (NPOE), (b) dioctyl phthalate (DOP), and (c) tri-(2-ethylhexyl) phosphate (T2EHP).*

The extractant in the PIMs acts as a mobile carrier for the target analyte in the membrane matrix. Tri-octylmethylammonium chloride (Aliquat-336) can used as an extractant to make PIM behave as anion exchange membrane. The important features of the PIMs are as following:

a) Simple method of preparation
b) Cost effective
c) Well-defined chemical properties
d) Tailor-made for the target analyte
e) More stable than SLMs
f) Extensively used in chemical sensor

The properties of these membranes can be tuned by appropriate selection of matrix forming polymer, plasticizer, and extractant. Therefore, these membranes can be tailor made for a specific application without involving exotic synthetic chemistry. These membranes exhibit many advantages, viz. ease of operation, minimum use of hazardous chemicals, and flexibility in membrane composition to achieve desired selectivity and separation efficiency. However, the transport of ions across PIMs has been found to be slower than SLMs. This is due to the fact that the viscosity of the liquid fraction and the hydrophobicity of PIMs are considerably higher than the other class of membranes [157]. The preparation of the PIMs and different components are shown in Fig. 1.5.

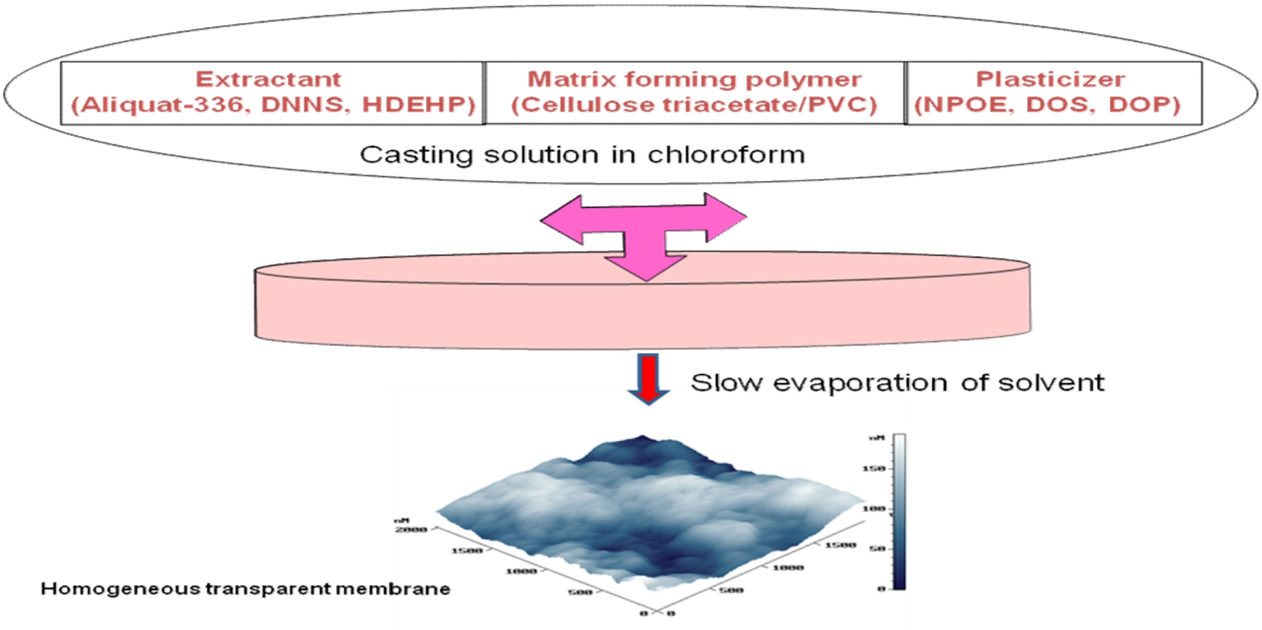

Fig. 1.5 *Schematic diagram showing steps involved in the preparation of PIMs.*

The extracted ions tend to form ion-pairs with the extractant (liquid ion-exchanger) present in the membrane. The electrostatic interaction makes a principal contribution to the stability of such ion pairs and would govern the distribution ratio of an ion between the solution and the membrane phase, which is a key factor in determining the selectivity of an ion with respect to other in a solution. However, the transfer of ions from aqueous to membrane phase is affected by the hydrophobicity and dielectric constant of the membrane phase. For example, the exchange of highly hydrated ions with less hydrated ions in a low dielectric medium is energetically unfavorable. In SLMs, which are very close to liquid-liquid solvent extraction systems, the effect of hydrated cationic radius on the permeation of cations has been studied [168]. The results show that the ion with smaller hydrated ionic radius forms a stronger complex with the extractant, thereby increasing its flux across the SLM. Therefore, it is possible to make ion-exchange membrane selective to less hydrated ions by properly tuning the properties of the membrane phase. In PIM, this can be achieved by appropriate choice of plasticizer and ion-exchanger immobilized in the membrane matrix.

The polymeric membrane has three important structural levels: (1) the molecular, which is equivalent to the chemical nature of the polymer, is characterized by polar, steric, and ionic factors and is also responsible for the membrane's microcrystalline nature; (2) the microcrystalline, which affects both the transport and mechanical properties of the membrane; and (3) the colloidal, which is concerned with the aggregation of macromolecules and governs the statistics of pores (size, size distribution, density, and void volume).

1.4. Nanoparticles in membrane

Polymer membrane have been considered one of the important matrix materials for the preparation and application of nanoparticles because of their mechanical, optical, electrical, and thermal properties [18]. The synthesis of size-controlled, well-dispersed metal nanoparticles in the membrane matrix is of great interest for a wide-range of emerging technological applications. In membrane matrix, aggregation of nanoparticles is avoided by restriction of the movement of nanoparticles of the polymer chains of the membrane and thus nanoparticles are stabilized in the polymer networks.

In general, there exist two different approaches to preparation of metal nanoparticle in the membrane e.g. *ex situ* and *in situ* methods. In the *ex situ* approach, the metal nanoparticles are chemically synthesized and their surface is organically passivated. The derivatized nanoparticles are dispersed into the polymer matrix during the preparation of the membrane. While in the *in situ* approach metal nanoparticles are prepared by reduction of precursor metal ions within the matrix of the membrane using chemical [27], electrochemical, thermal [28], gamma/UV irradiation [29,30] reduction method. The *ex situ* is simple and attractive, but often leads to undesired results because of aggregation and non-uniform distribution of nanoparticles during dispersion and unremoved capping agent of nanoparticles in the membrane matrix upon completion of the synthetic procedure. The *in situ* methods have become very popular because they are easy to implement and yield a homogeneous distribution of nanoparticles in the membrane. One of the *in situ* methodology involves the simultaneous synthesis of the polymer membrane from the monomer as well as the metal nanoparticles. Alternately, in a preformed membrane, the metal nanoparticles can be generated from suitable precursors within the membrane matrix. Conversion of precursors to nanoparticles within the polymer matrix can result in the generation of undesirable species in the membrane matrix; but, it can be overcome by careful choice of the precursor and reaction conditions.

Mbhele et al. followed *ex situ* method to prepared poly(vinyl alcohol) (PVA)-Ag nanocomposite membrane by dispersing preformed Ag nanoparticles in the PVA matrix. Incorporation of Ag nanoparticles into the PVA matrix induced significant changes in the thermal and mechanical properties of the PVA. It was shown that the glass transition of the membrane was shifted toward higher temperatures by 20 °C, and the thermal stability was improved by about 40 °C for the nanocomposite membrane containing 0.73 wt % of Ag [169].

Kim et al. [170] reported simultaneous *in situ* synthesis of silver nanoparticles and the polymer film through an in situ electron-transfer reaction and the copolymerization of styrene and amphiphilic urethane acrylate nonionomer. Similarly, Sangermano et al. [171] used simultaneous synthetic methodology for *in situ* generation of silver nanoparticles during photoinduced cationic curing of bisepoxides. Another method of formation of metal nanoparticles in polymer involves the synthesis of both nanoparticle and its stabilizing polymer matrix in one place and in one stage by thermolysis. The thermal decomposition is attended with evolution of gas and mass loss of the samples. Metal-forming precursors such as carbonyls, formates, acetates, oxalates and organometallic compounds are used in producing polymer-immobilized nanoparticles by thermolysis. For example, a metal–polymer composition can be prepared by thermolysis of copper formate triethylene-diaminic(EDA) complex $[Cu(EDA)_3](HCOO)_2$ into poly styrene (PS) through a common solvent (DMF) [172]. The same principle was used to get Rh, Pd, Pt, Ag, and Au nanoparticles in polymethyl methacrylate (PMMA) at the stage of methyl methacrylate (MMA) polymerization [173]. Matsubayashi et al. used interference light for the generation of multilayer structure of the metal nanoparticles by photoreduction of silver and palladium metal precursors homogeneously dispersed in polymer films of poly(methyl methacrylate) (PMMA) and polystyrene (PS) [174].

Another interesting way to prepare metal nanoparticles in polymer matrix is based on ion exchange membrane. Ion exchange mechanism was used to load metal precursor in the membrane and then metal precursor were converted into metal nano structures by reducing agent. The pores or self-assembled clusters in ion exchange membrane act as nanoreactors, where nanoparticles can be synthesized provided that other reactants are somehow able to interact with precursor ions. The membrane matrix efficiently separates the nanoparticles from one another and thus ensuring stability of nanoparticles. The advantage of this process is that the nanostructure properties such as particle size, distribution, particle concentration, and interparticle spacing can be controlled during nanoparticle synthesis by utilizing the ion exchange properties of the membrane. The amount of ion exchange sites and ion-exchange conditions, such as the pH and competitive ions, decide size and size distribution of the nanoparticles. For example, Wang and co-workers reported that silver nanoparticles with various sizes and concentrations were produced in the polyelectrolyte multilayer film [175]. Watanabe et al. prepared uniformly dispersed Pt nanoparticles inside the Nafion. Pt precursor, $[Pt(NH_3)_4]Cl_2$, was transfered to the Nafion by an ion-exchange process and subsequently reduced to Pt nano crystals with an aqueous solution containing neutral hydrazine [176,177]. Mau et al. has developed Nafion/Pt, Nafion/Pt/CdS nano composite systems for photocatalytic hydrogen generation by using similar production route [178]. Yoon and their group demonstrated the superparamagnetic behavior of Ni nanoparticles of size 1.5–3 nm that were formed within the perfluorinated sulfo-cation membrane (MF-4SK) by the reduction of Ni ions with aqueous solution of $NaBH_4$ [179]. They also prepared cobalt nanoparticles in the membrane using similar route of synthesis to study magnetic properties of nanocomposite membrane [180,181].

Corain, Prati, and co-workers reported well-defined gold nanoparticles supported by a gel-type polyacrylic resin, poly-(2-(methylthio)ethyl methacrylate-N,N-dimethyl acrylamide-N,N-methylene bisacrylamide). The thioether (R-S-R) functional group was used as a coordination site for Au precursor prior to its reduction to Au^0 with $NaBH_4$. The gel-type resin had small pores with a mean diameter of 2.5 nm, while the size of the obtained gold nanoparticles was 2.2 nm. The slightly smaller size of the nanoparticles relative to the pore size of the polymer gel suggested that the cavities in the polymer gel prevented the gold nanoparticles from aggregating [182,183].

Zhang and his coworker had used nano cavity of the Nafion as a templetes to produces silver nanoparticles [184]. The distribution of nanoparticles in the ion exchange membrane depends upon inclusion methodology. Wang et al. prepared CdS nanoparticles in Nafion ionomer membranes using two different precursors. Nafion membrane was first converted into Cd form and then converted into CdS by using both nonionic and ionic precursors. It was observed that the CdS nanoparticles were homogeneously dispersed across the membrane when a nonionic thioacetamide was used as a precursor, while CdS was predominantly formed near the surface of the membrane when ionic Na_2S was used as a precursor [185]. Ag_2S nanoparticles were prepared in Nafion using similar route of synthesis by Rollins [186]. Xu et al. modified the micropores of poly(vinylidene fluoride) (PVDF) membranes with the ion-exchange groups of poly(acrylic acid) (PAA). These ion-exchange groups were used to synthesize Fe/Pd bimetallic nanoparticles [187]. Zan et al. incorporated silver nanoparticles in polyelectrolyte multilayer flim made of filmspoly(diallyldimethylammoniumchloride) (PDDA)/ Poly (styrene sulfonate) PSS by counterion exchange and followed by *in situ* reduction [188].

Silver nanoparticles in Nafion using $NaBH_4$ as reducing agent were prepared form the Ag+-loaded Nafion-117 in our laboratory [189]. Ag nanoparticles, thus formed, were confined to the surface of the membrane. The average size of nanoparticles formed after reduction was found to be around 15 nm, which was irrespective of the concentration of silver ions present in the membrane before reduction.

1.5. Experimental techniques for characterization of nps

The structural characterization of nanoparticles in the nanocomposite membrane is performed mainly by transmission electron microscopy (TEM), X-ray diffraction (XRD), and optical spectroscopy (UV–Vis). These three techniques are very effective in determining particle morphology, crystal structure, composition, and particle size.

Membrane characterization has been carried out by atomic force microscopy (AFM), electrochemical impedance spectroscopy (EIS), differential scanning calorimeter (DSC) and non-stationary radiotracer method for measuring self-diffusion coefficient.

1.5.1. Measurement of self-diffusion coefficient

Diffusion is a process by which matter is transported from one part of the system to another as a result of random molecular motion [190]. In the absence of any external force, concentration gradient is the driving force for diffusion. In the context of ion-exchange membranes, diffusion is the process of transport of ionic species across the membrane [191]. The ionic flux involves a transfer of electric charge. In the absence of electric current, this charge transfer must be balanced by one or more ionic fluxes. Diffusion process in any isotropic substance, including ion-exchange membranes, can be expressed mathematically by Fick's laws [190]. According to Fick's first law of diffusion, the rate of transfer of diffusing substance through a unit area of a section is proportional to the concentration gradient measured normal to the section

$$J = -D\frac{dC}{dx} \tag{1.1}$$

where, D is the diffusion coefficient of the species (unit cm^2/s) and J is the flux in unit of moles/cm^2/s. The negative sign shows that diffusion occurs in the opposite direction to that of increasing concentration. The change in concentration with time is given by Fick's second law as

$$\frac{\partial C}{\partial t} = D\frac{\partial^2 C}{\partial^2 x} \tag{1.2}$$

Self-diffusion is diffusion of a species in a medium or between two media having no concentration gradient. In such a case, the diffusion constant, called the *self-diffusion* *coefficient* (SDC), gives the true mobility of any species in the matrix. The entropy of mixing is the driving force for self-diffusion.

Diffusion of ions in a membrane matrix is governed by two important factors, the physical and chemical architecture of the polymer matrix through which the counterions are moving and the nature of interaction of the counterions with the fixed sites on the polymer backbone. Non-stationary radiotracer method is extensively used for measuring self-diffusion coefficient in membranes. Other methods like ion exchange, conductivity measurements and pulse field gradient NMR also have been used for the same.

Non-stationary radiotracer method of measuring self-diffusion coefficient of ions and water in ion-exchange membranes is essentially based on the analysis of kinetics of isotopic exchange in an ion-exchange membrane using an analytical solution of Fick’s second law. This transient method is simple, does not require stringent control over hydrodynamics near the membrane, and is faster because a single measurement can yield the self-diffusion coefficient of the ions [33-35]. This method of determination of self-diffusion coefficient is based on the analysis of the time dependent concentration profile of the radioactive tracer ions diffusing in or out of a sheet of membrane sample kept in contact with an equilibrating solution. The method is based on the assumptions that (i) it is a membrane controlled diffusion process, (ii) the self-diffusion coefficient of given species within the membrane is constant, and (iii) diffusion process is one-dimensional. The first assumption is valid only if the concentrations of the radiotracer ions at membrane-water interface is same as that in the bulk solution. To achieve this, membrane samples are vigorously stirred in the equilibrating solution. The concentration profile of a radiotracer diffusing in or out of the membrane is a function of time and space and is governed by Fick’s second law given by equation 1.2. In the case of radiotracer sorption experiment, the membrane free of radiotracer is kept in contact with an equilibrating salt solution containing radiotracer ions. With the initial conditions t=0, 0<x<L, c=0 and boundary conditions t>0, c=c*, x=0, and x=L, the solution of equation 1.2 is

$$c(x,t) = c^* + \frac{2c^*}{\pi}\sum_{n=1}^{\infty}\frac{(\cos n\pi - 1)}{n}\sin\frac{n\pi x}{L}\exp\left(-D\frac{n^2\pi^2 t}{L^2}\right) \tag{1.3}$$

where *L* is the thickness of the membrane. For a fixed time ($t=t_k$), the amount of radiotracer sorbed by the membrane of area *A* is given by

$$N(t_k) = A\int_0^L c(x,t)dx \tag{1.4}$$

which on integration gives

$$\mathrm{N}(t_k) = N^*\left[1-\left(\frac{8}{\pi^2}\right)\left\{\exp\left(-\frac{D\,\pi^2 t_k}{L^2}\right)+\left(\frac{1}{9}\right)\exp\left(\frac{-9D\,\pi^2 t_k}{L^2}\right)+\ldots\ldots\ldots\ldots\right\}\right] \tag{1.5}$$

Where, *N** is the total amount of the radiotracer ions in the membrane at equilibrium ($t=\infty$). In the case of reverse experiment, that is, radiotracer diffusing out of the membrane, *N** will represent the total radiotracer ions in the salt solution at equilibrium ($t=\infty$). *D* has been deduced by a non-linear least-squared fit of equation 1.5 with both *N** and *D* as free parameters.

In the present thesis, self-diffusion coefficients of different ions in different types of ion-exchange membranes have been measured using the non-stationary radiotracer method.

1.5.2. Differential scanning calorimeter (DSC)

Differential scanning calorimetry (DSC) is a thermal analysis method designed to determine phase transformations events of a sample with respect to a reference [192]. The basic principle of DSC is that, as a sample undergoes a heating cycle, it may undergo exothermic and/or endothermic phase transformations. The DSC can quantify the heat change, which allows one to determine the nature and extent of the physicochemical change taking place.

Mettler Toledo DSC 822 has been used for measuring DSC profiles of the membrane samples. DSC scans were carried out at heating rate of 10 ^{o}C min^{-1}, under inert atmosphere with an empty aluminum pan as reference. Temperature and enthalpy calibration of the instrument has been carried out using cyclohexane and indium. The transition enthalpy of the curve has been calculated by using the software supplied by Mettler Toledo.

1.5.3. UV-Vis spectroscopy

Measurement of UV-visible absorption spectra has been carried out using the UV-visible spectrophotometer. Modern spectrophotometers employ double beam arrangements whereby the absorbance is measured through two cells, a reference cell and a sample cell [193].

UV-Vis spectra of nanoparticles embedded membrane samples has been recorded using UV-Vis Spectrophotometer (V-530, JASCO, Japan). The absorbance measurements has been carried out by mounting the membrane sample (1x2 cm) on to the inside wall of a (1x1x3 cm) quartz cell and placing it in a spectrophotometer to record spectrum with respect to air.

1.5.4. X-ray diffraction (XRD)

X rays are the electromagnetic radiations of wavelength ranging from 0.04 to about 100 Å. They occur in the electromagnetic spectrum between gamma rays and UV rays. X–rays are produced when the high energy charged particles, generally electrons, are accelerated through high potential and allowed to strike a metal target. The incident electrons have sufficient energies to knock out inner orbital electron. Simultaneously an electron from an outer orbital falls down immediately to the vacant orbital and the energy released appears as characteristic X – rays. For copper, the most commonly used target, 2p → 1s transition called K_{α} transition has a wavelength of 1.5418 Å.

X-ray diffraction has been in use since the early part of this century for the determination of structure of crystalline materials. In 1912, Max von Laue discovered X-ray diffraction from crystalline solids. When X-rays passes through crystalline materials, they get scattered by its constituent atoms. The scattered X-rays interfere with the incident X-ray constructively or destructively depending on the path difference. Condition for the constructive interference can be obtained from the Bragg law. These diffracted X-rays are then detected and counted in a range of 2θ angles. This technique is most extensively used for characterization of solid crystalline materials and determination of their unit cell, lattice parameters, and their probable structures [194,195].

X-ray diffraction is also being used as a method for determining the mean size of single-crystal nanoparticles or crystallites in nanocrystalline bulk materials [196]. In 1918, Paul Scherrer published his landmark paper on the effect of crystallite size on the width of X-ray diffraction peaks, which is known as Debye–Scherrer equation [197,198]. In this equation broadening of X-ray diffraction peak is used to estimate the size of crystallite.

$$D_{hkl} = \frac{K\lambda}{B_{hkl}\cos\theta} \tag{1.6}$$

Where,

D_{hkl} is the crystallite size in the direction perpendicular to the lattice planes,

K is a numerical factor frequently referred to as the crystallite-shape factor,

λ is the wavelength of the X-rays,

B_{hkl} is the FWHM (full-width at half-maximum) of the X-ray diffraction peak in radians and

θ is the Bragg angle.

The value of K, the Scherrer constant, depends on the shape of the crystal, and the size distribution. The most common value for K is 0.9 for spherical crystals.

In the present work, X-ray diffraction (XRD) measurements has been carried out in the range of 2θ (10-70^o) on the membrane using monochromatized Cu-K_α ($K_{\alpha 1}$ = 1.5406 Å and $K\alpha_2$ =

1.5444 Å) radiation by Philips X-ray diffractometer Model PW 1710, Netherlands. Silicon has been used as an external standard for correction due to instrumental broadening.

1.5.5. Energy dispersive X-ray fluorescence (EDXRF)

X-ray fluorescence (XRF) is based on the principle of measurement of the energies or wavelengths of the X-ray spectral lines emitted from the sample, which are the characteristic or signature of the elements present in the sample. There are two major modes of analysis in X-ray spectrometer: wavelength dispersive X-Ray fluorescence (WDXRF) and energy dispersive X-ray fluorescence (EDXRF) spectrometry. The difference in these two modes of analysis lies in the detection component. In EDXRF, the detectors directly measure the energy of the X-rays with the help of multichannel analyzer. Whereas in WDXRF, the X-rays emitted from the samples are made to disperse spatially using a dispersion crystal and each wavelength of the emitted X-rays is determined by the detector sequentially.

The EDXRF measurements have been carried out using ITAL STRUCTURES TX 2000 spectrometer. This spectrometer has been used in energy dispersive mode. In energy dispersive mode, the angle between the incident beam and sample is 45 degrees and the sample and detector is 45 degrees. Hence it’s called 45/45 degree geometry. A W-Mo dual target tube has been used for sample excitation. The spectrometer uses a Si(Li) detector having a resolution of 139 eV (FWHM) at 5.9 keV (Mn Kα). The X-ray spectra have been acquired and processed by computer programs EDXRF-32, provided with the instrument.

1.5.6. Transmission electron microscopy (TEM)

The transmission electron microscope (TEM) operates on the same basic principles as the light microscope but uses electrons instead of light to get enhanced resolution due to the shorter wavelengths of electron beams. The resolution of a microscope is defined as the distance between two details just separable from one another. It can be calculated using the Abb theory of images formation for optic systems and depends upon wave length of light. For optical microscopy, the resolution is therefore limited by the wavelength of light. In 1927, Hans Bush showed that a magnetic coil can focus an electron beam in the same way that a glass lens for light. In a TEM, the electrons are accelerated at high voltage to a velocity approaching the speed of light. The associated wavelength of the electrons is five orders of magnitude smaller than the light wavelength. Hence, TEM provides enhanced resolution due to the shorter wavelengths of electron beams. This resolution enables material imaging and structure determination at the atomic level. First image with a TEM was obtained by Ernst Ruska and Max Knoll in 1932 [199].

The TEM has a similar optical configuration to an optical microscope. By choosing the position of the aperture, either the diffracted beam (dark field) or the unscattered electrons (bright field) can be used to form the image. In the bright field (BF) mode of the TEM, image results from a weakening of the direct beam by its interaction with the sample. Therefore, mass-thickness and diffraction contrast contribute to image formation: thick areas, areas in which heavy atoms are enriched, and crystalline areas appear with dark contrast. In dark field (DF) mode, the direct beam is blocked by the aperture while one or more diffracted beams are allowed to pass the objective aperture. Since diffracted beams have strongly interacted with the specimen, very useful information is present in DF images, e.g., about planar defects, stacking faults or particle size [200].

For TEM analyses of cross-section of membrane, the membrane samples have been sectioned under cryogenic conditions in Leica ultramicrotome to 70 nm thicknesses by using glass and diamond knifes. The sections were picked on 200 mesh Cu grids. The grids have been examined in an FEI Technai G2 electron microscope at 120 KeV without any staining or post-treatment. The sizes of nanoparticles were measured manually using the image analyser software (Image Z, version 1.33 U).

1.5.7. Atomic force microscopy (AFM)

The AFM can be used to investigate the nanoscale topography of any surface, even poorly or non conducting surface [201]. Binnig, Quate, and Gerber invented the Atomic Force Microscope in 1985. The instrument measures forces on a surface by scanning the sample with the tip attached to a flexible cantilever. The AFM operates similar to the record player, in which the tip moves up and down in response to the surface features. The tip is attached to the end of a cantilever and an optical readout, or a piezoelectric crystal, translates the motion of the cantilever into an electronic signal. The outcome of the scan is a three-dimensional image of the surface. The resolution obtained by AFM is determined mainly by the size of the probe tip used for imaging [202]. Maximum resolution is typically on the atomic scale in the lateral and vertical directions. There are there main modes of scanning of the AFM e.g. contact mode, noncontact mode, and tapping mode.

In the present work, Nanosurf easy Scan 2 AFM (Nanosurf, Switzerland) with 10 µm scanner head is used for Atomic Force Microscopy (AFM) studies of membrane samples. The measurements have been carried out in non-contact mode at ambient temperature. The cantilevers in NCLR-10 (Nano World) cantilevers have been used having a resonance frequency of 190 kHz and force constant of 48 N/m. AFM data have been analyzed using Nanosurf Report 4.1 software.

1.5.8. Electrochemical impedance spectroscopy (EIS)

Electrochemical impedance spectroscopy (EIS) is the most important impedance measurement technique. EIS is a powerful diagnostic technique used in the fields of electrochemistry, corrosion, batteries and fuel cells. EIS involves measurements and analysis of materials in which ionic conduction strongly predominates. In, EIS an additional perturbation of a periodic small amplitude ac signal is added to the dc signal in order to obtain the frequency response of the system.

AUTOLAB Frequency Response Analyser 2 (Eco. Chemie B.V., Utrecht, The Netherlands) has been used for carrying out the ac-impedance measurements. A small sine wave AC potential has been applied to an electrochemical cell over a frequency range from 1 MHz to 10 Hz to obtain impedance spectra. The impedance spectra have been analyzed with the help of the Frequency Response Analyser software (Eco. Chemie B.V., Utrecht, Netherlands).

1.6. Scope of the thesis

The major objective of the present thesis is synthesis of metal nanoparticles in ion exchange membrane and to understand the interplay of different parameters, which affect the formation and spatial distribution of nanoparticles in ion exchange membrane. The selection of ion exchange membrane in the present thesis is based on the fact that they have immense potential in wide range of application. Incorporation of nanoparticles could impart desirable properties in the membrane that can enhance its functional properties for the given application.

In the present thesis, two types of ion exchange membranes have been used as a host for metal nanoparticles; (i) Nafion, a cation exchange membrane, and (ii) polymeric inclusion membrane. They represent different class of membranes. The presence of ion exchange groups in the ion exchange membrane enable precursor metal ions to be loaded by ion exchange mechanism. It is possible to control the amount of precursor ion loading in the matrix either by controlling the equilibration time of membrane in precursor metal ion solution or by controlling the precursor ion concentration in the equilibrating solution or by controlling the amount ion exchange sites in membrane. On subsequent reduction by the suitable process, metal ions have been converted into metal nanoparticles within the membrane. The nature of reductant and reducing condition has been varied to control the formation and distribution of nanoparticles. These nanoparticles containing membranes have characterized using different techniques for size and spatial distribution of nanoparticles.

Nafion-117 has been used for the preparations of silver and rhodium nanoparticles. These nanoparticles have been prepared by chemical reduction of the metal ion loaded membranes. Different ionic and nonionic reducing agents have been used for this purpose. Their effects on size and spatial distribution of nanoparticles in the membrane have also been studied. Change in the properties of the membrane such as water content and self-diffusion of counterions ions due to formation of nanoparticles in the membrane have been investigated.

Galvanic reduction method to reduce metal ion in Nafion has also been investigated in the thesis. Sacrificial silver nanoparticles have been used in galvanic reaction with salt solution of rhodium and mercury. Galvanic reduction of mercury ion by silver nanoparticles has been investigated for its possible use as colorimetric sensor for Hg^{+2} ions. Syntheses of gold and platinum nanostructures in the Nafion from their anionic precursor ion by galvanic reaction have been investigated using silver nanoparticles as templates.

Polymeric inclusion membrane having anion exchange groups have been developed to load metal ion which exist as anion such as $AuCl_4^-$. The composition of anion exchange polymeric inclusion membrane was optimised by varying the concentration of base polymer plasticiser and liquid anion exchanger. As polymeric inclusion membranes are not well studied. Surface topography, ion exchange capacity, glass transition temperature, self-diffusion of counter ions & water and counterions-exchange kinetics has been studied for polymeric inclusion membrane.

Gold nanoparticles have been prepared in the anion exchange polymeric inclusion membrane by loading gold precursor $AuCl_4^-$ in the membrane followed by chemical reduction. Multiple cycles of loading and reduction have been carried out by reusing the residual ion exchange capacity of the membrane. The effects on ion exchange capacity and transport property of the membrane due to formation of nanoparticles have been investigated. The accessibility of nanoparticles by counterions of the membrane has been studied using the surface plasmon band of nanoparticles.

Chapter -2

Metal nanoparticles in Nafion by direct reduction

2.1. Introduction

The cluster-network model of water-swollen Nafion, proposed by Geirke, is shown in Fig 1.2. It proposes that Nafion microstructure is divided into a hydrophobic domain consisting of the fluorinated backbones and a hydrophilic domain consisting of the ionic clusters. These ionic clusters are made of fixed sulfonic groups, their counter ions, and water. Elliott et al. proposed morphology of Nafion consists of independent bicontinuous networks of ionic clusters and fluorocarbon chains as shown in Fig 2.1 [123-125].

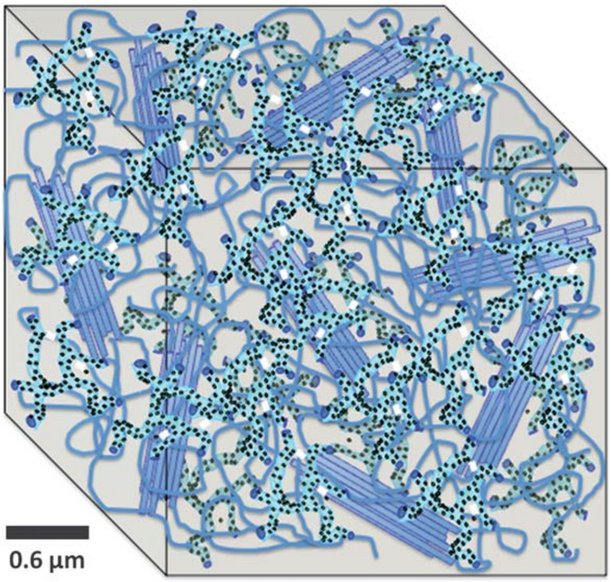

Fig. 2.1 *3D morphology showing continuous network of ionic clusters*

The presence of ionic water clusters in Nafion membrane makes it a promising host for nanoparticles (nps). A variety of monometallic, bimetallic, and ceramic nanoparticles have been incorporated in the Nafion membrane [184-186,189,203-207]. Jalani et al. synthesized Nafion/ZrO_2, Nafion/SiO_2, and Nafion/TiO_2 nanocomposite membranes via in situ sol–gel technique to improve water uptake and proton conductivity for fuel cell application [203]. Nafion/organic silica modified TiO_2 composite membrane was prepared by in situ sol–gel method for Vanadium redox flow battery [204]. Liu et al. prepared TiO_2 nano crystals in the nafion by hydrolysis of varying concentration of lower titanium alkoxide for photo catalytic applications [205]. Watanabe et al. modified Nafion by the incorporation of hygroscopic oxides such as SiO_2 and TiO_2 to increase water uptake [176,208]. They were prepared by casting from a Nafion solution with TiO_2/SiO_2 colloids prepared by the hydrolysis of Titanium/Si tetraisopropoxide. Thampan et al. modified Nafion by the incorporation of hygroscopic oxides or inorganic solid acids such as ZrO_2/SO_4 [209]. Malhotra et al. incorporated inorganic solid acids (such as heteropolyacids) in Nafion for improving water retention as well as providing additional acidic sites [210]. Mauritz et al. and Adjemian et al. introduced nanosized SiO_2 into pores of Nafion by in situ sol-gel method [211,212]. Krishnan et al. prepared CdS in Nafion by incorporating Cd^{2+} in the membrane by ion exchange followed by exposing the membrane to H_2S [213]. Similarly Rollins et al. prepared Ag_2S nanoparticles in nafion in silver form by reaction of Na_2S [186]. Sun et al. and Sachdeva et al. prepared silver nanoparticles in Nafion by borohydride reduction of silver form of Nafion [184,189]. Watanabe et al. synthesized platinum nanocrystallites, dispersed in the Nafion membrane, by the cation exchange treatment of Nafion with a $[Pt\ (NH_3)_4]\ Cl_2$ followed by reduction with hydrazine [176,208]. Ramon et al. synthesized bimetallic Ag–Au nanostructures homogeneously distributed on Nafion membranes by galvanic substitution reaction of silver island deposition on to the Nafion films [206].

Synthesis of nanocomposite membranes either by casting a bulk mixture of powder or colloidal state of inorganics with a polymer solution or in-situ formation of inorganic particles utilizing the membrane as template is very promising [212]. The advantage of in-situ method is that the particle size and dispersion of these solid particles can be controlled by the concentration of precursors. More often, the sizes of nanoparticles formed in the matrix of Nafion are much larger than the size of water clusters (4-5 nm) present in it [184,186,189,203-207]. Recently, Ag nanocubes have been synthesized by adenosine-5’-triphosphate (ATP) mediated reduction of Ag^+ ions in the Nafion membrane [214]. The results so far seem to suggest that the shape and size of nanoparticles in Nafion may not be dependent only on the dimensions of water clusters.

The synthesis of metal nanoparticles generally involves transfer of the desired metal ions by the ion-exchange process to the membrane matrix and subsequent reduction of metal ions by appropriate reductant in the membrane matrix [184,186,206,207]. The reductant plays an important role in the spatial distribution of metal nanoparticles in the ion-exchange membrane. Nafion is a cation-exchange membrane and, therefore, the anionic reductant would not enter in bulk matrix of the membrane due to “Donnan exclusion”. Wang et al. have observed that CdS nanoparticles in the Nafion membrane were confined to surface when Na_2S was used as a precursor [185]. Contrary to this, the CdS nanoparticles in Nafion have been found to be uniformly distributed across thickness of the membrane when thioacetamide used as a precursor. This has been attributed to the fact that non-ionic thioacetamide could diffuse into the cation-exchange membrane much more uniformly [185]. It has also been reported that the Ag nanoparticles formed in Nafion-117 membrane by reduction with BH_4^- ions were located mostly to a few μm surface layer of the membrane [189].

The transport properties of the Nafion-117 membrane were not found to be affected by the formation of Ag nanoparticles by BH_4^- ions reduction [189]. However, the proton conductivity was decreased significantly when SiO_2 nanoparticles were formed in matrix of the Nafion-115 membrane [215]. This indicates that the tortuosity of diffusion channels (three dimensional network connecting water swollen clusters) in membrane increases by incorporation of nanoparticles in the matrix.

In this chapter, the synthesis of nanoparticles by *in situ* chemical reduction of metal (Ag^+ & Rh^{+3}) ions in Nafion-117 membrane with borohydride (BH_4^-), formamide ($HCONH_2$), and dimethyl formamide ($HCON(CH_3)_2$), as reductant, have been studied. Formamide and dimethyl formamide (DMF) are non-ionic and can invade the membrane matrix [216-219].

The fraction of Ag^+ ions loaded in the membrane, that has been reduced, have been quantified using radiotracer. Shape, size, and spatial distribution of nanoparticles have been obtained by transmission electron microscopic (TEM) analyses of the cross-section of membrane samples. The membrane morphology strongly influences diffusion mobility of the counterions. Therefore, the self-diffusion coefficients of different valence counterions (Na^+, Cs^+, and Eu^{3+}) in the nanoparticles embedded membrane have been measured to understand the effects of inclusion of nanoparticles on diffusion mobility of the counterions.

2.2. Experimental

2.2.1. Reagents and apparatus

Analytical grade chemicals ($NaNO_3$, $AgNO_3$, $CsNO_3$, Eu_2O_3, $NaBH_4$, DMF, and formamide) from BDH (Poole, England) and deionized water (18 MΩ.cm) purified by model QuantumTM from Millipore (Mumbai, India) were used throughout the studies. Nafion-117 ion-exchange membrane with an equivalent weight of 1100 and thickness of 178 µm (Ion Power Inc.) was used after conditioning. The membrane samples were preconditioned by boiling in conc. HNO_3 for 3-4 h. to remove organic impurities introduced during manufacturing process. It was followed by washing and boiling the membrane samples in distilled water for one hour. Subsequently, the membrane samples were equilibrated with 0.5 mol L^{-1} NaOH and 0.5 mol L^{-1} HCl at room temperature (27 °C) for converting the membrane into the proton form [33,220]. Radiotracers ^{22}Na, ^{137}Cs, and ^{110m}Ag were obtained from the Board of Radiation and Isotope Technology, Mumbai, India. Radiotracer ^{154}Eu was prepared by irradiating known amount of Eu_2O_3 (having 99.1 % enriched ^{153}Eu obtained from Euriso-top, France) for appropriate time in Dhruva reactor at BARC, Mumbai, India. ^{154}Eu radiotracer solution was prepared by dissolving the irradiated Eu_2O_3 in concentrated HCl and evaporating it to near dryness. The acidity of stock solution of ^{154}Eu was adjusted to pH = 2 for preventing any hydrolysis during the period of storage. The γ-activity of ^{22}Na, ^{137}Cs,

^{110m}Ag, and ^{154}Eu in the membrane was monitored by a well-type NaI(Tl) detector connected to a multi-channel analyser. All the samples and standard containing radioactivity were counted in identical sample-detector geometry. The thickness of the membrane samples was measured using a digital micrometer (Mitutoyo, Japan) with a precision of ± 0.001mm.

2.2.2. Preparation of the nanoparticles

The conditioned membrane sample (2×2 cm) in Na^+ form was equilibrated with 25 mL of 0.25 mol L^{-1} of $AgNO_3$ solution to convert it into Ag^+ form. The Na^+ ions tagged with ^{22}Na radiotracer were used to study the quantitative replacement by Ag^+ ions. It was observed that > 98% of Na^+ ions in membrane was replaced by the Ag^+ ions from aqueous solution having 0.25 mol L^{-1} $AgNO_3$. Similarly the membrane was converted to Rh^{+3} from by ion exchange process. The metal ion loaded membrane samples were reduced by equilibrating it with 15 mL of reductant at fixed temperature for a known period of time with constant stirring. $NaBH_4$ (0.2 mol L^{-1}), formamide, and DMF were used as reductant. For formamide and DMF reduction, fully Ag^+ ions loaded samples were used. In case of BH_4^- reduction, the amount of Ag^+ ions was kept 15% of ion-exchange sites by equilibrating fully Ag^+ ions loaded membrane samples in the well-stirred 0.25 mol L^{-1} $NaNO_3$ for 45 s as described elsewhere [189]. Rh^{+3} loaded nafion membrane was reduced with formamide at 65^{o}C for 30 min.

After reduction, the membrane samples were thoroughly washed with water and equilibrated with $NaNO_3$ (0.25 mol L^{-1}) to remove unreduced metal ions, if any, from the membrane matrix.

2.2.3. Characterization

2.2.3.1. UV-Vis spectroscopy

Ag nanoparticles gives color due to surface plasmon resonance of electrons. UV-Vis spectra of Ag nanoparticles embedded membrane samples were recorded using UV-Vis Spectrophotometer (V-530, JASCO, Japan). The absorbance measurements were carried out by mounting the sample (1x2 cm) on to the inside wall of a (1x1x3 cm) quartz cell and placing it in a spectrophotometer to record spectrum with respect to air.

2.2.3.2. TEM

For TEM analyses of cross-section of membrane, the membrane samples were sectioned under cryogenic conditions in Leica ultramicrotome to 70 nm thickness. The sections were picked on 200 mesh Cu grids. The grids were examined in an FEI Technai G2 electron microscope in IIT Bombay [Central Facility at SAIF], Mumbai at 120 KeV without any staining or post-treatment. The sizes of nanoparticles were measured manually using the image analyser software (Image Z, version 1.33 U). The size distribution was obtained from 5-8 images obtained by TEM of samples from different locations of the membrane.

2.2.3.3. Determination of fractional conversion of Ag^+ ions to nps

In order to quantify Ag^0 content after the reduction of membrane, the membrane samples (2 x 2 cm pieces) were equilibrated with 0.1 mol L^{-1} $AgNO_3$ stock solution containing known activity of ^{110m}Ag radiotracer for 24 h. After equilibration, the membrane samples were thoroughly washed with de-ionized water to remove equilibrating solution clinging to the surface of the samples. These samples were subjected to reduction as described above. Post reduction, the membrane samples were equilibrated with 0.25 mol L^{-1} $NaNO_3$ for 30 min to remove un-reduced Ag^+ ions. This ensured that ^{110m}Ag radioactivity in the samples represent only content of Ag^0 and not Ag^+ ions, if any. The membrane samples were counted before and after reduction in a well type NaI(Tl) detector to monitor the γ-activity of ^{110m}Ag in the membrane samples. The percentage of Ag^+ ions reduced to Ag^0 in the sample was obtained as:

$$Ag^0 \text{ (\% of ion exchange sites)} = A_{(f)}/A_{(b)} \times 100 \qquad (2.1)$$

where $A_{(f)}$ and $A_{(b)}$ are the γ-activity of ^{110m}Ag before and after reduction followed by equilibration with $NaNO_3$, respectively.

2.2.3.4. Ion exchange capacity

Ion exchange capacity of membrane is defined as the number of equivalents of counter ions present in per unit mass of membrane. The total exchangeable sites (IES, in moles) available in the membrane samples (1 x 2 cm pieces) were measured by equilibrating them for 24 h with 0.05 mol L^{-1} NaCl stock solution containing known activity of ^{22}Na. After equilibration, the membrane samples were thoroughly washed with deionized water to remove equilibrating solution clinging to the surface of the samples. Filter paper standards were prepared by taking pieces of filter paper of the same dimensions (1 x 2 cm) as the membrane samples and adding known volume (50, 100 and 200 μL) of the radiolabeled 0.05 mol L^{-1} NaCl stock solution. NaCl stock solution used for preparing standard samples contained same ^{23}Na (natural) to ^{22}Na (radioactive) ratio as the solution used for equilibrating the membrane samples. Each standard was prepared in duplicate. The soaked filter papers were dried at room temperature and counted in a well type NaI(Tl) detector in a similar counting geometry as the membrane samples. The amount of Na^+ ion in the membrane sample was obtained by comparing the γ-activity of ^{22}Na in the membrane samples with filter paper standards as given below:

$$\text{Ion Exchange capacity} = \frac{A_{(\text{mem})}}{A_{(\text{std})}} \times \frac{M_{(\text{std})}}{W_{mem}} \tag{2.2}$$

where $A_{(\text{mem})}$ and $A_{(\text{std})}$ are ^{22}Na γ-radioactivities (counts min^{-1}) in membrane sample and standard, respectively. $M_{(\text{std})}$ is moles of Na^+ in the standard and W_{mem} is the weight of the membrane.

2.2.3.5. Water-uptake capacity

The water uptake capacity and dimensional changes after the reduction of the membrane samples were also measured. The water uptake capacity of the membranes, defined as the amount of water absorbed per unit dry weight of the membrane, was obtained from the difference in weight of wet and vacuum dried membrane samples in appropriate ionic form.

For measurements of water uptake capacity, the membrane samples were equilibrated with 0.25 mol L^{-1} relevant salt solution for 24 h. The water uptake capacity of the membranes was determined by using the following equation:

$$\text{Water uptake capacity (\%)} = \frac{(W_{\text{wet}} - W_{\text{dry}})}{(W_{\text{dry}})} \times 100 \qquad (2.3)$$

Where, W_{wet} is the weight of the wet membrane sample and W_{dry} is the weight of the same membrane sample dried under vacuum.

2.2.3.6. EDXRF analyses

Energy Dispersive X-ray Fluorescence (EDXRF) measurements of membrane samples were carried out using Total Reflection X-ray Fluorescence Spectrometer IX-2000 provided with EDXRF geometry (ITAL STRUCTRES, Italy). W L_α (8.398 keV) radiation was used as excitation source for EDXRF measurements.

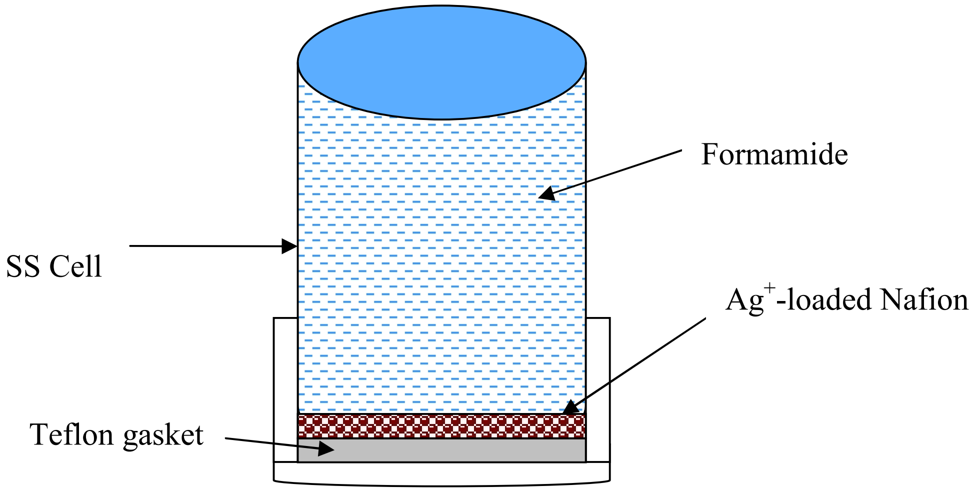

Fig. 2.2 *Arrangement for dead end cell experiment*

2.2.4. Dead end cell experiment

In order to study the penetration of reducing agent formamide across the thickness of membrane, the Ag$^+$-loaded membrane was exposed to formamide from one side in a dead end cell as shown in Fig. 2.2 for 24 hrs. After reduction, the membrane samples were equilibrated with the 0.25 mol L^{-1} $NaNO_3$ to ensure the removal unreduced Ag^+ ions from the membrane, if any.

2.2.5. Measurement of self-diffusion coefficients of the counterions

The self-diffusion coefficients of Na^+, Cs^+, and Eu^{3+} ions were obtained from analyses of the isotopic-exchange rate profiles as described in chapter 1, section 1.5.1 [33,34]. The measurements of isotopic-exchange rates of (M^{n+}=Na^+, Cs^+, and Eu^{3+}) were carried out using 2 x 2 cm pieces of the Nafion-117 membrane. The membrane samples in appropriate ionic forms were placed in 25 mL of respective equilibrating salt solution (0.25 mol L^{-1}) containing radioactivity tagged counterions. These radiotracer loaded membrane samples were again equilibrated with salt solution (0.25 mol L^{-1}) having same ions as the counterions in the membrane samples. The solution (at 25°C) containing membrane sample was stirred vigorously ($\approx$ 52 rad s^{-1}) to minimize the concentration gradient of counterions in the equilibrating solution. The amount of radiotracer counterions desorbed from the membrane sample was monitored by taking out the membrane sample from the equilibrating solution at regular time intervals. The membrane samples were washed with de-ionized water to remove traces of equilibrating solution adhering to its surface and then radioactivity in the membrane was counted with a γ-ray spectrometry in a fixed geometry. The membrane sample was again placed in the equilibrating solution after counting. The actual residence time of the membrane in the equilibrating solution was considered as time for the isotopic exchange of counterions.

2.3. Results and discussion

2.3.1. Formation of the metal nanoparticles

The formation of metal nanoparticles in the membrane matrix is a two steps process. First, the membrane samples have been loaded with M^{n+} ions by ion-exchange mechanism shown below:

$$n[\text{-R-SO}_3^-\text{H}^+]_{mem} + [\text{M}^{n+}]_{aq} \rightleftharpoons [(\text{-R-SO}_3^-)_n\,\text{M}^{n+}]_{mem} + n[\text{H}^+]_{aq} \quad (2.4)$$

Next metal ions in the loaded membranes have been reduced using a reducing agent. For formamide reduction, reaction is shown below:

$$2[(\text{-R-SO}_3^-)_n\,\text{M}^{n+}]_{mem} + n[\text{HCONH}_2]_{aq} + n[\text{H}_2\text{O}]_{mem} \rightleftharpoons$$
$$n[\text{NH}_2\text{COOH}]_{aq} + 2n[\text{-R-SO}_3^-\text{H}^+]_{mem} + 2n[\text{M}^0]_{mem} \quad (2.5)$$

The conversion of metal ion to its zero valent state in the membrane matrix is highly dependent on nature of the reductant as well as on the ion-exchange process operating during the reduction. Formamide and DMF are non-ionic reductants and the membrane matrix is swelled in them. They are, therefore, expected to invade the interior of Nafion-117 membrane.

In the case of Ag^+ ions, the reduction process occurring in the membrane matrix has been studied by tagging Ag^+ ions with ^{110m}Ag radiotracers and results of this study are summarized in the Table 2.1. It has been observed that the rate of formation of Ag nanoparticles in the membrane is quite slow with DMF at room temperature. The membrane sample has started dissolving on increasing the temperature of DMF and hence formamide has been used for reduction of Ag^+ ions in the membrane. The rate of formation of Ag nanoparticles has increased when formamide is used as reducing agent. As shown in Table 2.1, the amount of Ag nanoparticles formed with both formamide and DMF at room temperature are 2-3% of Ag^+ ions loaded in the membrane samples. This is due to loss of Ag^+ ions from the membrane sample to reducing solution as colour of reducing solution has been also changed. In order to increase the reduction rate as well as amount of Ag nanoparticles in the membrane, the Ag^+-loaded membrane samples have been equilibrated with formamide at 40°C and 65°C. It is evident from the Table 2.1 that the formation of nanoparticles has enhanced considerably on increasing the temperature i.e. 16 % of Ag^+ ions present in the ion-exchange sites have been converted to Ag^0 within 15 min at 65°C. The amount of Ag^0 formed in the membrane during reduction with formamide at 65°C has been found reproducible within ±1% in five experiments. Unlike formamide and DMF reduction, the reduction of Ag^+-loaded membrane samples with BH_4^- ions is quite fast and quantitative. 15% Ag^+ ions loaded membrane samples, prepared by controlled by desorption of Ag^+ ions from ion-exchange sites of the membrane with Na^+ ions [189], are reduced by BH_4^- ions. Nearly 94 % of Ag^+ ions present in the membrane have been converted to Ag^0 within 5 min.

The ion-exchange capacity of the membrane has not changed significantly after reduction of Ag^+ ions in the membrane. After reduction with BH_4^-, the dimensions of the membrane have not changed significantly. However, the area of the membrane has reduced after formamide reduction and increased by 5-8 % after DMF reduction of the membrane. The thickness of the membrane has changed corresponding to change in the area. Similarly, Rh nanoparticles have been prepared in Nafion by the reduction of Rh^{3+}-loaded membrane with formamide at 65°C for 30 min.

2.3.2. Size and spatial distribution of Ag nps

The size and spatial distributions of Ag nanoparticles have been studied by ultra-thin sectioning of the cross-section of membrane samples reduced with BH_4^-, DMF at room temperature, and formamide at 65°C. The choice for these samples are based on the fact that Ag^+ reduction rates in these cases are slowest and fastest as given in Table 2.1 and also they represent ionic and non-ionic reductants. The TEM analyses of the cross-section of the membrane samples are given in Figs. 2.3-2.5 and the results of statistical analyses of TEM micrographs are summarized in Table 2.1. It is seen from Table 2.1 that size distributions of Ag nanoparticles in the samples varied significantly depending upon the reducing conditions. It is clear from the TEM micrographs analyze that the shape of Ag nanoparticles is nearly spherical in all the cases.

Table 2.1 *Results of the reduction of Ag^+ ions in Nafion-117 membrane with different reducing agents.*

Reducing Reagent	Temp. (°C)	Equilibration Time	Amount of Ag^+ reduced (%)	Average size (nm)
$HCON(CH_3)_2$	25	7 days	2-3	5±1 & 18±5
$HCONH_2$	25	24 h	3	-
$HCONH_2$	40	30 min	7	-
$HCONH_2$	65	15 min	16	9±2
BH_4^-	25	5 min	94	15±4

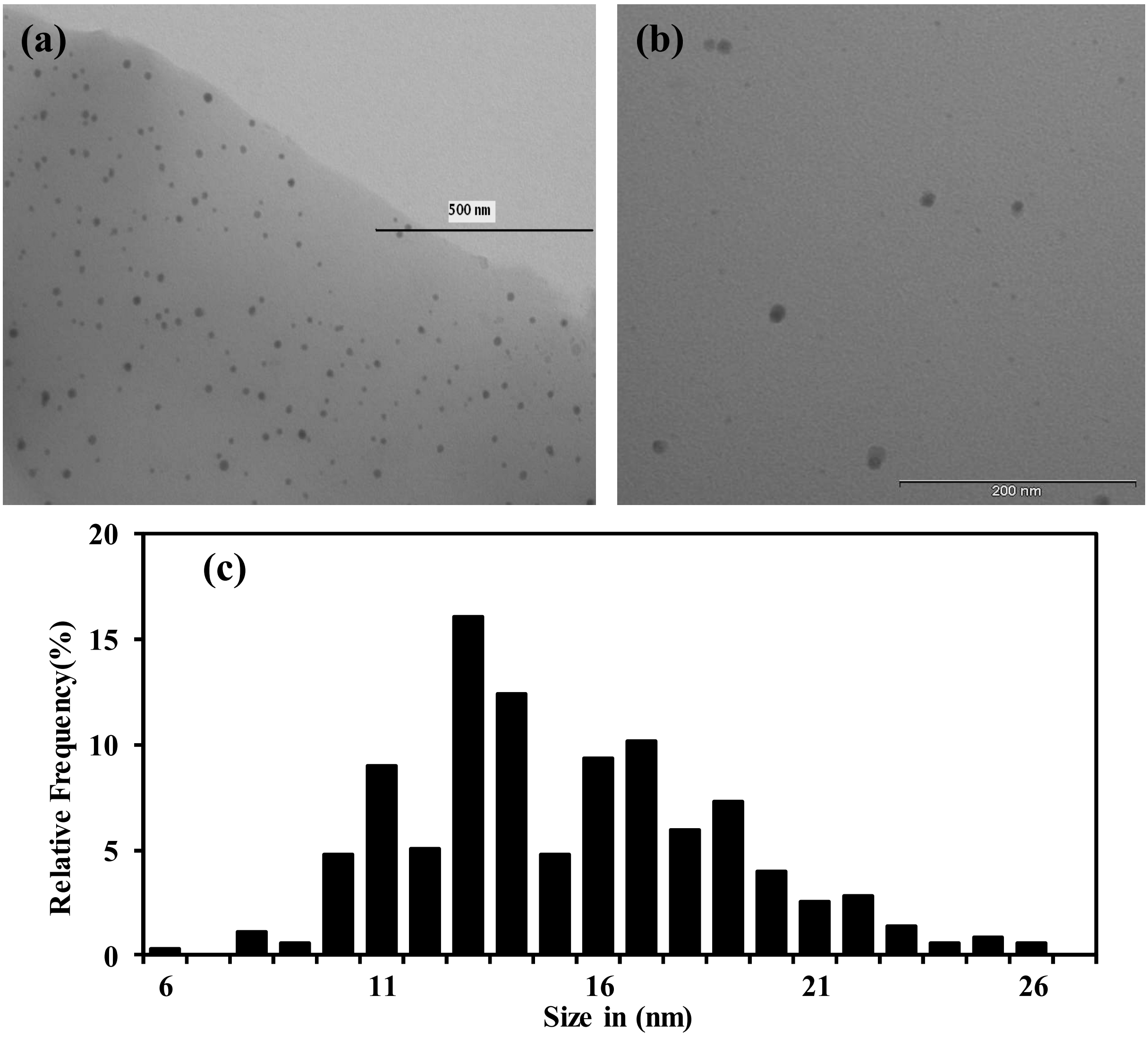

Fig. 2.3 *TEM analyses of Ag nanoparticles in BH_4^- reduced membrane samples. (a) Ag nanoparticles distributions at the surface, (b) Ag nanoparticles distributions in the interior, & (c) statistical analysis of Ag nanoparticles.*

As can be seen from Fig. 2.3(a & b), the Ag nanoparticles are mostly located at the surface of the BH_4^- ions reduced membrane samples. Sachdeva et al. showed that Ag nanoparticles, formed by reduction with BH_4^-, were mostly positioned at the surface layer of the membrane [189]. This is due to inability of BH_4^- ions to invade interior matrix of the cation-exchange membrane. However, few Ag nanoparticles are observed throughout the matrix of membrane. In present experiment, 0.2 mol L^{-1} concentration of $NaBH_4$ solution is used. This concentration is high enough to produce leakage of BH_4^- ions in the matrix of membrane [221-223]. This, in turn, reduces some amount of Ag^+ ions in the bulk matrix. The average size of Ag nanoparticles in this sample is found to be 15 nm, which is close to 13.4 ± 2.2 nm reported by Sun et al. for Ag nanoparticles formed by BH_4^- reduction in Nafion-117 membrane under similar conditions [184].

The TEM of cross-section of membrane samples reduced with DMF under ambient conditions does not also show uniform distribution of Ag nanoparticles. It is seen from Fig. 2.4(a) & 2.4(b) that the Ag nanoparticles are slightly more concentrated at the surface of the membrane than the bulk matrix. The statistical analysis given in Fig. 2.4(c) indicated that there was a bimodal size distribution of Ag nanoparticles. The smaller nanoparticles are in significantly larger number having 5 nm size and bigger nanoparticles (18 nm) are lesser in number but dispersed throughout the matrix. DMF is a mild reducing agent and require 7 days to form 2-3 % nanoparticles in the membrane matrix. As DMF swells Nafion membrane readily, the physical structure of the membrane changes continuously during reduction from water swollen membrane having water cluster-channel network to that corresponding to DMF swollen homogenous membrane. Swelling and ion-exchange processes operating during prolong equilibration with DMF seems to be responsible for non-uniform bimodal size distribution in the membrane matrix. It appears that bigger nanoparticles have been formed

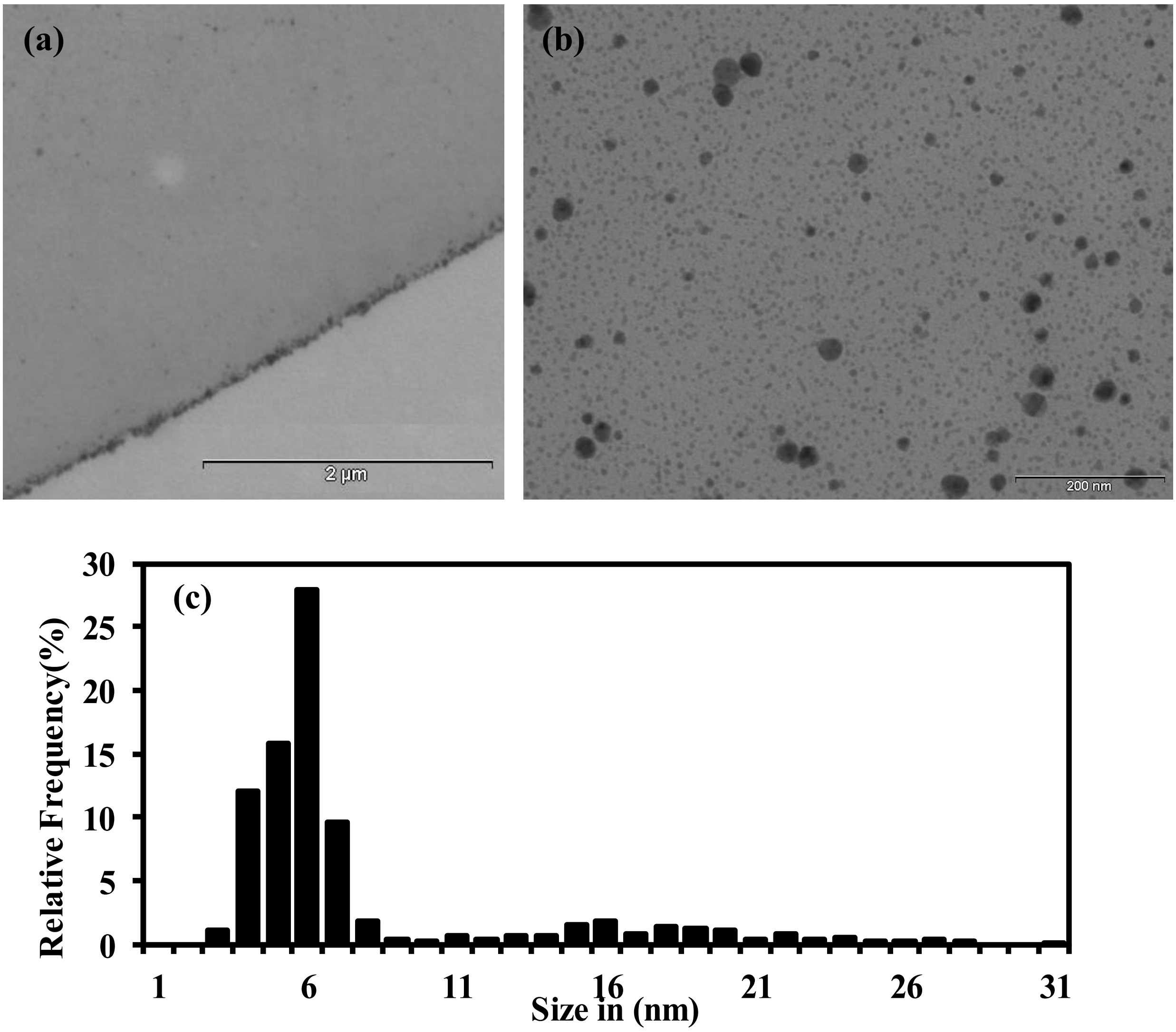

Fig. 2.4 *TEM analyses of Ag nanoparticles in DMF reduced membrane samples. (a) Ag nanoparticles distributions at the surface, (b) Ag nanoparticles distributions in the interior, & (c) statistical analysis of Ag nanoparticles.*

during initial reduction of Ag^+ nanoparticles in membrane sample still containing water cluster-channel network structure. This was based on the fact that the size of bigger nanoparticles (18 nm) is comparable to that of the Ag nanoparticles (15 nm) formed by BH_4^- reduction in the membrane. As reduction time progress, the swelling of membrane samples with DMF would destroy the cluster-channel network structure. This would lead to the homogeneous matrix that might restrict the growth of nanoparticles to a smaller size. The radiotracer studies indicate that there is considerable loss of Ag content from the membrane sample to equilibrating DMF solution. H^+ ions formed during reduction occurring both in membrane matrix and DMF solutions would displace Ag^+ ions from the ion-exchange sites at interior of membrane to the surface leading to slightly higher reduction at the surface of membrane as seen in Fig. 2.4(a).

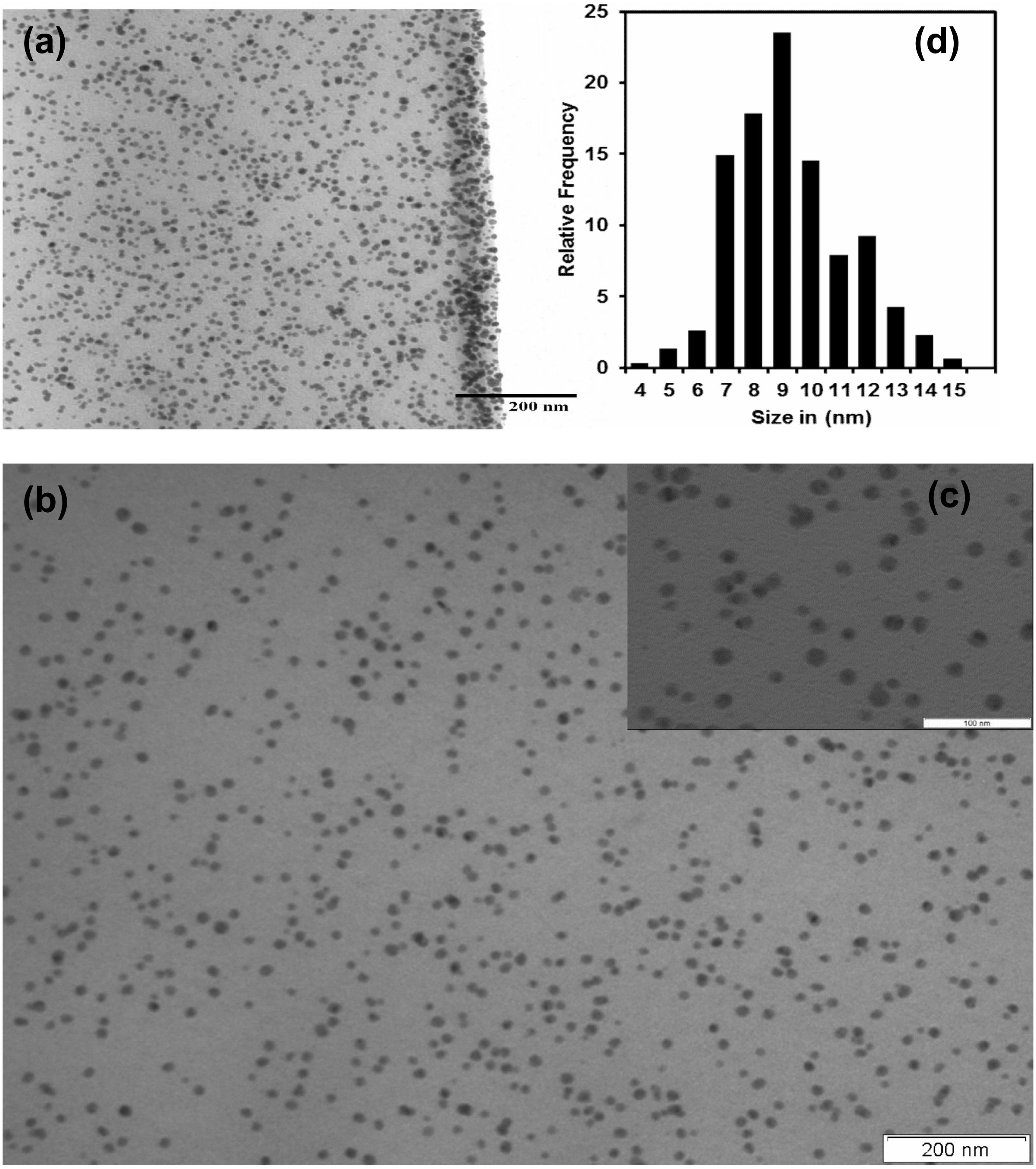

Fig. 2.5 *TEM analyses of Ag nanoparticles in formamide reduced membrane samples. (a) Ag nanoparticles distributions at the surface, (b) Ag nanoparticles distributions in the interior, (c) enlarged view of b, & (d) statistical analysis of Ag nanoparticles.*

It is seen from Fig. 2.5(a, b, & c) that the Ag nanoparticles of average size 9 nm are uniformly distributed across the thickness of membrane sample reduced with formamide at 65^{o}C with constant stirring. This indicates that fast reduction produced nanoparticles uniformly throughout the membrane. However, the sizes of Ag nanoparticles are considerably higher than the expected size of water cluster (4-5 nm) in Nafion-117 membrane [109,224]. The number of Ag^+ ions in any of the initial water domains is small. In a typical hydrophilic domain of 4-5 nm there may not be more than 100 cations. So reducing all the Ag^+ ions in that domain would produce Ag nanoparticles that would have ~ 1 nm size. The particles observed are ≈ 10-15 times larger. There is a possibility that the Ag^0 atoms form adjacent clusters may be diffusing fairly rapidly to the site of seeding. The growth of Ag nanoparticles leads to strain at different location along the cluster where seeding of nanoparticles has occurred. Due to this strain, a point comes when the cluster cannot take further strain and either the channel structure is disrupted or the silver nps is excluded out of the channel due to rearrangement of physical structure by hydration forces. It is known that the Nafion-117 membrane rearrange its physical structure depending upon the pretreatment conditions and counterions [33].

2.3.3. Characterization of the reduced samples

The variation of intensity of surface plasmon absorption bands (SPB) of nanoparticles as a function of reduction time in a well stirred formamide at 65^{o}C has been studied. It is seen form UV-Vis spectra given in Fig. 2.6 that the intensity of SPB was quite high though only 15-16 % of Ag^+ ions present in the ion-exchange sites of membrane sample was converted to Ag nanoparticles. In order to study the penetration of reducing agent formamide across the thickness of membrane, dead end cell experiment has been carried out. The EDXRF analyses of both the surfaces of membrane samples have been carried out. The EDXRF spectra are shown in Fig. 2.7. It is seen from the comparison of the EDXRF spectra that the Ag content

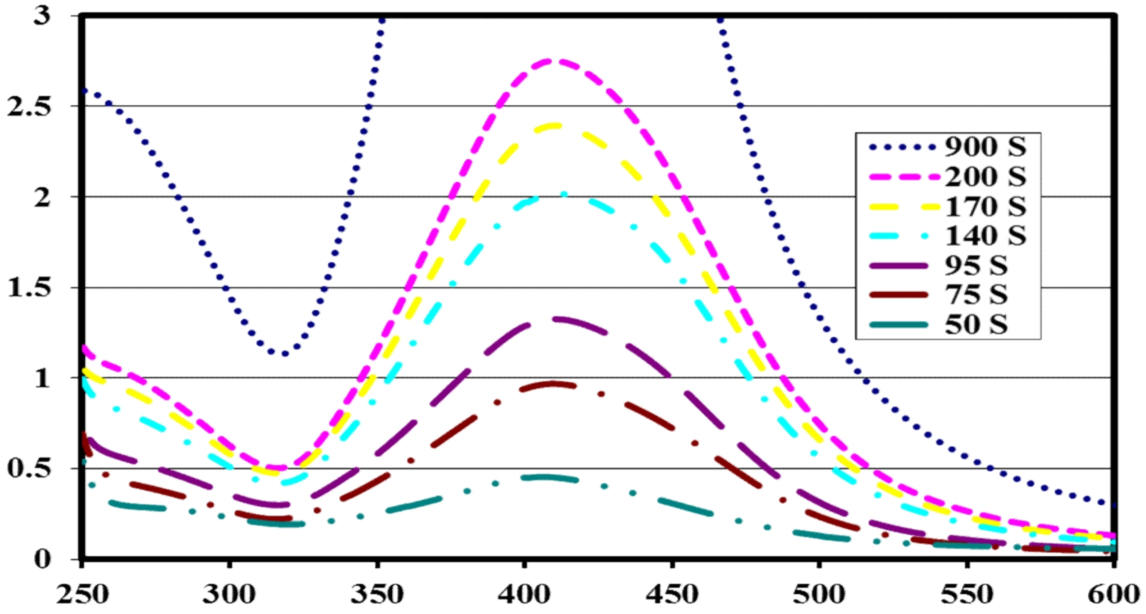

Fig. 2.6 *Variation of UV-Vis spectra corresponding to growth of Ag nanoparticles as a function of equilibration time of Ag$^+$-loaded membrane sample in well-stirred formamide solution at 65 °C.*

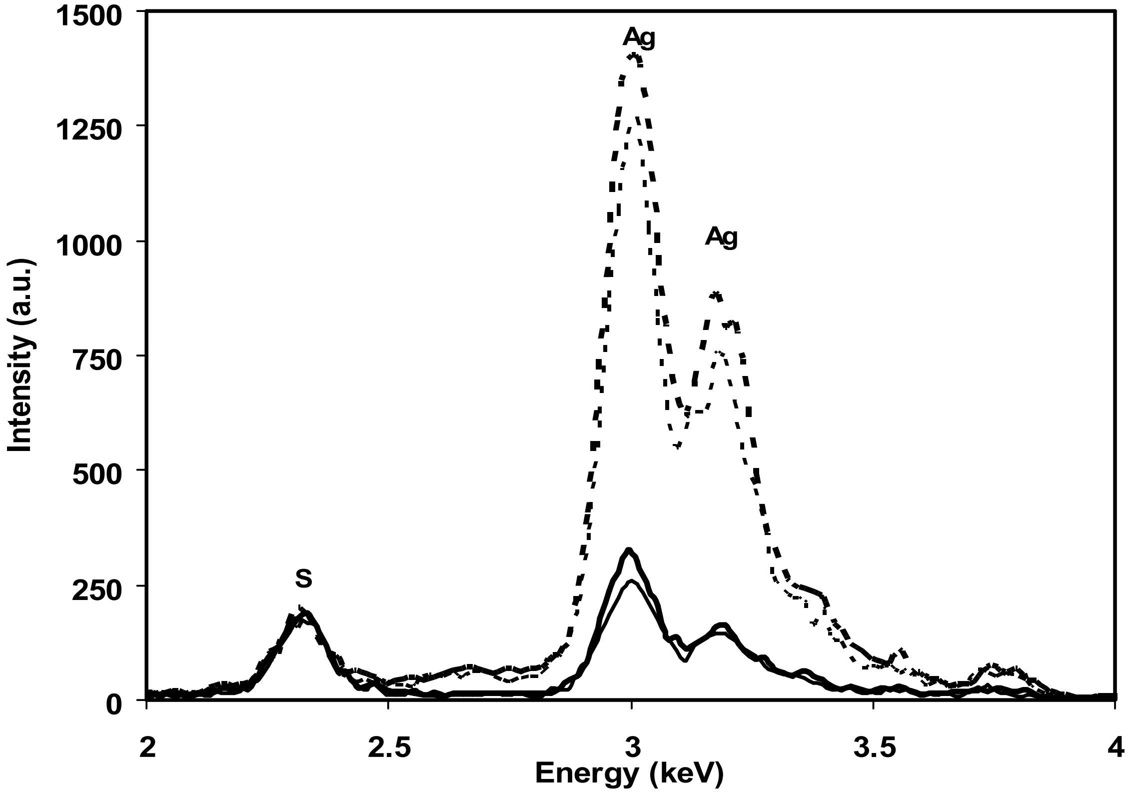

Fig. 2.7 *Comparison of EDXRF spectra of both the surfaces of Ag$^+$-loaded membrane samples before reduction (broken lines) and after reduction (solid lines) with a formamide at 65 °C.*

in membrane decreased considerably after reduction but the intensity of S K_α peak has not changed. As intensities of S K_α peak representing -SO_3 groups are same, the lower intensity of Ag in the reduced sample with that in nascent sample has been attributed to loss of Ag^+ ions during reduction process. However, the distributions of Ag contents on both the surfaces of the dead end cell reduced membrane sample have been almost same. This indicated that formamide could diffuse to unexposed side of membrane and reduced Ag^+ ions in bulk matrix of the membrane. In case of BH_4^- reduction under similar conditions, the Ag^+ ions have been found to reduce only on the side of the membrane that was exposed to the reductant [189].

2.3.4. Size and spatial distribution of Rh nps

TEM of the cross section of formamide reduced Rh^{+3} loaded membrane are shown in Fig. 2.8. It is evident from the TEM image given in Fig. 2.8 that the clusters containing Rh nanoparticles of size 2-4 nm have been formed. It is seen in TEM image given in Fig. 2.8(a & b) that the most of Rh nanoparticles aggregated in the clusters throughout the matrix. The fractal dimension (D) of the two dimensional cluster has been calculated by the power law relationship between no. of particles and radius, $N(r) \propto r^D$ where r is the radius of the searching circle assuming the centre of mass of the cluster as the origin. The fractal dimension of cluster has been found to be 1.8 (Fig. 2.8 c). It has been reported that the self-diffusion mobility of the trivalent counterions in the Nafion-117 membrane is quite slow [35,225]. This would lead to the reaction-limited as well as diffusion limited aggregation of Rh atoms. This would produce fractals normally observed in diffusion controlled growth of crystals [226-229]. However, the exact reason for the formation of clusters in the membrane matrix could not be understood.

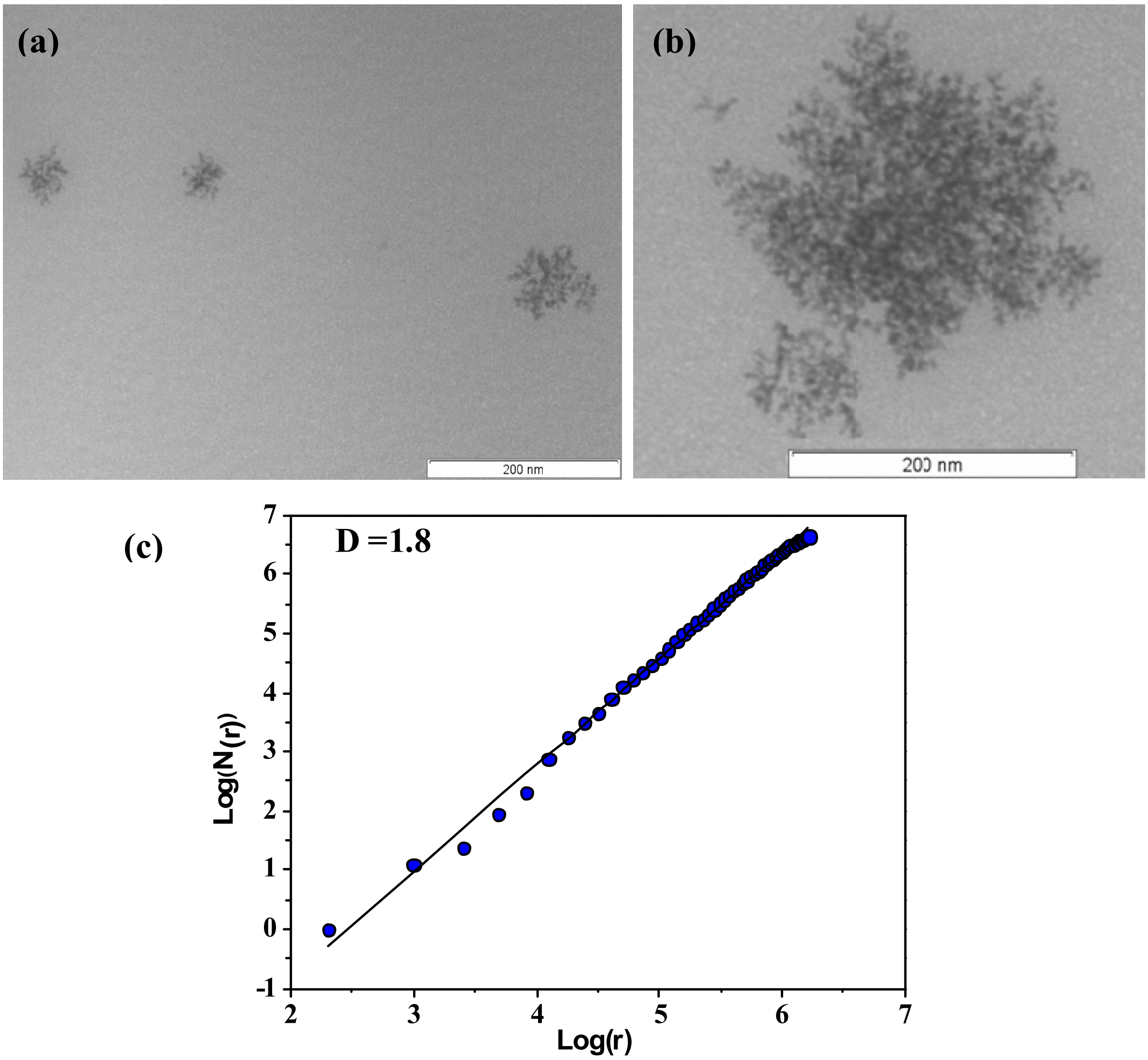

Fig. 2.8 *a)TEM image showing cross-section of membrane containing Rh cluster formed by in situ reduction of* Rh^{3+} *ions in the membrane with formamide at* $65^{o}C$*, (b) enlarged view of a, and (c) plot for fractal dimension.*

2.3.5. Self-diffusion coefficients of the counterions

The self-diffusion of ions in a homogeneous medium is due to continuous random motions that give rise to a definite probability of their arrival at some point within a given time. The precise information about the matrix effect on mobility of the ions can be obtained from the self-diffusion coefficient of the ions. Self-diffusion coefficients of ions in ion-exchange membranes provide information about the physical as well as the electrostatic interactions between the fixed charged sites and the diffusing ions [225]. In order to study the effects of formation of nanoparticles on the membrane marphology and matrix, the isotopic-exchange rate profiles of Na^+, Cs^+, and Eu^{3+} counterions have been measured in the Ag nanoparticles embedded membrane samples formed by reduction with formamide at 65°C. The choice for this membrane sample was based on the fact that Ag nanoparticles are uniformly dispersed in it. The self-diffusion coefficients of Na^+, Cs^+, and Eu^{3+} counterions have been measured as Na^+ and Cs^+ ions lead to extreme of water contents in the membrane (see Table 2.2), and Eu^{3+} ions represent higher valence counterions.

Table: 2.2 *Effects of Ag nps formation on the water uptake capacity and the self-diffusion coefficients (D) of the counterions in nascent Nafion-117 membrane and Ag nps dispersed Nafion-117 membrane formed after reduction at 65 °C.*

Ionic form	**Water uptake (wt. %)**		**D (x 10^{-6} cm^2 s^{-1})**	
	Without Ag nps	**With Ag nps**	**Without Ag nps**	**With Ag nps**
Na^+	17.2^a	18±1	1.03±0.04^a	1.06±0.03
Cs^+	8.2^a	10±1	0.194±0.007^a	0.38±0.04
Eu^{3+}	13.2^b	15±1	0.045±0.005^b	0.22±0.01

a: taken from Ref. 24; b: taken from Ref. 29, c: average of three experiments

The profiles of isotopic-exchange rate of $^*Na^+_{(mem)} \rightleftharpoons Na^+_{(aq)}$, $^*Cs^+_{(mem)} \rightleftharpoons Cs^+_{(aq)}$, and $^*Eu^{3+}_{(mem)} \rightleftharpoons Eu^{3+}_{(aq)}$ (* represents radioactivity tagged ions) isotopic exchanges were analysed by using an analytical solution of Fick's second law described in chapter 1, section 1.5.1 [33-35]. The equation 1.5 was used for deducing self-diffusion coefficients from isotopic-exchange rate profile. The variation of the fractional attainment of isotopic-exchange equilibrium F(t) as a function of square root of equilibration time $t^{1/2}$ for the Ag nanoparticles embedded membrane samples with the different counterions are shown in the Fig. 2.9. It is evident from the figure that the $F(t_k)$ varies linearly with $t^{1/2}$ during initial stages of the exchange process, which is a characteristics of the Fickian diffusion. The value of D has been obtained by a non-linear least-square fit of experimental profile with equation 1.5. The comparisons of experimental data point for the isotopic-exchange rate for Ag nanoparticles embedded membrane and calculated isotopic- exchange rate profiles for nascent membrane are shown in Fig. 2.9. The values of D, thus obtained are given in Table 2.2. It is seen from

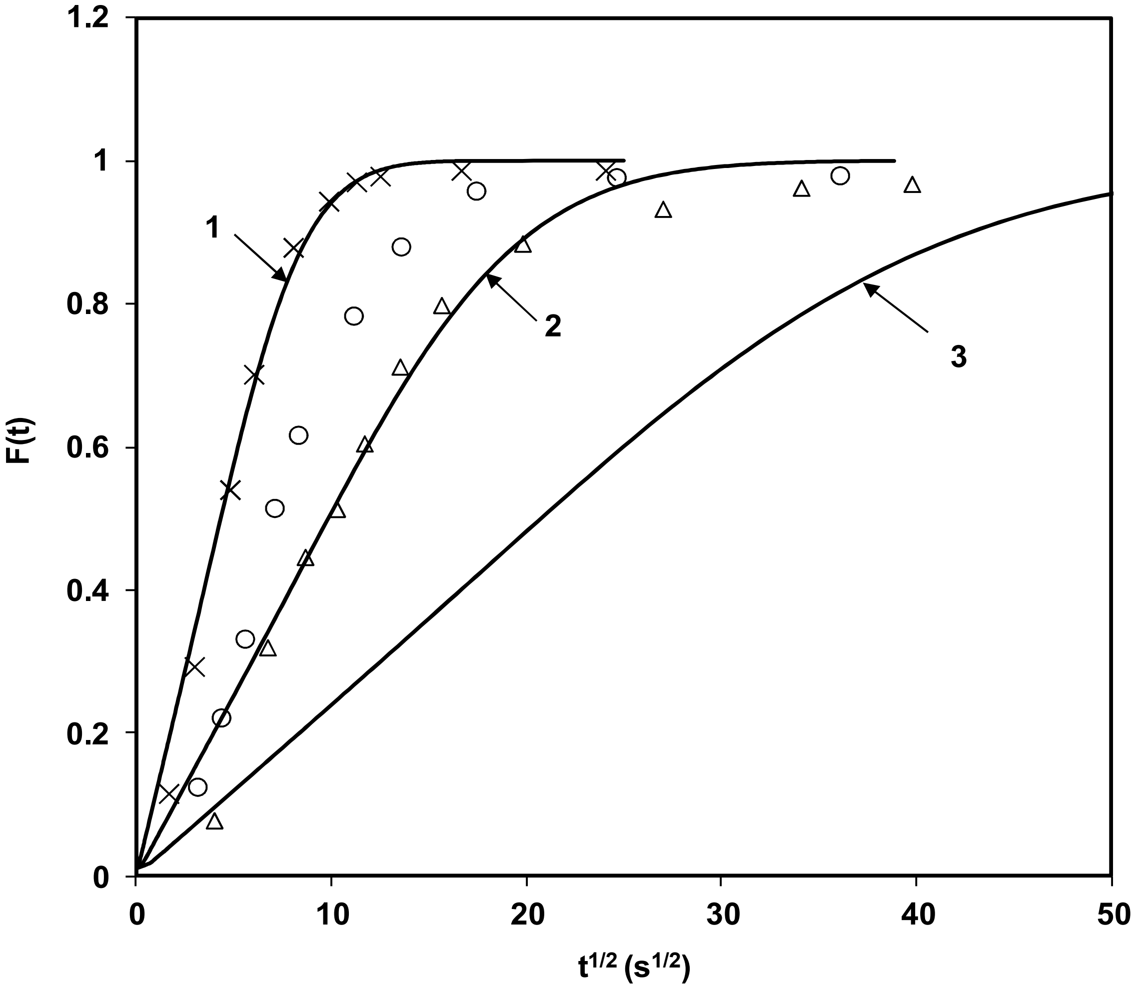

Fig. 2.9 *Fractional attainment of isotopic-exchange equilibrium (F(t)) as a function of square root of equilibration time t. The symbols x , o , and Δ represent* $^{*}Na^{+}_{(mem)} \rightleftharpoons Na^{+}_{(aq)}$, $^{*}Cs^{+}_{(mem)} \rightleftharpoons Cs^{+}_{(aq)}$, *and* $^{*}Eu^{3+}_{(mem)} \rightleftharpoons Eu^{3+}_{(aq)}$ *isotopic-exchange rate profiles between Ag nps embedded Nafion membrane in contact with a well stirred aqueous salt solution. The solid lines 1, 2, and 3 represent isotopic-exchange rate profiles of* Na^{+}, Cs^{+}, *and* Eu^{3+} *ions, respectively, calculated using self-diffusion coefficients of ions in the nascent Nafion-117 membrane and equation 1.5.*

experimental isotopic-exchange profiles shown in Fig. 2.9 that the Na^+-exchange profile in membrane is not affected by the formation of Ag nanoparticles in the membrane. However, the Cs^+ and Eu^{3+} exchange rates have been considerably enhanced in Ag nanoparticles embedded membrane as compared to that in nascent membrane.

As can be seen from Table 2.2, there is no significant difference in the D values of Na^+ and water contents in the nascent and Ag nanoparticles embedded membrane samples. However, there is a significant difference in the D values of Cs^+ and Eu^{3+} in the membrane samples with and without Ag nanoparticles. The value of D has increased 2 and 5 times for Cs^+ and Eu^{3+}, respectively, after the formation of Ag nanoparticles in the membrane. The water content in Cs^+ form of membrane has been found to increase from 8 wt.% to 10 wt.% on formation of Ag nanoparticles in the membrane by reduction with formamide at 65°C. Similarly water content in Eu^{+3} form of membrane has been increased from 13.2 wt.% to 15 wt.% due to the formation of Ag nanoparticles. It appears that the inclusion of Ag nanoparticles prevents the dehydration of membrane with least hydrated counterions like Cs^+ ions. It has been reported that increase in the water fraction of the Nafion-117 membrane, which leads to the morphological change, is reponsible for higher self-diffusion coeffceints of the counterions [33].

2.4. Conclusion

The present study indicated that the fast reduction of silver ions with non-ionic reductant produced Ag nanoparticles monodispersed throughout the bulk matrix of the Nafion-117 membrane. It has been achieved by increase in the reaction temperature and using formamide as reducing agent. Contrary to this, the anionic reductant BH_4^- produced Ag nanoparticles near the surface of the membrane due to Donnan exclusion of anions in the fixed negative charged membrane. DMF, being slow reductant, produced a bimodal distribution of nanoparticles throughout the membrane matrix. In case of slow moving ion Rh^{+3}, formation of fractal was observed. The diffusion properties of the membrane changed significantly when nanoparticles were uniformly dispersed in the membrane matrix. For example, the self-diffusion coefficients of the slow moving counterions like Cs^+ and Eu^{3+} increased significantly membrane samples. The inclusion of Ag nanoparticles in the membrane leads to the higher water content than the corresponding ionic form of the nascent Nafion-117 membrane. This, in turn, leads to higher diffusion mobility of less hydrated ions.

Chapter -3

Metal nanoparticles in Nafion by galvanic reaction

3.1. Introduction

There are many methods for *in situ* reduction of metal ions in the membrane such as reduction through ionic and non ionic reductants, UV reduction, and reduction by galvanic reaction. Compared to conventional reduction process, galvanic reduction process has advantage that no additional reducing agent is required. Galvanic replacement reactions of nano-scaled materials have been extensively investigated and developed in the recent decade. They are proved to be an effective approach to form various porous or hollow nanostructures with unique and attractive properties [230-233]. Nanostructures of active metals have been commonly used as sacrificial seeds and noble-metal ions with lower chemical activities compared with the seeds have been used as reactants to produce nanostructures of noble-metal.

Several attempts have been made to synthesized bimetallic, core- shell, hollow and porous nanostructures of noble metal using inexpensive transition metals as seeds by galvanic exchange reaction. Xia and co-worker have used the galvanic replacement reaction for synthesis of the hollow spheres, nanoboxes, nanorattles, multiple-walled nanoshells/nanotube and other hollow nanostructures of various noble metals such as Au, Pd, and Pt for the various applications [37,230-232,234-238]. Mohl et al. synthesized porous Au, Pt, and Pd nanorods via galvanic exchange reaction using Ni nanorods as a sacrificial template which were grown in porous alumina template by electrodeposition technique [239]. Li et al. prepared various Cu nanostructures by redox reaction using Zn nanowire as template and reducing agent [240]. Platinum nanoparticles catalyst supported on the surface of Mn_3O_4 nanoparticles were prepared for oxygen reduction reaction using galvanic reaction by Kim et al [241]. Galvanic reaction was used for dealloying of Cu from Cu-rich Pt−Cu alloys to form "core-shell" structure consisting of a Pt-Cu alloy core and Pt shell [242,243]. Khalavka et al. have synthesized rod-shaped gold nanorattles having hollow gold nanostructures with a solid nanorod inside by galvanic reaction for exploiting the advantages of nanorods with the high surface area of hollow structures [244].

There is an interesting possibility of synthesizing metal nanoparticles and their alloys by using the galvanic reaction of Ag nanoparticles embedded in Nafion membrane with the metal ions whose redox potential is more positive than the Ag^+/Ag pair. If this approach can be adopted for Nafion membrane, the process of formation of noble metal nanoparticles can be controlled in terms of shape, amount, and distribution by minimizing the role of ion-exchange process. Due to fixed negative charge sites (sulphonate groups), the anionic species like $AuCl_4^-$, $PdCl_4^{2-}$, and $PtCl_6^{2-}$ would not enter in bulk matrix of the Nafion-117 membrane due to "Donnan exclusion" of the co-ions. This makes syntheses of Au, Pd, and Pt nanoparticles in the matrix of Nafion-117 membrane complicated.

In present chapter, galvanic reactions of Hg^{2+}, Rh^{3+}, $AuCl_4^-$ and $PtCl_6^{2-}$ ions with spherical Ag nanoparticles embedded in the matrix of Nafion-117 membrane have been studied. Hg^{2+}, Rh^{3+}, $AuCl_4^-$, and $PtCl_6^{2-}$ ions are representative ionic species having different complexity and nanoparticles of these metals have many potential applications [245,246]. Ag nanoparticles in the host Nafion-117 membrane samples have been formed by in situ reduction of Ag^+ counterions with ionic (sodium borohydride) and non-ionic (formamide at 65°C) reagents. The reduction with BH_4^- ions leads to Ag nanoparticles (15±4 nm size) mostly positioned near the surface of membrane, while reduction with formamide at 65°C produces Ag nanoparticles dispersed uniformly in the membrane matrix with narrow size distribution (9±2 nm) [32,189].

3.2. Experimental

3.2.1. Reagents and apparatus

AR grade chemicals and deionized water (18 MΩ.cm, Gradient A-10 model, Milli-Q USA) were used in the present study. Nafion-117 ion-exchange membrane with an equivalent weight of 1100 and thickness of 178 μm (Ion Power Inc.) was used after conditioning as described in the chapter 2 section 2.2.1 [226]. Radiotracer ^{110m}Ag was obtained from the Board of Radiation and Isotope Technology, Mumbai, India.

The γ-activities of the radiotracers in the membrane and equilibrating solution were monitored by a well-type NaI(Tl) detector based gamma ray spectrometer. All the samples and standard containing radioactivity were counted in identical sample-detector geometry. The thickness of the membrane samples was measured using a digital micrometer (Mitutoyo, Japan) with a precision of ± 0.001mm.

3.2.2. Preparation of nanoparticles in membrane

The conditioned membrane samples (2×2 cm) were equilibrated with 25 mL of 0.25 mol L^{-1} of $AgNO_3$ solution to convert it in Ag^+ form. The Ag^+-loaded membrane samples were reduced by equilibration for a 30 min with 15 mL of formamide at 65°C temperature with a constant stirring. In case of BH_4^- reduction, the amount of Ag^+ ions was kept 15% of ion-exchange sites by equilibrating fully Ag^+ ions loaded membrane samples in the well-stirred 0.25 mol L^{-1} $NaNO_3$ for 45 s as described in earlier work [35]. After this, the membrane samples were subjected to reduction in well stirred 0.2 mol L^{-1} $NaBH_4$ solution at room temperature for 30 min. After reduction, the membrane samples were thoroughly washed with water and equilibrated with $NaNO_3$ (0.25 mol L^{-1}) to remove unreduced Ag^+ ions from ion-exchange sites of the membrane sample.

3.2.3. Galvanic reaction of Ag nanoparticles embedded membrane

For galvanic reactions experiments, the 10 mL aqueous solutions containing Hg^{2+} (0.01 mol L^{-1} $HgNO_3$), Rh^{3+} (0.01 mol L^{-1} $RhCl_3$), $AuCl_4$ (0.01 mol L^{-1} $HAuCl_4$), and $PtCl_6^{2-}$ (0.01 mol L^{-1} H_2PtCl_6) ions were used. The membrane samples (2×2 cm) containing Ag nanoparticles were equilibrated in aqueous solution for known period of time with a constant stirring. The membrane samples equilibrated with chloride salt solution was washed with ammonia and 0.5 mol L^{-1} NaCl to remove AgCl deposited on surface of the membrane samples.

3.2.4. Characterization

3.2.4.1. UV-Vis spectroscopy

Ag nanoparticles give characteristic color due to surface plasmon resonance of electrons. UV-Vis spectra of Ag nanoparticles embedded membrane samples were recorded using UV-Vis Spectrophotometer (V-530, JASCO, Japan). The absorbance measurements were carried out by mounting the sample (1x2 cm) on to the inside wall of a (1x1x3 cm) quartz cell and placing it in a spectrophotometer to record spectrum with respect to air.

3.2.4.2. TEM

For TEM analyses of cross-section of membrane, the membrane samples were sectioned under cryogenic conditions in Leica ultramicrotome to 70 nm thickness. The sections were picked on 200 mesh Cu grids. The grids were examined in an FEI Technai G2 electron microscope in IIT Bombay [Central Facility at SAIF], Mumbai at 120 KeV without any staining or post-treatment. The sizes of nanoparticles were measured manually using the Image Analyzer Software (Image Z, version 1.33 U). The size distribution was obtained from the images obtained by TEM of samples from different locations of the membrane.

3.2.4.3. EDXRF analyses

Energy Dispersive X-ray Fluorescence (EDXRF) measurements of membrane samples were carried out using Total Reflection X-ray Fluorescence Spectrometer IX-2000 provided with EDXRF geometry (ITAL STRUCTRES, Italy). W L_{α} (8.398 keV) radiation was used as excitation source for EDXRF measurements.

3.2.4.4. XRD analyses

X-ray diffraction (XRD) measurements were carried in the range of 2θ (10-70^{o}) on the thin films of polymer for phase identification using monochromatized Cu-K_{α} ($K_{\alpha 1}$ = 1.5406 Å and

$K\alpha_2$ = 1.5444 Å) radiation by Philips X-ray diffractometer Model PW 1710, Netherlands. Silicon was used as an external standard for correction due to instrumental broadening. The presence of broad peak around $2\theta=17^o$ is due to the polymer film.

3.2.5. Measurement of Ag metal content

The amount of Ag nanoparticles embedded the membrane samples (2 x 2 cm pieces) were measured by procedure described in chapter 2, section 2.2.3.3. Filter paper standards were prepared by taking pieces of filter paper of the same dimensions (2 x 2 cm) as the membrane samples and adding known a volume (50, 100 and 200 μL) of the radiolabeled 0.1 mol L^{-1} $AgNO_3$ stock solution. $AgNO_3$ stock solution used for preparing standard samples was same solution used for equilibrating the membrane samples. Each standard was prepared in duplicate. The soaked filter papers were dried at room temperature and counted in a well type NaI(Tl) detector in a similar counting geometry as the membrane samples. The amount of Ag in the membrane sample was obtained by comparing the γ-activity of ^{110m}Ag in membrane samples with the filter paper standards.

$$\text{Metal Content (moles/gm)}= \frac{A_{(mem)}}{A_{(std)}} \times \frac{M_{(std)}}{Wt_{(mem)}} \tag{3.1}$$

where $A_{(mem)}$ and $A_{(std)}$ are ^{110m}Ag radioactivity (counts min^{-1}) in membrane sample and standard, respectively. $M_{(std)}$ is moles of Ag in the standard and $Wt_{(mem)}$ is the weight of the membrane.

3.3. Results and Discussion

3.3.1. Galvanic reaction with Hg^{2+} ions

The standard redox potentials of the systems Hg^{2+}/Hg (+0.85 V) and Ag^+/Ag (+0.80 V) lie close together. It is known that the electrochemical potentials of silver nanoparticles are rather electronegative and galvanic reaction between Ag^0 and Hg^{2+}, given below, may become possible in the membrane [247,248].

$$Ag^0_m + (m/2)Hg^{2+} \rightarrow mAg^+ + (m/2)\,Hg^0 \qquad (3.2)$$

^{110m}Ag radiotracer tagged Ag nanoparticles have been prepared to determine the yield of the galvanic reaction. The membrane samples containing radiotracer tagged Ag nanoparticles has been equilibrated for 15 min with 0.01 mol L^{-1} $Hg(NO_3)_2$. After equilibration, the Ag^+ ions formed by the galvanic reaction have been removed from the ion-exchange sites of membrane samples by treating these with 0.1 mol L^{-1} $NaNO_3$. As shown in Table 3.1, 99 % and 97 % of Ag^0 are replaced from the membrane samples reduced with BH_4^- ions and formamide, respectively. Ag nanoparticles, formed by formamide reduction, are dispersed throughout the membrane matrix. Some of the Ag nanoparticles may be excluded from the water channel network. Hg^{+2} ions cannot reach to these Ag nanoparticles and hence lead to 97 % reduction of Ag nanoparticles. The comparison of energy dispersive X-ray fluorescence (EDXRF) spectra of the membrane samples before and after equilibration with aqueous solution containing Hg^{2+} ions also indicates that the galvanic reaction proceeded quantitatively; see Fig. 3.1(a), (b), & (c).

The transmission electron microscopic (TEM) images of the cross-section of the membrane samples before and after partial treatment with Hg^{2+} ions are shown in Fig. 3.2 (a) & (b). The statistical analyses of nanoparticles size indicate that the nanoparticles size dispersion broadened in the membrane sample subjected to 50% galvanic reaction from average size 9 nm (range 4 to 15 nm) to average size 15 nm (range 4 to 28 nm). Also, the distribution of nanoparticles is not evenly spread as before galvanic reaction. A few bigger particles (2%) ranging from 50 nm to 70 nm are also seen in the TEM image given in Fig. 3.2 (b). The TEM images of the samples subjected to complete galvanic replacement of Ag^0 with the Hg^{2+} ions are shown in Fig. 3.2 (c) & (d). The radiotracer studies and EDXRF spectra confirmed the complete galvanic replacement of Ag in these samples.

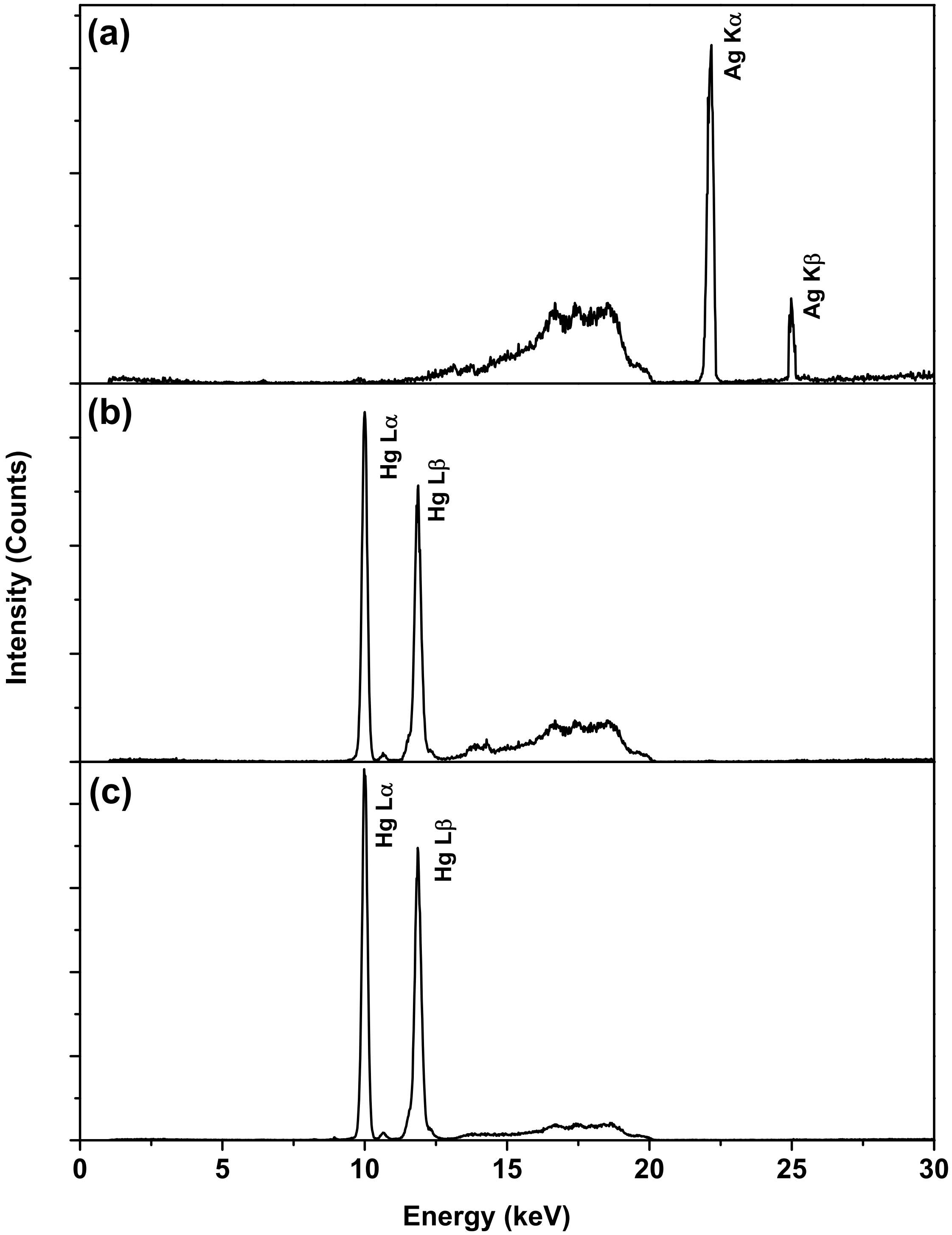

Fig. 3.1 *Energy Dispersive X-ray Fluorescence spectra of (a) the Ag nps embedded membrane samples before the galvanic reaction, (b) after the galvanic reaction by* Hg^{2+} *ion on the membrane samples containing Ag nps throughout the matrix (formed by formamide reduction at 65°C), and (c) after the galvanic reaction by* Hg^{2+} *ion on the membrane samples containing Ag nps at the surface (formed by* BH_4^- *reduction).*

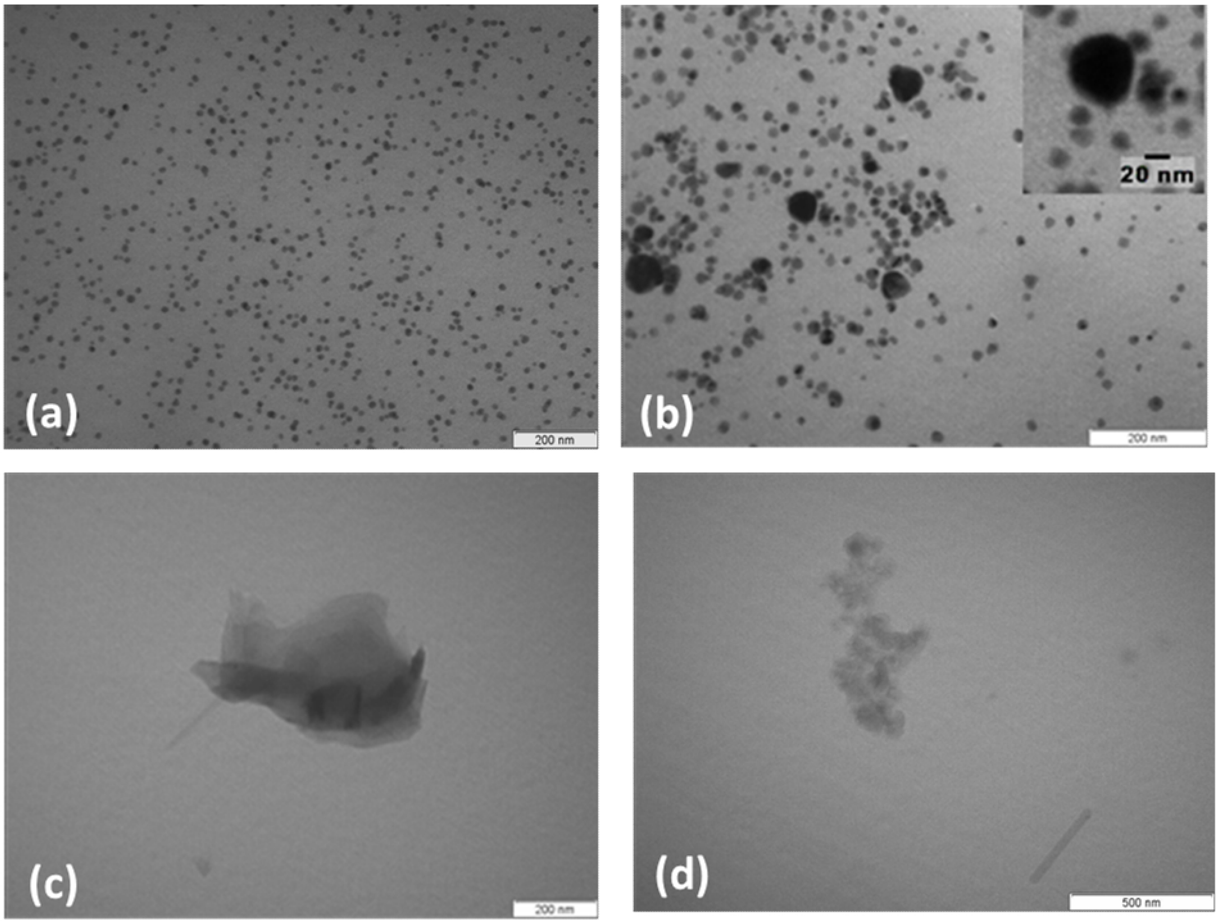

Fig. 3.2 *TEM images of the across sections of the membrane samples subjected to quantitative galvanic replacement of Ag nps with* Hg^{2+} *ions. (a) before galvanic reaction (b) at 50 % of the galvanic reaction (c), & (d) after completion galvanic reaction*

The spherical Ag nanoparticles are not seen in any TEM image of the sections of the membrane sample subjected to complete galvanic reaction with Hg^{2+} ions. Hg^0, thus formed, has coalesced to bigger size nanostructure that does not have well-defined shape; see Fig. 3.2 (c) & (d). The quantitative uptake of Hg^{2+} ions in the cation-exchange membrane can be attributed to the concentration gradient of Hg^{2+} ions between aqueous solution and membrane maintained by the galvanic reaction that changes Hg^{2+} ions to Hg^0. It is important to remove the Hg accumulated in the membrane matrix for its reuse. It has been observed that Hg could be re-oxidized and removed from the membrane by its equilibration in 0.5 mol L^{-1} HNO_3 at room temperature. EDXRF spectra of membrane sample after treatment with HNO_3 does not show any peak for Ag & Hg (Fig. 3.3 a & b).

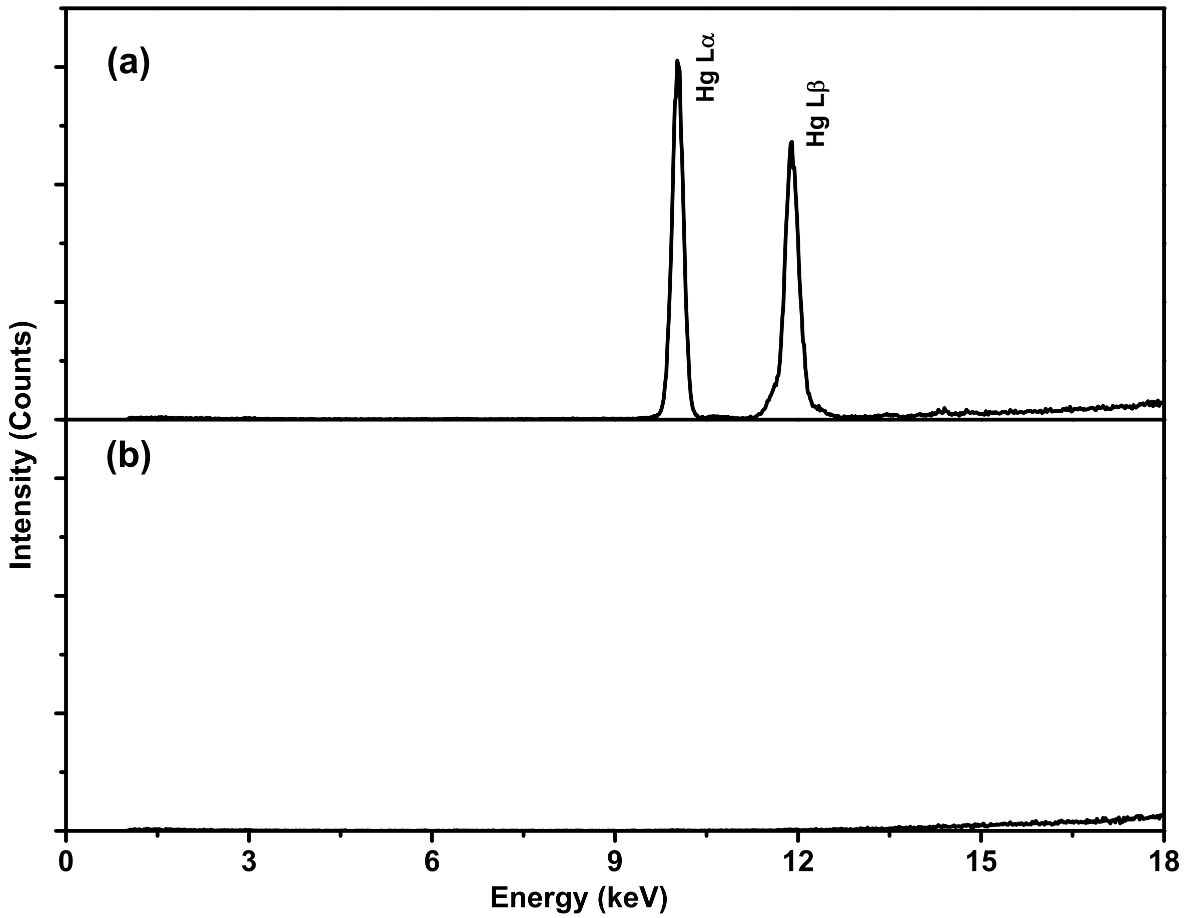

Fig. 3.3 *Energy Dispersive X-ray Fluorescence (EDXRF) spectra of the* Hg^0 *loaded membrane samples before (a) and after (b) the equilibration with 0.5 mol* L^{-1} HNO_3 *at room temperature.*

Table 3.1 Radiotracer *studies of formation of metal nanoparticles during galvanic reactions of ions with Ag nanoparticles in the matrix of Nafion-117 membrane.*

Ions	**Method of the Formation of Ag nps***	**Equilibration Time in salt solution (0.01 mol L^{-1})**	**Replacement of Ag^0 from membrane (%)**
Hg^{2+}	BH_4^- reduction	5 min	99±2
Hg^{2+}	FA reduction at 65°C	5 min	97±2
$AuCl_4^-$	BH_4^- reduction	4 h	95±2
$AuCl_4^-$	FA reduction at 65°C	overnight	70±1
$PtCl_6^{2-}$	BH_4^- reduction	6 h	90±2
$PtCl_6^{2-}$	FA reduction at 65°C	overnight	60±1

*BH_4^- *reduction produces Ag nanoparticles of size 15 nm positioned near surface of the membrane and formamide reduction at 65°C produces Ag nanoparticles of size 9 nm uniformly spread in the membrane matrix.*

3.3.2. Formation of core-shell structure

It has been reported in the literature that Hg adsorption on Ag nanoparticles induces a blue shift and a decrease in the intensity of the surface plasmon absorption band (SPB) of Ag nanoparticles due to formation of the core–shell structure [247,249]. The extent of the blue shift has been found to increase with an increase in the Hg shell around Ag nanoparticles [247,249]. The blue shift and decrease in the intensity of SPB of Ag nanoparticles can be used for generating the response signal for detection and quantification of Hg^{2+} ions by using the galvanic reaction. To explore such a possibility, UV-Vis spectra of the membrane sample has been studied as a function of equilibration time in the solution containing excess of Hg^{2+} ions.

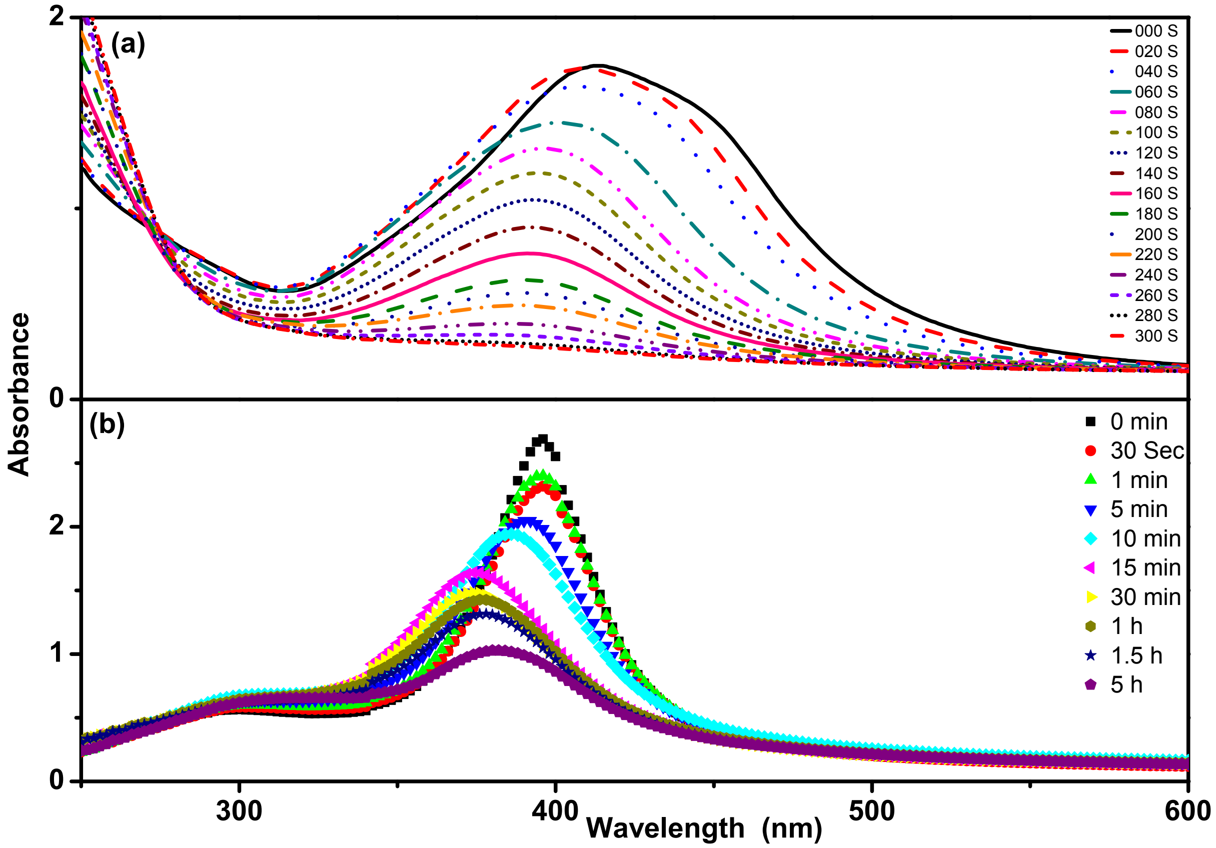

Fig. 3.4 *Surface plasmon absorption of Ag nps embedded Nafion-117 membrane as a function of equilibration time (t) in solution: (a) containing Hg^{2+} ions for complete reduction of Ag^0, and (b) containing Hg^{2+} ions less than that required for complete replacement of Ag^0.*

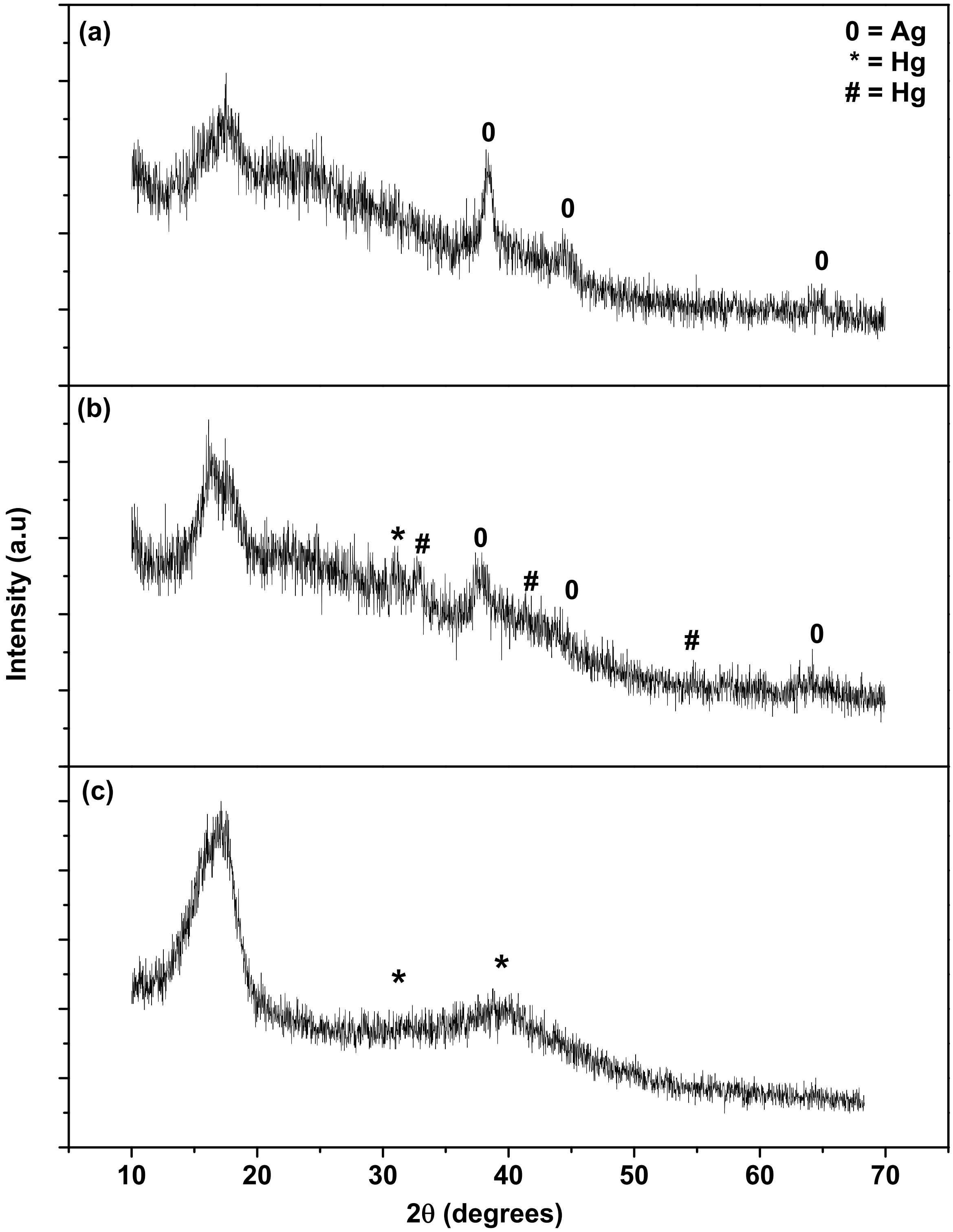

Fig. 3.5 *XRD membrane samples subjected to galvanic replacement of Ag nanoparticles with* Hg^{2+} *ions. (a) before galvanic reaction, (b) at 50 % of the galvanic reaction, and (c) after completion galvanic reaction.*

It is observed that the intensity at $\lambda_{max} \approx 400$ nm continuously has decreased and completely disappeared after 5 min equilibration; Fig. 3.4(a). UV-Vis spectra of the membrane sample subjected to partial galvanic reaction of Ag nanoparticles with Hg^{2+} ions are shown in Fig. 3.4(b). In this experiment the membrane sample has been equilibrated with well-stirred solution containing concentration of Hg^{2+} ions five times less than that required for complete galvanic replacement of Ag nanoparticles. The intensity of absorption band of Ag nanoparticles embedded membrane sample at $\lambda_{max} \approx 400$ nm has decreased continuously up to 5 min, and thereafter gradually shifted to ≈ 375 nm with increase in the equilibration time. The XRD pattern of the membrane samples are shown in Fig. 3.5. Absence of the diffraction peak corresponding to the Hg-Ag amalgam in XRD indicates that that no well-defined amalgam has formed during partial oxidation of Ag nanoparticles with Hg^{2+} ions. The experimental observations like broadening of size distribution of nanoparticles, blue shift in SPB of Ag nanoparticles, and XRD pattern seem to suggest that core–shell structure is formed after partial oxidation of Ag nanoparticles with Hg^{2+} ions.

3.3.3. Galvanic reaction with Rh^{3+} ions

The galvanic replacement of Ag nanoparticles with Rh^{3+} in the membrane has been found to be nearly complete as indicated by EDXRF. TEM image of the cross-section of the membrane is shown in Fig. 3.6. It is evident from the figure that Rh nanoparticles of size range 5–11 nm (average 8 nm) were uniformly dispersed throughout the matrix of the membrane. It is contrary to the direct reduction of Rh^{+3}ions loaded membrane, where fractals of Rh were observed (Chapter 2, section 2.3.4). This clearly shows that the mechanism of formation determines the size and shape of the nanoparticles. Bi et al. have synthesized the hollow rhodium nanotubes through galvanic replacement reaction between Ag nanowires and $RhCl_3$ controlled by iodide ions [250]. It appears that Rh nanoparticles has nucleated and grown independently without alloying with Ag due to the lack of solid-solid inter diffusion between Rh and Ag at the reaction temperature [37,238,251,252]. This appears to be the most probable reason for the complete galvanic replacement of Ag.

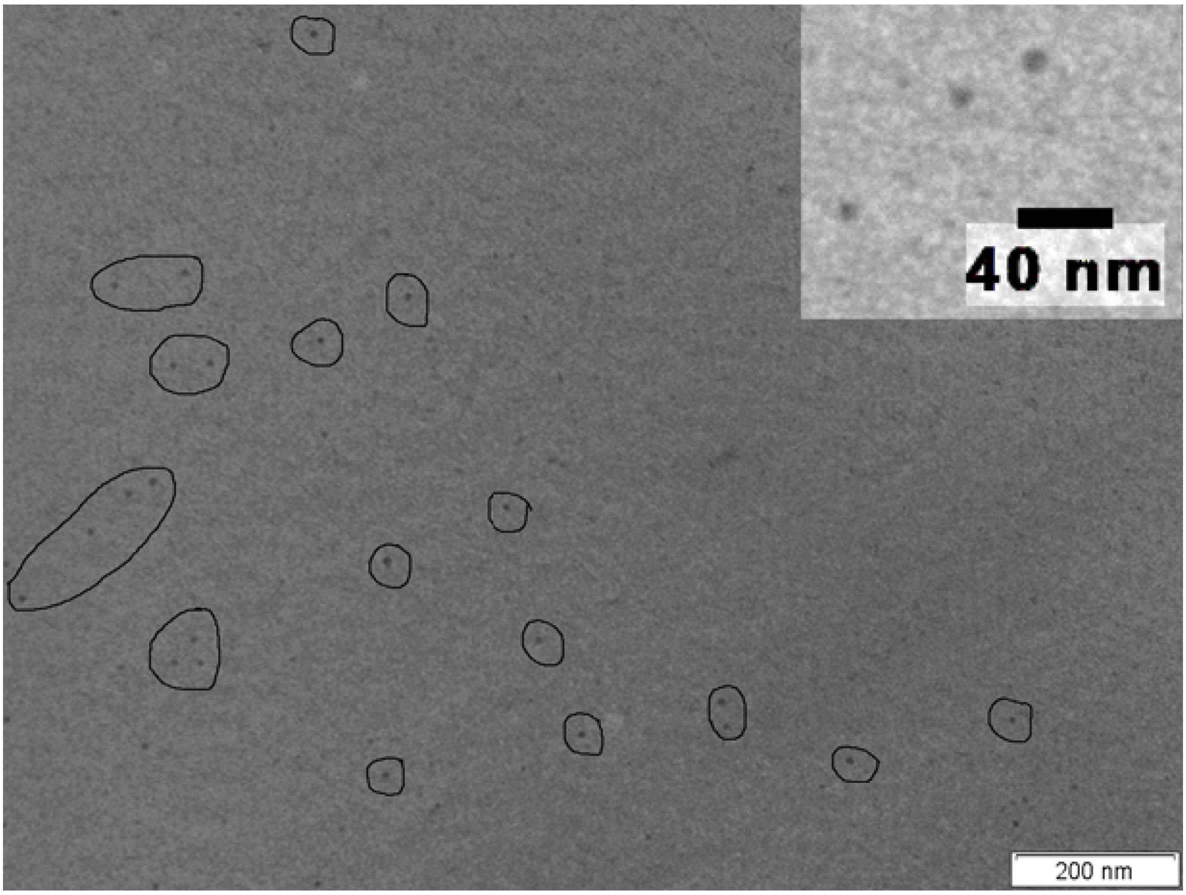

Fig. 3.6 *TEM image of the across sections of the membrane samples in which Ag nanoparticles were formed by reduction with formamide (at 65 ^oC) and subsequently treated with aqueous solution containing Rh^{3+} ions.*

3.3.4. Galvanic reaction with $AuCl_4^-$ ions

The galvanic reaction of $AuCl_4^-$ anions with Ag nanoparticles have studied using BH_4^- ions reduced membrane samples that produce Ag nanoparticles at surface of the cation-exchange membrane [189]. The TEM images of cross-sections of this membrane sample after galvanic reaction with $AuCl_4^-$ anions are shown in Fig.3.7 (a) & (b). It is seen from TEM images that the particles concentration is very high at the both surfaces of the membrane, and different shaped nanostructures of Au are formed. Similar to the Rh nanoparticles formation, Au nanoparticles also have grown independently during the galvanic reactions. This resulted in quantitative replacement of Ag and formation of different Au nanostructures at the surface of membrane. The quantitative replacement of Ag has been confirmed by radiotracer and EDXRF studies, which showes that 95 % of Ag^0 has been replaced by galvanic reaction with $AuCl_4^-$ ions (Fig. 3.8 and Table 3.1).

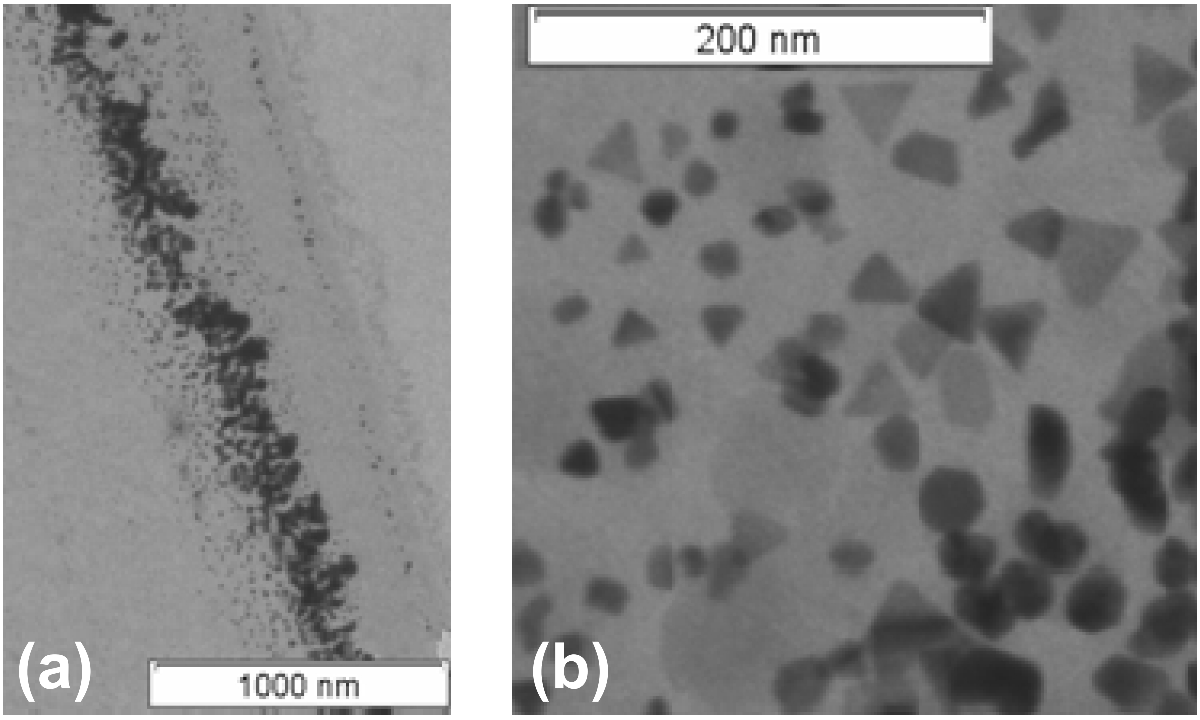

Fig. 3.7 *TEM images of cross-section of membrane samples showing Au nps formed after galvanic reactions with Ag nps formed by the* BH_4^- *ions reduction. TEM image "b" is enlarged view of Au nps present as the surface of membrane shown in TEM image "a".*

The galvanic reaction of $AuCl_4^-$ anions in bulk matrix has been studied using the formamide reduced samples having Ag nanoparticles dispersed throughout the matrix. It has been observed in radiotracer study (Table 3.1) that 70% of Ag^0 are replaced during equilibration of the membrane sample for overnight. EDXRF spectra (Fig. 3.8 a) also shows the presence of a small amount of Ag in the membrane sample. It is observed that 30% of Ag content of the membrane sample present at the interior matrix could not be oxidized by $AuCl_4^-$ ions. This is due to the fact that $AuCl_4^-$ ions could not invade the interior matrix of the membrane due to ''Donnan exclusion'' of the co-ions from the cation-exchange membrane. The TEM images of a cross-section of this membrane sample show that Au nanoparticles of size ranging from

4 nm to 22 nm with average size 12 nm (Fig. 3.9) were uniformly dispersed in the membrane matrix. The size and shape of Ag nanoparticles (before galvanic reaction) and Au nanoparticles (formed after galvanic reaction) are similar, but the concentration of Au nanoparticles in the membrane matrix is significantly lower than that of the original Ag nanoparticles due to the stoichiometry of the galvanic reaction.

UV-Vis spectra of the Ag nanoparticles embedded membrane sample showed disappearance of ≈400 nm absorbance peak after galvanic reduction (Fig. 3.10). A new peak emerged at ≈530 nm, which is a characteristic absorption band of Au nanoparticles.

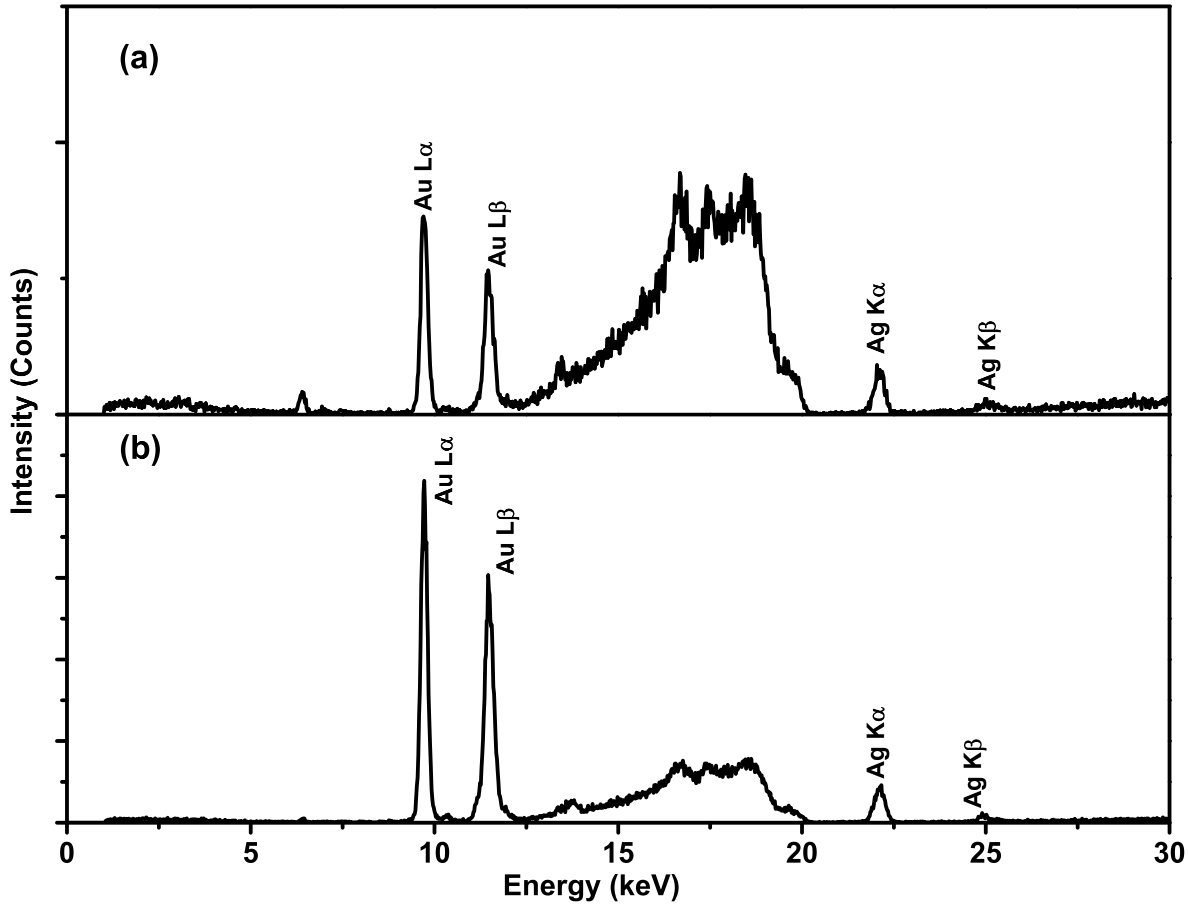

Fig.: 3.8 *EDXRF Spectra of the Ag nanoparticles embedded membrane samples treated with aqueous solution containing excess of* $AuCl_4^-$ *anions for 3 hrs. with constant stirring. The spectra (a) and (b) are of the membrane samples in which Ag nanoparticles were formed by reduction with formamide and sodium borohydride, respectively.*

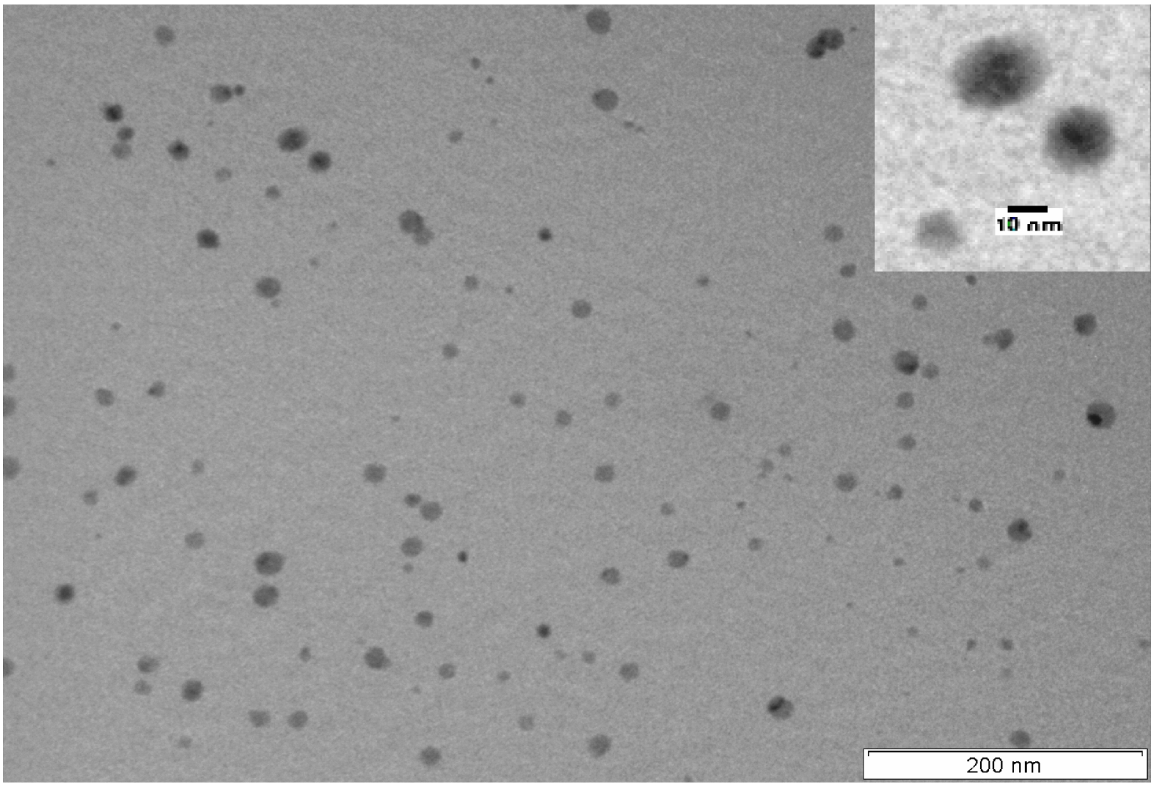

***Fig.:3.9** TEM image of cross-section of membrane sample showing Au nps formed after galvanic reaction with Ag nps containing membrane formed by the formamide reduction.*

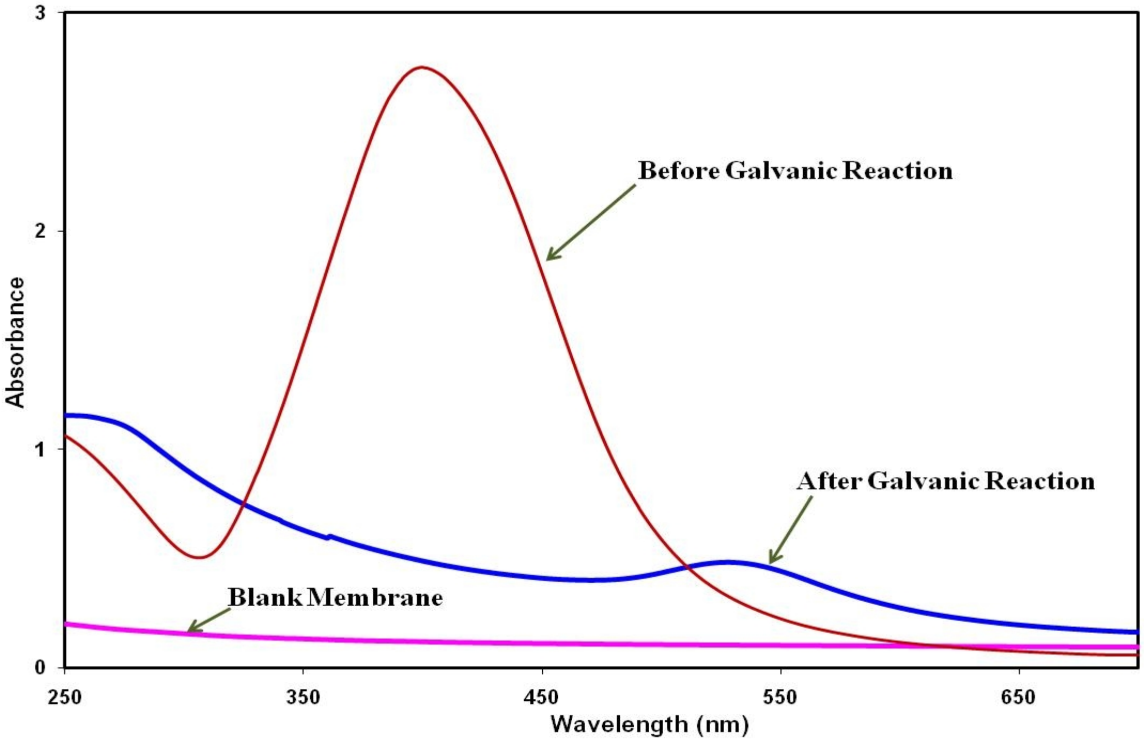

Fig.:3.10 *UV-Vis absorbance spectra of the membrane samples showing surface plasmon absorption bands of Ag nps (before galvanic reaction), Ag+Au nps (after galvanic reaction), and blank membrane.*

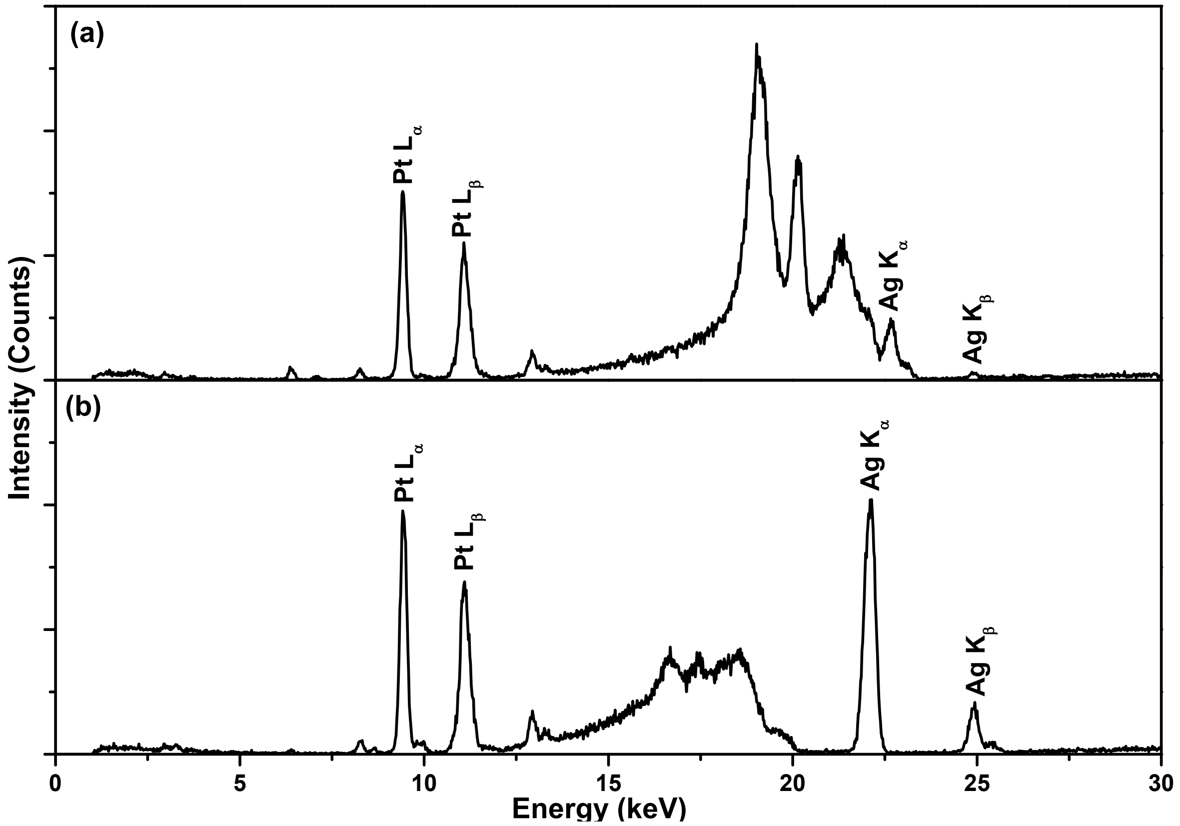

Fig. 3.11 *EDXRF Spectra of the Ag nanoparticles embedded membrane samples treated with aqueous solution containing* $PtCl_6^{2-}$ *solution. The spectra (a) and (b) are of the membrane samples in which Ag nanoparticles have been formed by reduction with* BH_4^- *and formamide, respectively.*

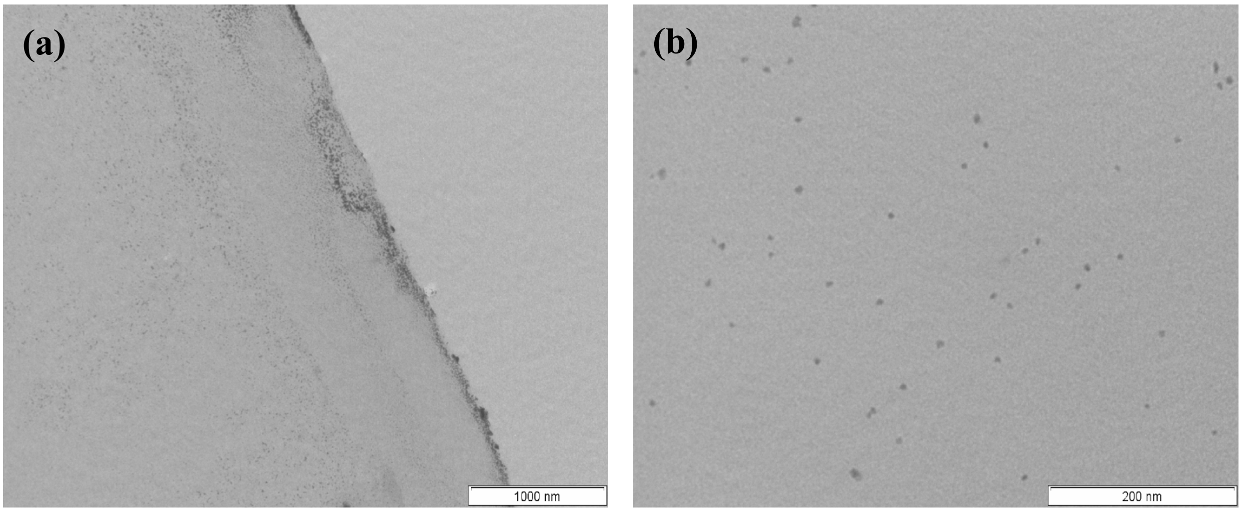

Fig.3.12 *TEM images of the (a)* BH_4^- reduced, (b) formamide reduced *membrane samples subjected to galvanic replacement of Ag nanoparticles with* $PtCl_6^{2-}$ *ions.*

3.3.5. Galvanic reaction with $PtCl_6^{2-}$ ions

The galvanic reaction of $PtCl_6^{2-}$ anions with Ag nanoparticles has been studied using BH_4^- ions and formamide reduced membrane samples. EDXRF spectra of the membrane after galvanic reduction are shown in Fig. 3.11. The radiotracer and EDXRF studies showed that 90 % of Ag nanoparticles of BH_4^- reduced membrane have been replaced by galvanic reaction with $PtCl_6^{2-}$ ions (Fig. 3.11 and Table 3.1). While in case of formamide reduced membrane samples only 60 % Ag nanoparticles has been replaced by galvanic reaction. This is attributed to fact that $PtCl_6^{2-}$ ions would not enter the bulk matrix as these are co-ions that are excluded from the cation-exchange membrane. The TEM images of the cross-section of membrane sample after galvanic reaction are given in Fig. 3.12. It is seen from figure that the spherical Pt nanoparticles are formed after the galvanic reaction and particles measure approximately from 2 nm to 8 nm sizes. Pt nanoparticles concentration has been found very high at both surfaces of the membrane sample in case of BH_4^- reduced sample; see Fig. 3.12(a). A uniform distribution of Pt nanoparticles throughout the matrix has been observed in the formamide reduced membrane samples; see Fig. 3.12(b).

3.4. Conclusion

In conclusion, the *in situ* galvanic reactions involving Ag nanoparticles in the membrane matrix are quite different from that in solution in terms of mechanism as well as possible applications. Galvanic reaction with Hg^{+2} showed blue shift of with the decrease in the surface plasmon resonance absorption of Ag nanoparticles. This properties can be used for the development of chemical sensor for Hg^{2+} ions which produces optical response in the form of blue shift and decrease in intensity of the SPB of Ag nanoparticles [253]. Contrary to direct reduction where fractal of Rh has been formed, Rh nanoparticles have been formed by galvanic replacement reaction. Au and Pt nanoparticles have been prepared in cation exchange membrane using anionic species $AuCl_4^-$ or $PtCl_6^{2-}$ which are excluded from the membrane matrix.

Chapter - 4

Anion exchange polymer inclusion membrane: preparation and characterization

4.1. Introduction

In situ synthesis of nanoparticles in the membrane requires transfer of the metal ions to the membrane and their subsequent reduction to zero valence state in the membrane matrix. Poly(perfluorosulfonic) acid membrane is a cation-exchange membrane and, therefore, the formation of nanoparticles in its highly perm-selective matrix from the anionic species like $AuCl_4^-$ is not a straightforward process as explained in chapter 3.

A promising alternative to poly(perfluorosulfonic) acid membrane may be the polymer inclusion membranes or solvent polymeric membranes [152-156]. Polymer inclusion membranes (PIMs) are widely used in the membrane based chemical sensor [160,162,163,254,255] and facilitated transport based separation of the metal ions [152,154,157,256-259]. This class of membranes is prepared by physical immobilization of an organic extractant in plasticized polymer matrix. The components of the matrix of a typical polymer inclusion membrane are base polymer, compatible plasticizer, and a carrier (extractant) responsible for transferring the ions from aqueous to the membrane phase and subsequent ionic diffusion in the membrane matrix.

Poly(vinyl chloride) (PVC), cellulose triacetate (CTA) or their analogues are used as the matrix forming base polymer [165,166]. The base polymer forms skeleton of the PIM to provide mechanical strength. The chemical structure of the base polymer also plays an important role in transport of ions across the PIMs. For example, the polymer inclusion membranes containing bis-tert-butylcyclohexano-18-crown-6 as a metal cation carrier showed that flux of K^+ diminished with increasing size of the cellulose side chains [166]. However, the length of alkyl side chain of cellulose has been found to influence stability of the PIM in acidic conditions that lead to hydrolytic cleavage of the polymer β-glucosidic linkages [166]. These membranes can be tailored for hosting the desirable nanoparticles by appropriate choices of the carrier and plasticizer immobilized in the membrane matrix. The physical structure of the PIMs is a key issue in understanding the transport mechanism of ions across these membranes. Ye et al. have suggested three dimensional grid structures for plasticized PVC membrane based on small angle neutron scattering studies [260]. AFM images and surface roughness profiles of the PIM made up of plasticized CTA seem to suggest a regular pattern of plasticized blobs of CTA nodes in the membrane [261]. X-ray diffraction spectra of the PIMs consisting of CTA, NPOE, and varying concentration of Lasalocid A were studied by C. Fontas et al [38]. It was found that the XRD pattern of the crystalline part of CTA was not affected significantly on addition of the plasticizer 2-nitrophenyl octyl ether (NPOE). However, the amorphous part of the CTA diffraction pattern was altered. The transmission infrared mapping microspectroscopy of PIM samples containing CTA, plasticizer NPOE or tri-(2-ethylhexyl) phosphate (TEHP), and carrier bis(2,4,4-trimethylpentyl)phosphinic acid (CYANEX 272) revealed that distribution of the carrier in the PIM was highly dependent on the hydrogen bonding and dipolar interactions of the carrier with the plasticizer and matrix forming polymer CTA [262].

Though selectivity of the PIMs (partition coefficient of the ions at aqueous-membrane interface) is governed by the chemical property of the carrier, the physical properties of plasticizer like viscosity and dielectric constant strongly influence transport of the ions across the membrane [152,157,263-266]. The mechanism of solutes (ions/molecules) diffusion across the PIMs may occur through fixed-site jumping [267,268], carrier-diffusion [269], or mobile-site jumping depending upon the composition of the membrane [270]. It has been reported earlier that the competition of the anions with the I^- ions for available exchange sites of the liquid anion-exchanger trioctylmethylammonium chloride in the NPOE plasticized CTA matrix (PIM) was dependent upon the hydration energy of the anions and followed the pattern of the Hofmeister series [265,266]. Malewitz et al. observed during competitive uptake of the anions in the Neosepta^R AMX and Selemion^R AMV anion-exchange membranes that the selectivity pattern of anions was $NO_3^- > Br^- > Cl^-$ [271]. However, the selectivity in anions transport through polymer inclusion membranes facilitated by transition metal containing carriers was found to be depended not only on their electrostatic interactions but also on affinity of the carrier towards specific anion [272].

In the present chapter, the physical characteristic and diffusional transport properties of the plasticized anion-exchange polymer inclusion membrane have been studied for synthesis of nanoparticles formed from anionic precursors like $AuCl_4^-$, $PtCl_6^{2-}$ etc. The samples of PIM have been prepared by physical immobilization of a liquid anion-exchanger trioctylmethylammonium chloride (Aliquat-336) in the plasticized matrix of cellulose triacetate (CTA). Three different plasticizers used in the PIM are 2-nitrophenyl octyl ether (NPOE), dioctyl phthalate (DOP), and tri-(2-ethylhexyl) phosphate (TEHP) having different dielectric constant and viscosity. Since carrier and plasticizer are the important constituents of the PIM, the amounts of both of these have been varied in the samples. The effect of concentration variation of the carrier (Aliquat-336) and plasticizer on microscopic structure, glass transitions, and ion-exchange capacity of the membrane are explained in this chapter. The diffusional-transport properties of the membrane based on the study of self-diffusion coefficients of the water, I^- and counterions are also discussed in this chapter.

4.2. Experimental

4.2.1. Reagents and apparatus

Analytical grade reagents and de-ionized water (18 MΩ.cm) purified by model Quantum™ from Millipore (Mumbai, India) were used throughout the work. Cellulose triacetate (molecular weight 72000-74000, acetyl value = 43.2%), Aliquat-336, and 2-nitrophenyl octyl ether (NPOE) were obtained from Sigma-Aldrich (Steinheim, Germany). Tris-(2-ethylhexyl) phosphate (TEHP) (Koch-Light Laboratories, Coinbrook Bucks, England) and dioctyl phthalate (DOP) (BDH, Poole, England) were used as obtained. These chemicals were having high purity (> 98%). The radiotracer ^{131}I used in the present work was obtained from the Board of Radiation and Isotope Technology, Mumbai, India. The aqueous solution containing $^{131}I^-$ ions was purified from I_2 by equilibration with chloroform. The stock solution was prepared by spiking 0.1 mol L^{-1} KI solution with a known amount of radioactivity of ^{131}I radiotracer. The γ-ray activity of ^{131}I radiotracer (364 keV) was monitored by using a well-type NaI(Tl) γ-ray detector connected to a multi-channel analyzer. All the samples and standard containing radioactivity were counted in identical geometry. β-radioactivity of the tritiated water (HTO) was measured by adding the 50 μL sample drawn from equilibrating solution to a vial containing 5 mL of scintillation cocktail-w (2,5-diphenyl oxazole = 10 g, 1,4-di-2-(5-phenyloxazolyl) benzene = 0.25 g, and naphthalene = 100 g in 1000 mL 1,4-dioxane solvent), and counting β radioactivity in the vial with a Packard Liquid Scintillation Analyser (model TRI-CARB 2100 TR). The thickness of membrane samples was measured using a digital micrometer (Mitutoy, Japan) with an accuracy of ± 0.001mm.

4.2.2. Preparation of the membrane

The solution of cellulose triacetate (CTA) was prepared by dissolving CTA (0.2 g or 0.4 g) in 5 mL of dichloromethane. A separate solution in dichloromethane (5 mL) containing known amounts of a plasticizer (0.2 to 0.6 g) and Aliquat-336 (0.05 to 0.25 g) were prepared. A casting solution was prepared by mixing the two solutions, and homogenized by ultrasonication for two minutes. This casting solution was poured on a leveled 9-cm diameter flat bottom casting plate. Dichloromethane was allowed to evaporate slowly over a period of two days. After the evaporation of dichloromethane, the transparent membrane was formed. The membrane was annealed at 50°C for 3 h to remove residual solvent, and then water was poured into casting plates before its peeling off from the casting plate. The membrane was cut into pieces of required dimensions for the experiments [265]. The membrane samples were stored in 0.1 mol L^{-1} NaCl solution to keep them in Cl^- forms.

4.2.3. Characterization of the membrane

4.2.3.1. Microscopy characterization

For Atomic Force Microscopy (AFM) studies of membrane samples, non-contact mode AFM measurements were performed at ambient temperature conditions using a Nanosurf easyScan 2 AFM (Nanosurf, Switzerland) with 10 μm scanner head. The cantilevers in use were NCLR-10 (Nano World) with a resonance frequency of 190 kHz and force constant of 48 N/m. AFM data were analyzed using Nanosurf Report 4.1 software. The root mean square roughness (Sq) of 100 μm^2 surface area of membrane samples were obtained by following equation:

$$Sq = \sqrt{\frac{1}{MN}\sum_{k=0}^{M-1}\sum_{l=0}^{N-1}(Z(X_K Y_l))^2} \tag{4.1}$$

Image is divided into a number of lines and each line is further divided into a number of points. N is the number of measured data lines and M is the number of measured data points per line in an image. In this case the number of measured data lines is equal to the number of measured data points per line i.e. N = M. The data is acquired and stored at each point during the scan/measurement. $Z(X_k,Y_l)$ is the Z-position of the tip (local sample height) at the point with coordinates (k,l) in the image.

4.2.3.2. Differential scanning calorimetry

DSC was used to measure the glass transition temperature of the membrane samples. DSC profiles were recorded at heating rate of 10 ^{o}C min^{-1}, under inert atmosphere using a Mettler Toledo DSC 822 with an empty aluminum pan as reference. Temperature and enthalpy calibration of the instrument were done, using cyclohexane and indium. The transition temperature reported is the peak temperature. The transition enthalpy of the endothermic curve is calculated by using the software supplied by Mettler Toledo. About 7 to 8.5 mg membrane samples were used to record the scans.

4.2.3.3. Electrochemical impedance spectroscopy

The instrument used for carrying out the ac-impedance measurements was the AUTOLAB Frequency Response Analyser 2 (Eco. Chemie B.V., Utrecht, The Netherlands). A small sine wave AC potential was applied to an electrochemical cell arrangement shown in Fig. 4.1(a) over a frequency range from 1 MHz to 10 Hz. The area of the membrane under study in the measuring cell exposed to mercury was 1.227 cm^2. Thus obtained impedance spectra were analyzed with the help of the Frequency Response Analyser software (Eco. Chemie B.V., Utrecht, Netherlands). The equivalent circuit, which refers to the experiment, is shown Fig. 4.1(b). The runs were analyzed assuming that the membrane behaved as a parallel RC circuit in the frequency range used [273]. Bulk resistance of the membrane samples, loaded with different anions, was measured using same experimental set up. For this experiment, the membrane samples were equilibrated with 0.1 mol L^{-1} salt solutions containing Cl^-, NO_3^-, I^-, and SO_4^{2-} ions for 24 h. The selection of Cl^-, NO_3^-, ClO_4^-, and SO_4^{2-} ions for the diffusion studies has been based on the fact that these ions have systematic variation of degree of hydration and thus represent Hofmeister series from highly hydrated to least hydrated ions [265]. The self-diffusion coefficient of the anion in PIM sample was determined using the relation [274]:

$$D = (k\ T / \bar{e}\ F\ A\ C)*(d / R\ z^2) \tag{4.2}$$

Where k is the Boltzmann constant, T is the absolute temperature in K, $\bar{e}$ is the charge of the electron, F is the Faradays constant, A is the area of the membrane, C is the concentration of the anions in membrane (= ion-exchange sites in the membrane sample), d is the thickness of the membrane, R is the bulk resistance of the membrane, and z is the charge of the anion. The values of D for the anions were normalized with D values of I^- ion in the same membrane obtained by the radiotracer method.

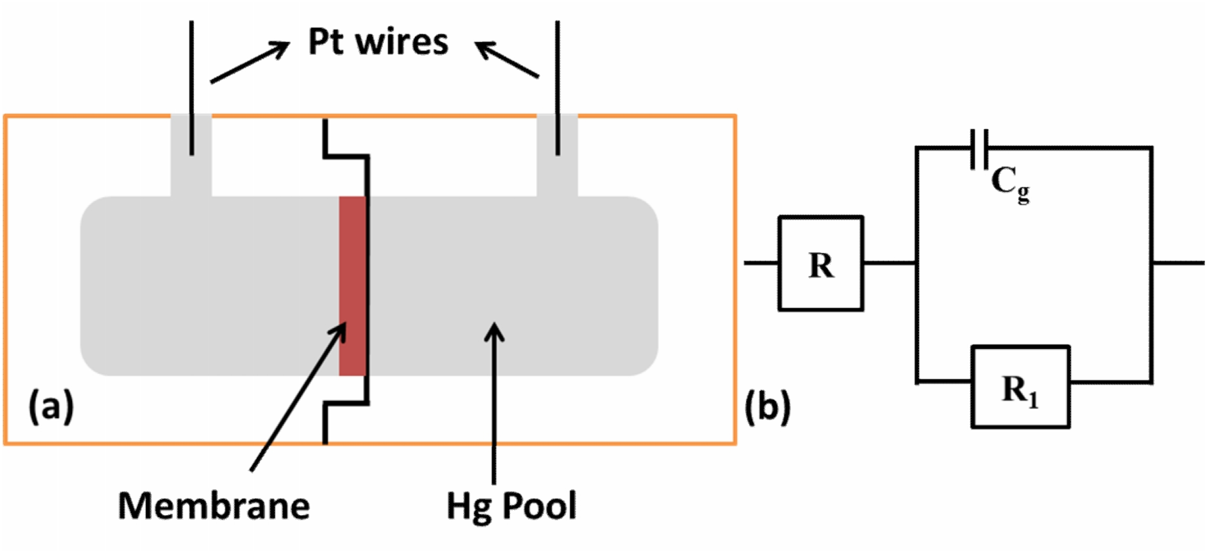

Fig. 4.1 *(a) Schematic diagram of electrochemical cell for impedance measurement, (b) Equivalent circuit for the impedance experiments, where* C_g *is geometric capacitance and* R_1 *is bulk membrane impedance.*

4.2.4. Measurement of anion-exchange capacity

Total exchange capacity available in the membrane samples (2 x 2 cm pieces) were measured by equilibrating them for 24 h with 15 mL of 0.05 mol L^{-1} KI stock solution containing known activity of ^{131}I radiotracer. The concentration of KI in the equilibrating solution was varied up to 0.1 mol L^{-1}. It was observed that the ion-exchange capacities of the membrane samples remained constant above 0.01 mol L^{-1} concentration of KI. The saturation equilibration time of membrane sample in well stirred KI solution was found to be 45 min. However, membranes were equilibrated for 24 hrs. in 0.05 mol L^{-1} KI stock solutions for the measurement of the ion-exchange capacity. After equilibration, the membrane samples were thoroughly washed with deionized water to remove equilibrating solution clinging to surface of the samples. Filter paper standards were prepared by taking pieces of filter paper of the same dimensions (2 x 2 cm) as the membrane samples and spreading known volume (50, 100 and 200 μL) of the radiolabeled 0.05 mol L^{-1} KI stock solution. KI stock solution used for preparing standard samples contained same ^{131}I (radioactive) to ^{127}I (natural) ratio as the solution used for equilibrating the membrane samples. Each standard was prepared in duplicate. The soaked filter papers were dried at room temperature and counted in a well type NaI(Tl) detector in a similar counting geometry as the membrane samples. The amount of I^- ions in the membrane sample was obtained by comparing the γ-activity of ^{131}I in the membrane samples with the filter paper standards as given below:

$$\text{Ion exchange capacity} = \frac{A_{(\text{mem})}}{A_{(\text{std})}} \times \frac{M_{(\text{std})}}{Wt_{(\text{mem})}} \tag{4.3}$$

where $A_{(mem)}$ and $A_{(std)}$ are γ-radioactivities of ^{131}I (counts min^{-1}) in membrane sample and standard, respectively. $M_{(std)}$ is equivalents of I^- in the standard and $Wt_{(mem)}$ is the weight of the membrane.

4.2.5. Measurements of self-diffusion coefficient

The measurements of self-diffusion coefficients of I^- ions and water in the PIMs with different compositions were carried out using 2.5 x 2.5 cm pieces of samples. A membrane sample in the I^- ionic form was loaded with $^{131}I^-$ radiotracer ions by equilibrating it with 25 mL of the vigorously stirred 0.1 mol/L KI solution spiked with ^{131}I radiotracer [264]. After equilibration, the membrane samples were washed with deionized water to remove equilibrating solution clinging to surface of the samples. The isotopic-exchange profiles were obtained by equilibrating the radiotracer loaded membrane sample with 25 mL aqueous solution of 0.1 mol L^{-1} KI with constant stirring (≈ 400 rpm). The amount of radiotracer ions diffusing out of the membrane sample was monitored by taking out 50 μL samples of equilibrating salt solution at regular time intervals and counting γ-activity of radiotracer ^{131}I using a well-type NaI(Tl) detector connected to a multi-channel analyzer.

In some experiments, the radioactivity of ^{131}I diffusing in/out of the membrane were monitored by taking out the membrane sample for γ-activity measurements at different time intervals and placed again in equilibrating solution. For the measurements of HTO exchange rates, the PIM samples with I^- counterions were equilibrated with water containing known radioactivity of tritiated water (HTO) for overnight. The HTO-loaded PIM sample was immersed in a 25 mL of well-stirred deionized water (without HTO radiotracer) at 25 ^{0}C. The amount of radiotracer HTO diffusing out of the membrane sample was monitored by taking out 50 μL samples from the equilibrating deionized water at regular time intervals and measured the β-radioactivity of HTO by scintillation counting.

The exchange rate profiles of radioactivity tagged I^- ions/HTO diffusing out of the membrane samples in the well-stirred solution as a function of equilibrium time were analyzed by using an analytical solution of Fick's second law explained in chapter 1, section 1.5.1 [33,34]:

4.2.6. Measurement of counterions exchange rates

The membrane samples having fixed dimensions were converted to required ionic forms of counter ions (X^-= NO_3^-, Cl^-, and ClO_4^-) by equilibrating them with aqueous sodium/potassium salt solutions of 0.1 mol L^{-1} concentration of relevant anions. The counter ions (X^-= NO_3^-, Cl^-, and ClO_4^-) exchanges with I^- ions between the membrane sample and well stirred aqueous salt solution (0.1 mol L^{-1}) were measured using ^{131}I radiotracer tagged I^- ions. Both forward exchange rate involving $(I^-)_m \rightleftharpoons (X^-)_{aq}$ system and reverse exchange rate involving $(X^-)_m \rightleftharpoons (I^-)_{aq}$ system were experimentally measured by monitoring the radioactivity of ^{131}I sorbed or desorbed in the membrane sample as a function of equilibration time in the well-stirred appropriate salt solution.

4.3. Results and discussion

4.3.1. Anion exchange capacity

The compositions of PIMs studied in the present work are given in Table 4.1. The densities and anion-exchange capacities of these membrane samples have been measured.

Table 4.1 *The comparison of experimental and calculated ion-exchange capacities of the membrane samples having varying proportions of different plasticizers. The calculated ion-exchange capacities were obtained from the weight fraction of Aliquat-336 in the casting solutions. The amounts of CTA and Aliquat-336 were kept as 0.2 g and 0.05 g, respectively.*

Id.	**Plasticizer**	**Composition (wt.%)**			**Density (g cm^{-3})**	**Exp. I.E.C (meq g^{-1})**	**Cal. I.E.C. (meq g^{-1})**	**Exp. I.E.C./ Cal. I.E.C.**
		CTA	Aliquat-336	Plasticizer				
C-1	None	100	-	-	1.18	N. D	0	-
C-2	None	78.66	21.34	0	1.14	0.44	0.53	0.84
C-2	None§	79.85	20.15	0	-	0.43	0.50	0.85
N-1	NPOE	55.99	16.24	27.78	1.06	0.34	0.40	0.84
N-2	NPOE	42.22	12.21	45.57	1.08	0.28	0.30	0.92
N-3	NPOE	36.11	9.84	54.05	1.17	0.22	0.24	0.90
T-1	TEHP	55.66	16.50	27.84	1.01	0.37	0.41	0.91
T-2	TEHP	44.29	11.50	44.21	0.99	0.25	0.28	0.88
T-3	TEHP	36.01	9.68	54.31	1.05	0.21	0.24	0.89
D-1	DOP	55.53	15.37	29.10	1.06	0.30	0.38	0.77
D-2	DOP	43.90	12.31	43.79	1.08	0.26	0.30	0.85
D-3	DOP	35.16	9.59	55.25	1.12	0.21	0.24	0.89

§Thickness of the membrane sample was doubled from 40±4 μm to 80 μm by doubling the contents of CTA and Aliquat-336 in the casting solution.

Density varied depending upon composition of the membrane sample. In general, the density of membrane sample increases on addition of Aliquat-336 and plasticizer in its matrix. It is seen from the data given in the Table 4.1 that the ion-exchange capacities systematically varied depending upon concentration of Aliquat-336 in the membrane sample. In order to understand the effect of plasticization on accessibility of the anion-exchanger molecules, the ion-exchange capacities of membrane samples have been calculated from the weight fraction of Aliquat-336 in homogenized casting solution. The comparison of experimental and expected ion-exchange capacities given in Table 4.1 seems to indicate that 85% of Aliquat-

336 molecules anion-exchange sites are available even in the absence of plasticizer. The addition of plasticizer slightly improve the ion-exchange capacity of the PIM to around 90% of the expected ion-exchange capacity.

4.3.2. Surface characterization

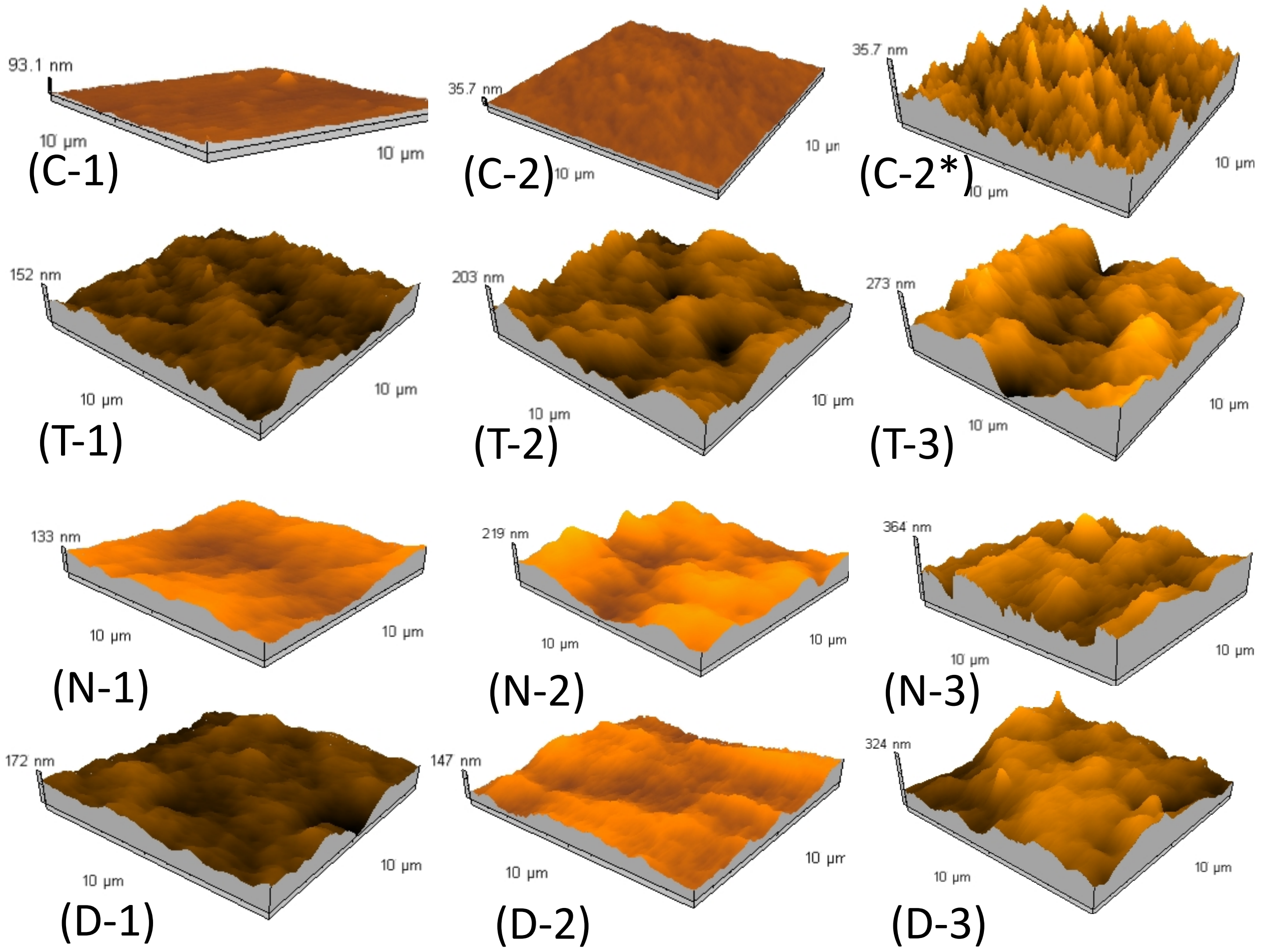

Fig. 4.2 *AFM images of the polymer inclusion membrane samples with and without plasticizers. The compositions of membrane samples are given in Table 1. The scales of Z-axis for all the images were kept same except for C-2*, which is the enlarged view of C-2.*

The AFM images of the membrane samples with and without plasticizer and having varying amount of the different plasticizers are shown in Fig. 4.2. It is evident from the AFM images that the surface morphology changes significantly on addition of the plasticizer. The surfaces of membrane samples having only CTA (C-1) and CTA + Aliquat-336 (C-2) are almost flat. The enlarged AFM image of sample C-2 showed surface roughness that appears like egg-basket. The small features seen in the AFM image of sample C-2 appears to get swelled on addition of the plasticizer, which increases the surface roughness. The comparison of AFM images given in Fig. 4.2 suggests that surface roughness of the membrane sample has increased with amount of the plasticizer.

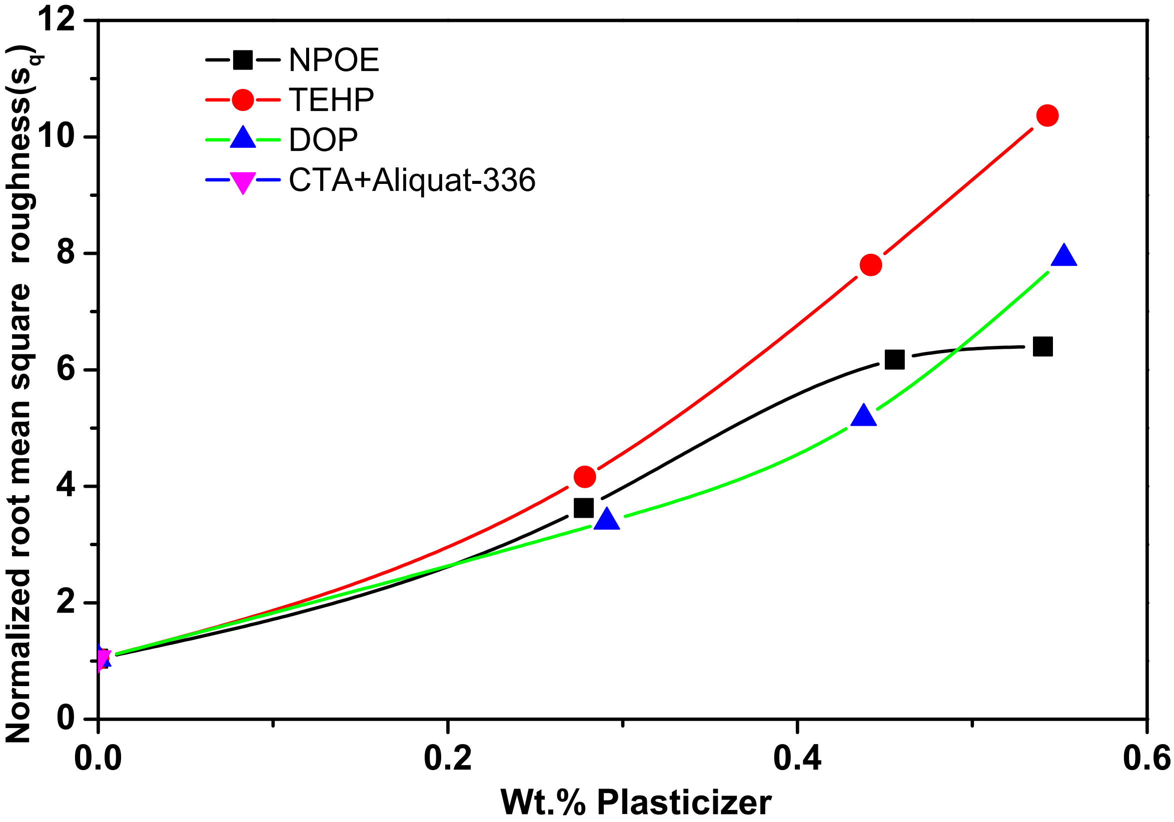

Fig. 4.3 *Variation of root-mean-square roughness (Sq) of the membrane samples, normalized with Sq of the sample made up of only CTA, as a function of weight fraction of the plasticizer.*

In order to correlate the extent of surface roughness with plasticization, the root mean square roughness (S_q) of fixed area of the membrane samples having different plasticizers have been plotted (Fig. 4.3) as a function of the weight fraction of plasticizer. The value of S_q of different membrane samples in Fig. 4.3 has been normalized with the value of S_q of membrane sample containing CTA and Aliquat-336 (C-2). The value of S_q has increased with amount of plasticizer used for the experiment. However, increase in the value of S_q is higher in the membrane sample having TEHP than other membrane samples having same weight fraction of either DOP or NOPE. This seems to suggest that plasticization of CTA is better with TEHP than other two plasticizers.

4.3.3. Glass transition of the membrane

The rubber-to-glass transition temperature (T_g) of the polymeric film is dependent on structural, compositional and conformational factors as well as on the degree of crosslinking, average molecular weight, presence of additives, stabilizers, and plasticizers in the polymeric matrix. Miguel et al. measured the T_g of the PIM made up of CTA, LIX^R 84-I (carrier) and tris(2-n-butoxyethyl)phosphate (plasticizer), which was found to be 175 °C [155]. However, it is not clear how T_g would vary with respect to pure CTA and with addition of different components. Therefore, a systematic study has been carried out to study the change in T_g on addition of different components.

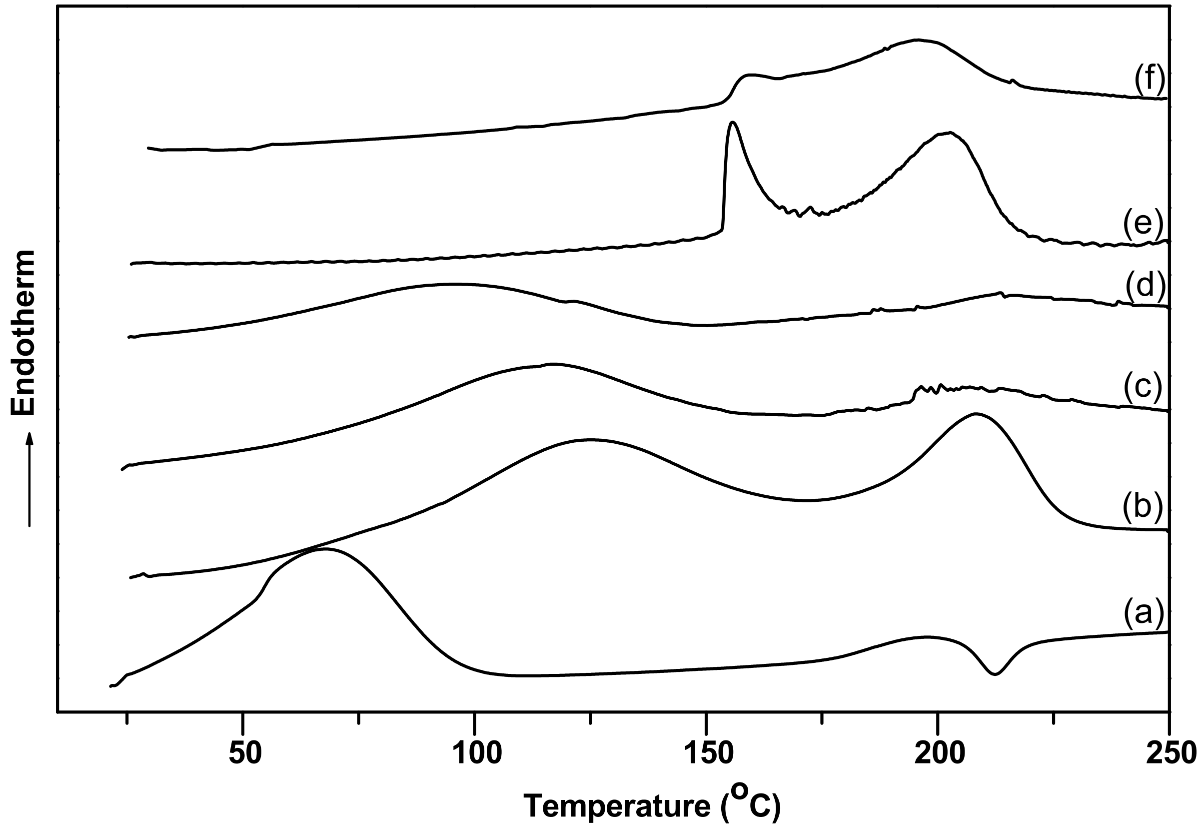

Fig. 4.4 *DSC heating thermograms of membrane samples containing (a) CTA only (C-1), (b) CTA+Aliquat-336 (C-2), (c) CTA+Aliquat-336+TEHP (T-1), (d) CTA+Aliquat-336+TEHP (T-3), (e) CTA+Aliqu-336+NPOE (N-3), and (f) CTA+Aliquat-336+DOP(D-3).*

Table 4.2 *Differential Scanning Calorimetry of the Membrane Samples*[*]

Sample Id.	T_{g1}(°C)	ΔH_{g1} (J g^{-1})	T_{g2}(°C)	ΔH_{g2}(J g^{-1})
C-1	68.1	55.2	196.6	4.3
C-2	122.5	43.3	208.7	26.6
T-1	116.5	40.7	210	8.9
T-3	95.4	26.0	212	6.0
N-3	Peaks are overlapping		155.6 & 202.8	53.6
D-3	Peaks are overlapping		158.3 & 195.9	24.1

[*] Tg_1 and Tg_2 are glass transition temperatures, and ΔHg_1 and ΔHg_2 are corresponding glass transition enthalpies.

The DSC thermograms have been obtained at heating rate of 10 °C min^{-1} in the temperature range 20 °C to 250 °C. The glass transition data obtained by analyses of DSC heating thermograms of PIM samples made up of CTA, CTA+Aliquat-336, and CTA+Aliquat-336+plasticizer (TEHP/NPOE/DOP) are given in Fig. 4.4 and Table 4.2, respectively. It is clear that PIM containing only CTA has two Tg values corresponding to two different kinds of crystalline phases. It has been reported elsewhere that CTA has multiple glass transitions [275,276]. The glass transition of CTA has been followed by an exothermic transition at peak temperature 212 °C. Freshly prepared CTA sample, CTA sample vacuum heated at 60 °C, and prepared from fibrous CTA have also displayed this exothermic transition. Therefore, this exothermic transition could be due to partial decompositional changes in the CTA chain. It is seen from Table 4.2 that T_{g1} and T_{g2} have been shifted from 68.1 °C and 196.6 °C in pure CTA to 122.5 °C and 208.7 °C in CTA+Aliquat-336, respectively. The glass transition enthalpy (ΔH) corresponding to T_{g2} has also increased significantly from 4.3 J g^{-1} to 26.6 J g^{-1}. This seems to suggest that Aliquat-336 may have polar interactions with CTA leading to higher crystalline phases in the PIM. The value of ΔH has decreased as a function of amount of TEHP in the PIM containing fixed proportion of CTA+Aliquat-336, Table 4.2. This can be attributed to reduction of ionic interactions of Aliquat-336 with CTA chains by TEHP leading to good plasticization of the PIM which has also been observed in surface roughness analyses. As can be seen from the Table 4.2, the glass transition of PIMs is also dependent on the nature of the plasticizer. The PIMs containing NPOE and DOP has different T_g and higher ΔH values than TEHP plasticized PIMs having the same weight fraction of the plasticizer. The higher ΔH values in NPOE and DOP plasticized membrane indicates more crystalline phases in the matrices of these membranes. In all the cases, the CTA crystalline phases have been modified as indicated by a shift in Tg but has not disappeared even in the PIMs containing as high as 55 wt % of the plasticizer. Thus, CTA could provide mechanical strength to the PIMs having high amount of the plasticizer.

4.3.4. Effects of plasticizer on diffusion mobility

Plasticizer in the PIM also acts as a solvent for the carrier Aliquat-336. Therefore, the nature and amount of the plasticizer is expected to influence intrinsic diffusion property of the PIM. It has been reported earlier that the log of the self-diffusion coefficients of I^- ions ($D^m(I^-)$) increased linearly with increase in liquid volume fraction (NPOE+Aliquat-336) in the PIM [264]. The polymer chains of CTA in the liquid fraction of PIM matrix offer obstruction in the path of the moving ions. This obstruction is reduced due to increase in liquid fraction in PIM. This fact is also corroborated by the microscopy studies discussed above. Hence, the plasticizer, which is the major component of the liquid phase, acts as a medium for the diffusional transport of ions in the PIM. In present work, the self-diffusion coefficients of I^- ions and water have been measured in the PIM samples having fixed proportion of different plasticizers. The values of self-diffusion coefficients have been obtained by least square fit of the profile of fractional attainment of exchange equilibrium (F(t)) as a function of equilibration time (t) using eq. 1.5. The results of the experiment and fitted profiles of F(t) as a function of equilibration time are shown in the Fig. 4.5, and the values of D for I^- ions and H_2O obtained from the analyses of the exchange profiles are given in Table 4.3. It is seen from the Fig. 4.5 that F(t) varies linearly square root of equilibration time ($t^{1/2}$) up to attainment of 70% of exchange equilibrium, which is characteristic of the Fickian diffusion.

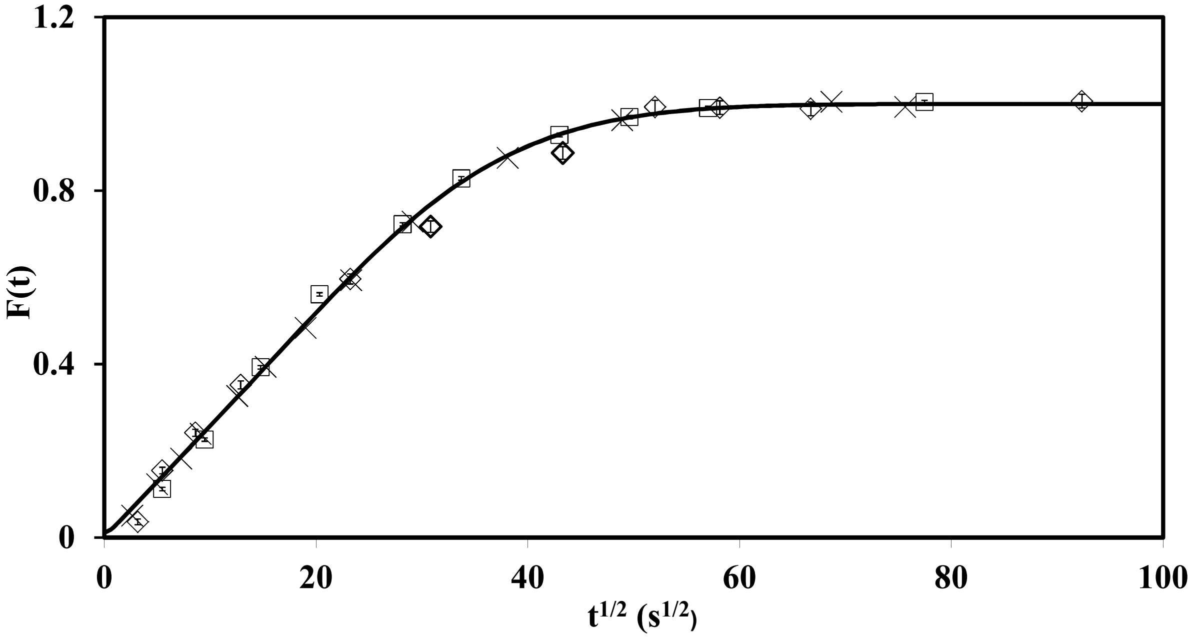

Fig. 4.5 *Fractional attainment of isotopic-exchange equilibrium F(t) of* I^- *ions between membrane sample (PIM-1) and well-stirred 0.1* $molL^{-1}$ *KI solution as a function of square root of equilibration time* $t^{1/2}$. *The symbols represent different sets of repeated experiment. The solid line represents the fitted data in terms of* eq. 1.5 *for deducing the self-diffusion coefficient of* I^- *ions in the membrane.*

Table 4.3 *Self-diffusion coefficients of* I^- *ions and water in the PIM samples having different plasticizers*

Id.	Plasticizer[a]			D(I^-) (cm^2 s^{-1})	D(H_2O) (cm^2 s^{-1})
	Type	Dielectric constant	Viscosity (cP)		
N-3	NPOE	24	13.1	$(3.2\pm0.7)x10^{-8}$	$(1.9\pm0.1)x10^{-7}$
T-3	TEHP	4.8	11.1	$(1.3\pm0.1)x10^{-8}$	$(1.3\pm0.2)x10^{-7}$
D-3	DOP	5.1	40.4	$(2.5\pm0.5)x10^{-9}$	$(1.2\pm0.2)x10^{-7}$

[a] Taken from refs [157,277]. [b] Taken from ref [264].

As seen from Table 4.3, the maximum value of D(I^-) is $3.2x10^{-8}$ cm^2 s^{-1} in the membrane sample N-3 consisting of CTA, NPOE, and Aliquat-336. This value is three orders of magnitude lower than the aqueous self-diffusion coefficient of I^- ions ($2.05x10^{-5}$ cm^2 s^{-1}) in aqueous medium [278]. The value of D(I^-) is found to be $2.91x10^{-7}$ cm^2 s^{-1} in hydrophilic anion-exchange membrane that is also ≈10 times higher than value of D(I^-) in PIM [279]. This seems to suggest that anions diffusion in the PIM is a quite slow process. This may be due to the viscosity of the liquid fraction in the PIM as well as homogeneous gel-like physical structure of the membrane. The comparison of the values of D(I^-) of PIMs having same fractions of the components but different plasticizers indicates that the intrinsic properties of the plasticizer strongly influence the diffusion of I^- ions in the membrane matrix. For example, the PIMs consisting of NPOE (N-3), TEHP (T-3), and DOP (D-3) have been found to have D(I^-) in order: 3.2×10^{-8} cm^2 s^{-1} > 1.3×10^{-8} cm^2 s^{-1} > > 2.5×10^{-9} cm^2 s^{-1}, respectively. The values of dielectric constant (ε_r) and viscosity of the plasticizers are given in Table 4.3 [157,277]. It is evident from the Table 4.3 that the self-diffusion coefficient of I^- ions is highest in the sample made up of the plasticizer (NPOE) having higher ε_r and lower viscosity. Therefore, the values of D(I^-) in following NPOE > TEHP > DOP order indicates that both viscosity and ε_r of the plasticizer affects diffusion mobility of ions in the PIM matrix. The viscosity is known to influence the diffusion mobility of ions in liquid medium as described by Stokes-Einstein and Eyring's equations [278]. The greater local dielectric constant would lead to lower activation barrier for the anions to move between positively charged sites.

The measurement of the self-diffusion coefficient of water in the PIMs by radiotracer (HTO) is based on the assumption that the exchange occurs via displacement of HTO by H_2O in the membrane in contact with equilibrating water. This means that tritium transfer from a water molecule to another in pure water is negligible, and isotopic effect on diffusion mobility is also within uncertainty limit of the experimental measurements. The validity of these assumptions is based on the fact that the values of the self-diffusion coefficients of water traced by three isotopes D, T and ^{18}O have been found to be very close to each other [280].

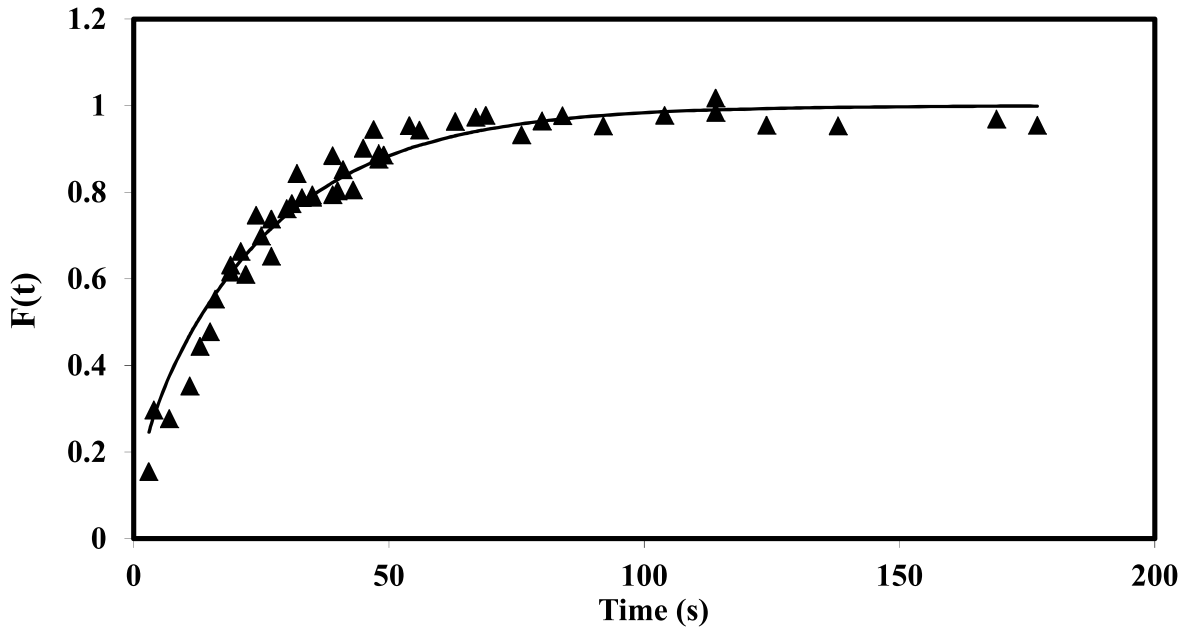

Fig. 4.6 *Fractional attainment of HTO-exchange equilibrium between equilibrating water and PIM sample in Cl⁻ form (N-3). Symbol and solid line represent experimental (normalized data of three experiments) and fitted data using* eq. 1.5*, respectively.*

Therefore, the HTO-exchange rate profiles have been analyzed using eq. 1.6 to deduce self-diffusion coefficients of water in the PIMs. The results of experiments and fitted data are shown in Fig. 4.6. The self-diffusion coefficients of water D(H_2O) measured in the membrane with Aliquat-336 and different plasticizers are given in Table 4.3. The self-diffusion coefficients of water in the PIMs are considerably lower than the self-diffusion coefficient of water in pure water (2.5×10^{-5} cm^2 s^{-1} at 25 ^{o}C) [281]. As values of D(H_2O) is one magnitude higher than the values D(I^-) ions in the membrane, the bulk water may be diffusing independent of the counterions. The apparent water diffusion coefficient in NPOE plasticized PVC based PIM has been reported to be 2x10^{-8} cm^2 s^{-1} [282]. This can be attributed to clustering of water in PVC based PIM [282,283]. There is a trend in the variation of D(H_2O) with counter ions in the membrane, though values are not drastically different. The comparison of data given in Table 4.3 indicates that the value of D(H_2O) in N-3 sample is slightly higher than that in T-3 and D-3 membranes. This may be due to higher dielectric constant of the NPOE than TEHP or DOP.

4.3.5. Effects of concentration of carrier on diffusion mobility

The other component of PIM that can significantly influence the diffusion mobility of the ions is the concentration of carrier (Aliquat-336) in the membrane. In order to study the effects of Aliquat-336 concentration on diffusion mobility, the values of D(I^-) in the PIMs having constant proportion of CTA and NPOE (1:1) and varying concentration of Aliquat-336 were deduced from $(^*I^-)_{mem} \rightleftharpoons (I^-)_{aq}$ exchange rate profiles and the values of D(I^-) are plotted against carrier concentration as shown in Fig. 4.7. As can be seen from this Fig., the value of D(I^-) has not changed significantly up to 0.5 meq g^{-1} concentration of Aliquat-336 in PIM. Thereafter, it has increased significantly from $(1.59\pm0.09)x10^{-8}$ cm^2 s^{-1} to $(3.18\pm0.08)x10^{-8}$ cm^2 s^{-1} at 0.6 meq g^{-1} concentration of Aliquat-336 in the membrane. Fontas et al. has also observed similar variation of $PtCl_6^{2-}$ anions initial flux vs. Aliquat-336 weight per unit area of the membrane consisting of NPOE plasticized CTA [159]. They has observed a Aliquat-336 concentration threshold is required to give a significant flux of Pt(IV) anionic species across PIM. After the threshold, initial flux varies linearly with Aliquat-336 concentration [159]. It is expected that the value of D(I^-) would not change with Aliquat-336 concentration if the transport of anions occur only through the carrier diffusion process. In the present work, the value of D(I^-) in PIM has varied with amount of plasticizer as well as its viscosity. These are characteristics of the 'carrier-diffusion' process. The variation of D(I^-) as a function of Aliquat-336 has shown a Aliquat-336 concentration threshold barrier in I^- ions diffusion. This indicated involvement of 'fixed-site hopping' in the transport process. The increase in value of D(I^-) with dielectric constant of plasticizer also support fixed-site hopping mechanism. Therefore, the mechanism of transport is neither pure carrier-diffusion nor fixed-site hopping. It may be intermediate of these two processes i.e. 'mobile-site hopping mechanism'. The mobile-site hopping transport mechanism would involve limited diffusion mobility of the carrier Aliquat-336 as well as hopping of anions between the mobile carriers. This is expected as Aliquat-336 has a long hydrocarbon chains, and its diffusion mobility may be limited in the high viscosity liquid channels.

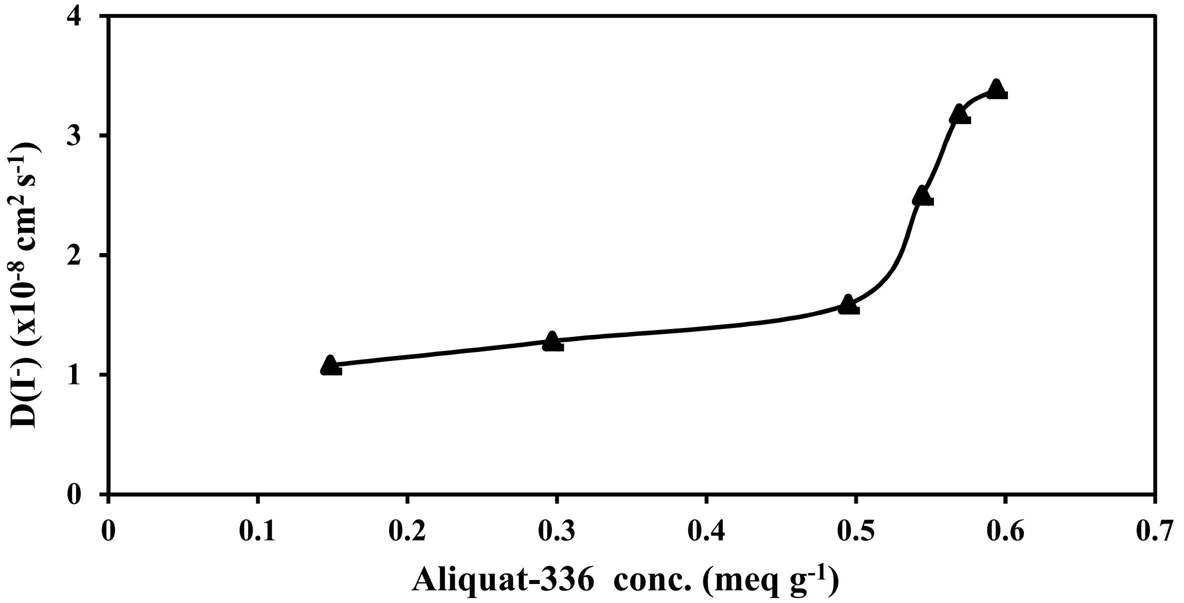

Fig. 4.7 *Variation of self-diffusion coefficients of* I^- *ions as a function of Aliquat-336 concentration in the membrane samples having fixed proportion (1:1) of CTA and NPOE. The concentration of Aliquat-336 in the membrane was varied by keeping of the amount of CTA = 0.40 ± 0.01 g, NPOE = 0.40 ± 0.01, and varying amount of Aliquat-336 from 0.05 to 0.26 g in 9 cm diameter membrane.*

4.3.6. Electrochemical impedance spectroscopy

Bulk resistance of N-3 membrane sample, loaded with different anion, was measured using EIS technique [276]. It is seen from the data given in Table 4.4 that the bulk resistance of the membrane sample varies significantly with different counterions. The membrane sample with NO_3^- counterions is found to have lower resistance as compared to that samples with Cl^-, I^-, or SO_4^{2-} counterions. This seems to indicate that NO_3^- ions have higher mobility in PIM than other anions. To understand variation in the self-diffusion mobility of anions in PIM, the data obtained from the EIS have been used to calculate the self-diffusion coefficients of anions using eq 4.2, and normalized with self-diffusion coefficient of I^- ions in the same membrane. The normalization with respect to I^- ions has been done as the self-diffusion coefficient of I^- ions in N-3 membrane sample has accurately been measured by the radiotracer method.

Among the four anions studied, NO_3^- ions has highest mobility and SO_4^{2-} ions has the lowest mobility in the membrane. The mobility of Cl^- and I^- ions are almost comparable. SO_4^{2-} ions is expected to bind with two anion exchanger molecules. Therefore, it has shown lower mobility as compared to that of the monovalent anions.

Table 4.4 *Self-diffusion mobility of anions in PIM (sample N-3) with respect to iodide ions* ($D(X^-) / D(I^-)$) *as obtained by Electrochemical Impedance Spectroscopy (EIS).*

Counter ions	Resistance (KΩ)	$D(X^-)/D(I^-)$
I^-	1.02±0.10	1.00
Cl^-	1.01±0.10	1.11
NO_3^-	0.42±0.05	1.66
SO_4^{2-}	0.86±0.10	0.45

4.3.7. Counterions exchange kinetics

The fluxes of the inter-changing counterions are governed by their inter-diffusion coefficients in the membrane matrix, which changes as the ion-exchange progresses. The Nernst-Planck theory predicts different rate of forward $(A^{n+})_{mem}\rightleftharpoons(B^{n+})_{aq}$ and reverse exchange $(B^{n+})_{mem}\rightleftharpoons(A^{n+})_{aq}$ in the case where inter-changing ions do not have same diffusion coefficients [35,284]. If the ion "A" initially present in the membrane has higher diffusion coefficient than the ion "B" (initially in the solution), then the exchange of "A" for "B" is faster than the reverse process, when "B" is exchanged for "A". In present work, NO_3^- and Cl^- anions forward and reverse exchanges with I^- ions have been studied. The experimentally measured counterion-exchange rate profiles are shown in Fig. 4.8 & 4.9. As seen in these figures, the forward $(I^-)_{mem}\rightleftharpoons(NO_3^-)_{aq}$ and reverse $(NO_3^-)_{mem}\rightleftharpoons(I^-)_{aq}$ exchange rate profiles are different, but forward and reverse exchange rate profiles of Cl^- with I^- ions are almost similar. This is because of the fact that NO_3^- ions has 1.66 times faster diffusion mobility than I^- ions in the same membrane, (see Table 4.4) Cl^- and I^- ions have comparable diffusion mobility, which would result in similar forward and reverse exchange rate profiles.

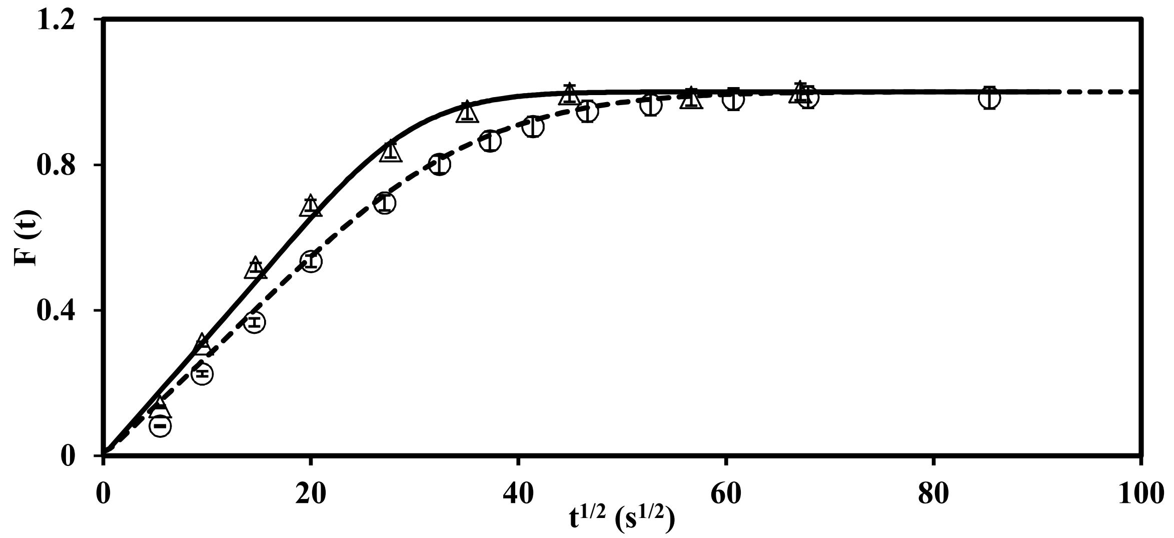

Fig. 4.8 *Profiles of fractional attainment of* NO_3^- *exchange equilibrium F(t) with* I^- *ions in membrane sample (N-3) as a function of square root of equilibration time t. The symbols Δ and O represent* $(NO_3^-)_{mem}\rightleftharpoons(I^-)_{aq}$ *and* $(I^-)_{aq}\rightleftharpoons(NO_3^-)_{mem}$ *exchanges, respectively. The solid and broken lines represent the predicted* $(NO_3^-)_{mem}\rightleftharpoons(I^-)_{aq}$ *and* $(I^-)_{mem}\rightleftharpoons(NO_3^-)_{aq}$ *exchange profiles, respectively, using Nernst-Planck equation for inter-diffusion of the exchanging counterions.*

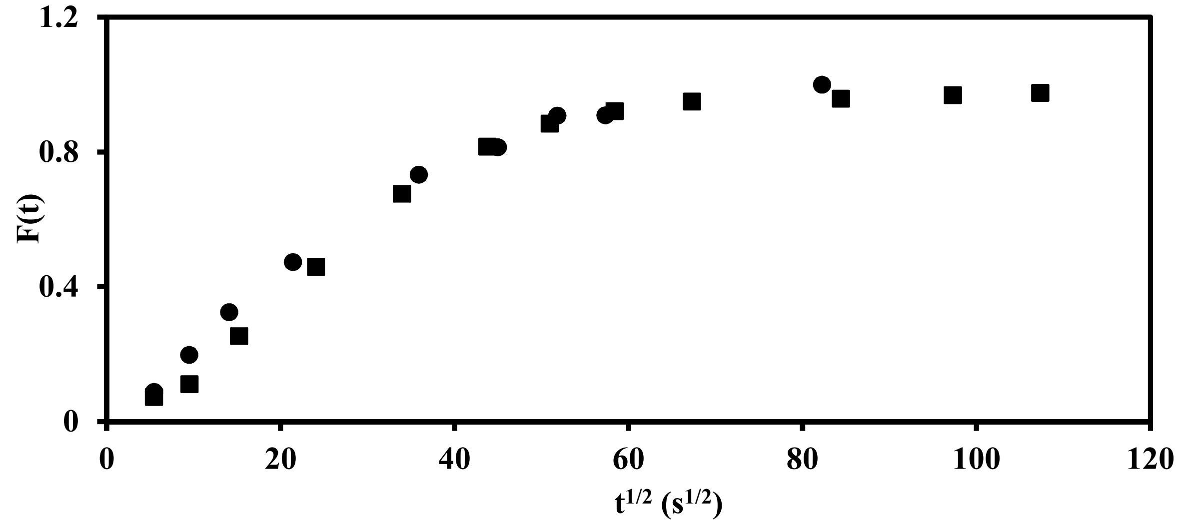

Fig. 4.9 *Profiles of fractional attainment of* Cl^- *exchange equilibrium F(t) with* I^- *ions in membrane sample (N-3) as a function of square root of equilibration time t. The symbols* ● *and* ■ *represent* $(Cl^-)_{mem}\rightleftharpoons(I^-)_{aq}$ *and* $(I^-)_{mem}\rightleftharpoons(Cl^-)_{aq}$ *exchanges, respectively.*

A numerical solution of the Nernst-Planck (N-P) equation for inter-diffusion has been used to interpret the kinetics of NO_3^- ions exchanges with I^- ions. The details of procedure are given elsewhere [35,284]. In this analyses, the exchange rate profiles have been obtained using values $D(I^-)$ and ratio $D(NO_3^-)/D(I^-)$ given in the Table 4.3 and Table 4.4, respectively. A reasonably good agreement between experimental and predicted exchange rate profiles clearly indicates that NO_3^- ions indeed have higher mobility in PIMs than the Cl^- and I^- ions.

4.4. Conclusions

The physical structure of PIM was studied by AFM of the samples having different compositions. The microscopy studies showed that PIMs are homogeneous gel-like membrane due to swelling of CTA with the plasticizer. The plasticizer was found to influence physical structure as well as diffusion mobility of the ions in the membrane matrix. However, the ion-exchange capacity of PIMs studied in the present work was not found be significantly dependent on nature and amount of the plasticizer. The heating thermograms of DSC indicated that the crystalline phases of CTA did not disappear even in the presence of high amount of the plasticizer in the membrane. However, the crystalline phase of CTA was significantly affected by the Aliquat-336 and plasticizer. The self-diffusion mobility of I^- ions in the PIM was found to be affected by the dielectric constant and viscosity of the plasticizer used in the preparation of the PIM. The variation of $D(I^-)$ as a function of Aliquat-336 concentration seems to suggest that transport of the anions could be enhanced significantly by increasing the amount of the carrier in the membrane. The self-diffusion coefficients of water in PIMs were found to one magnitude higher than the self-diffusion coefficients of iodide ions. This indicated that water molecules diffuse across the PIM independent of counterions. The electrochemical impedance spectroscopic and counterions-exchange kinetics studies indicated the variation of self-diffusion mobility of anions in order: $NO_3^- > Cl^- \approx I^- > SO_4^{2-}$.

Chapter - 5

In situ formation of gold nanoparticles in polymer inclusion membrane

5.1. Introduction

Synthetic polymer membranes are being developed for a variety of advance applications such as chemical sensors, actuators, fuel cell, water splitting, sequestering of ions etc. [105]. Many of these applications require tuning of the membrane properties by manipulating physical or chemical architecture of the membrane [132,245,285]. Nanoparticles (nps) have the characteristic properties that would be highly useful in a specific application [15,16]. Therefore, anchoring of the desirable nanoparticles in the membrane matrix would significantly enhance the functional property of the membrane.

In situ formation of nanoparticles in a cation-exchange membrane from the anionic species like $AuCl_4^-$ is complicated due to exclusion of anion from cation exchange matrix. Polymeric inclusion membrane prepared with a liquid anion-exchanger can facilitate transfer of anionic metal ions to the membrane matrix. Metal nanoparticles can be formed by subsequent reduction of anionic species to zero valence state in the membrane matrix. It is interesting to note that there is a possibility of tuning spatial distribution of the metallic nanoparticles in the matrix of membrane by appropriate manipulation of the ion-exchange process involved in formation of the nanoparticles [185,189].

In the present chapter, we have explored a plasticized anion-exchange membrane as a tunable host for stable metal nanoparticles. The host membrane was prepared by physical immobilization of a liquid anion exchanger trioctylmethylammonium chloride (Aliquat-336) in the matrix formed by cellulose triacetate (CTA) plasticized with different plasticizer. The choice of different components in the membrane has been based on the considerations for obtaining the optically transparent and stable anion-exchange host membrane for metal nanoparticles. Metal anions are transferred in the membrane matrix by anion-exchange process and these membranes are subsequently reduced with BH_4^- to form nanoparticles in the membrane matrix. The metal nanoparticles embedded membrane samples have been characterized with different techniques to obtain information on the size, shape and spatial distribution of nanoparticles in the membrane. The information obtained from these studies has been used for understanding the mechanism involved in the formation of nanoparticles in the polymer inclusion membrane. The self-diffusion coefficient of I^- ions have been measured to evaluate the change in diffusional transport properties of the membrane after incorporation of metal nanoparticles.

5.2. Experimental

5.2.1. Reagents and apparatus

Reagent and apparatus used for the studies discussed in this chapter is described in the chapter 4 section 4.2.1.

5.2.2. Preparation of the membrane

Membrane samples were prepared by casting of the solution containing 0.2 g of cellulose triacetate (CTA) and varying amounts of a plasticizer and Aliquat-336 [265]. The detailed procedure for the preparation of membrane is explained in the chapter 4, section 4.2.2. The membranes were cut into the (2x2 cm) pieces of required dimensions for the experiments. The membrane samples were stored in 0.1 mol L^{-1} NaCl solution to keep them in Cl^- forms.

5.2.3. Synthesis of metal nanoparticles in the membrane

The membrane samples (2x2 cm) were equilibrated with 15 mL of 0.01 mol L^{-1} $HAuCl_4$ solution for overnight. These $AuCl_4^-$ loaded membrane samples were reduced by immersing them in 25 mL of well stirred 0.1 mol L^{-1} $NaBH_4$ solution for 30 min at 25 ^oC. After reduction, membrane samples were thoroughly washed with water and conditioned with 0.1 mol L^{-1} NaCl.

To increase the Au^0 contents in the membrane sample having fixed composition, the cycle of loading and reduction of $AuCl_4^-$ anions in the membrane matrix were repeated up to three times. After each cycle, the membrane sample was conditioning with 0.1 mol L^{-1} NaCl.

5.2.4. Characterization

5.2.4.1. UV-Vis spectroscopy

UV-Vis spectra of Au nanoparticles embedded membrane samples were recorded using UV-Vis Spectrophotometer (V-530, JASCO, Japan). The absorbance measurements were carried out by mounting the sample (1x2 cm) on to the inside wall of a (1x1x3 cm) quartz cell and placing it in a spectrophotometer to record spectrum with respect to air.

5.2.4.2. TEM

The membrane samples were sectioned under cryogenic conditions in Leica ultramicrotome to 70 nm thickness for TEM analyses. The sections were picked on 200 mesh Cu grids. The grids were examined in an FEI Technai G2 electron microscope in IIT Bombay [Central Facility at SAIF], Mumbai at 120 KeV without any staining or post-treatment. The sizes of nanoparticles were measured manually using the image analyser software (Image Z, version 1.33 U).

5.2.4.3. EDXRF analyses

Energy dispersive X-ray fluorescence (EDXRF) measurements of membrane samples were carried out using Total reflection X-ray fluorescence spectrometer IX-2000 provided with EDXRF geometry (ITAL STRUCTRES, Italy). W L_α (8.398 keV) radiation was used as excitation source for EDXRF measurements.

5.2.4.4. XRD analyses

X-ray diffraction (XRD) measurements of the membrane were carried in the range of 2θ (10-70°) for phase identification using monochromatized Cu-K_α ($K_{\alpha1}$ = 1.5406 Å and $K_{\alpha2}$ = 1.5444 Å) radiation by Philips X-ray diffractometer Model PW 1710, Netherlands. Silicon was used as an external standard for correction due to instrumental broadening.

5.2.4.5. Dead end cell experiment

To reduce $AuCl_4^-$ from one side of membrane, the $AuCl_4^-$-loaded membrane sample was mounted on a dead end cell (volume=15 cm^3, and 2.5 cm dia.) that ensured the contact of only one surface of membrane with $NaBH_4$. The design of dead end cell is shown in Fig.2.2. This cell was filled with 10 mL of $NaBH_4$ (0.1 mol L^{-1}) solution. The solution was stirred using magnetic stirrer for 30 min. After the reduction, the membrane samples were washed with deionized water and equilibrated with 0.1 mol L^{-1} NaCl.

5.2.5. Measurement of anion-exchange capacity

Total ion exchange capacity available in the membrane samples (2 x 2 cm pieces) were measured by the procedure explained in the chapter 4, section 4.2.4. Total available ion exchange capacity for nanoparticles loaded membrane was also measured in similar way using the equation 4.3.

5.2.6. Measurements of self-diffusion coefficients

The measurements of self-diffusion coefficients of I^- ions in the PIMs with and without nanoparticles were carried out by radiotracer method. The details procedure for the measurements of self-diffusion coefficients by radiotracer method is described in the chapter 4, section 4.2.5.

5.2.7. Interactions of the counter ions with nanoparticles

The Au nanoparticles embedded membrane samples containing fixed proportion of CTA, DOP, and Aliquat-336 were equilibrated with 0.1 mol L^{-1} aqueous solutions of sodium or potassium salts of CH_3COO^-, ClO_4^-, I^-, Cl^-, and molecular iodine. The characteristic surface plasmon band (SPB) of Au nanoparticles at ≈ 530 nm was monitored to study the interactions of different anions and I_2 with Au nanoparticles in the membrane matrix.

5.3. Results and discussion

As described in the previous chapter, the formation of nanoparticles in ion exchange membrane involves two steps process i.e. loading of precursor ions and their subsequent reduction with reducing agent. The loading of the precursor ion in the membrane would depend upon ion exchange capacity of the membrane. Therefore, ion exchange capacity plays an important role in controlling the amount of nanoparticles in the membrane matrix.

5.3.1. Anion exchange capacity

The compositions of the membrane samples having a varying concentration of Aliquat-336 are given in the Table 5.1. The expected and experimentally determined anion-exchange capacities of the membranes are also given in the Table 5.1. The anion-exchange capacity of the membrane sample increased with the increase in concentration of the Aliquat-336. However, the experimentally measured anion-exchange capacities have been found to be lower than those calculated from the concentration of Aliquat-336 in case where the membrane samples have higher fraction of Aliquat-336. This seems to suggest the inaccessibility of some of the Aliquat-336 molecules for the ion exchange processes in the membrane matrix.

Table: 5.1 *Composition and anion-exchange capacities of the membranes.*

Membrane Id.	CTA (wt%)	DOP (wt%)	Aliquat-336 (wt%)	I.E.C. (Cal)[a] (meq g^{-1})	I.E.C.(Exp)[b] (meq g^{-1})
M-1	46.5	46.5	7.0	0.17	0.16
M-2	44.5	44.5	11.0	0.32	0.24
M-3	38.5	38.5	23.0	0.57	0.48

[a] *Calculated from concentration of Aliquat-336 in the membrane.* [b] *Experimentally measured using radioactivity tagged* (^{131}I) I^- *ions. The uncertainty in the experimentally measured I.E.C. was on the order of 5%.*

5.3.2. Preparation of Au nanoparticles in the membrane

The $AuCl_4^-$ loaded membrane samples has been placed in the well-stirred 0.1 mol L^{-1} aqueous solution of $NaBH_4$ at 25°C. The characteristic color of Au nanoparticles ($\lambda_{max} \approx 530$ nm) appeared immediately on contact with $NaBH_4$ solution. This indicates the onset of *in situ* reduction of $AuCl_4^-$ with BH_4^- and formation of Au nanoparticles in the membrane matrix. The external solution also acquired a low intensity color of characteristic Au nanoparticles, indicating a slight loss of $AuCl_4^-$ ions from membrane matrix due to their exchange with BH_4^- ions or loss of Au nps from the surface. The process of formation of Au nanoparticles in membrane matrix has almost been completed in 30 min.

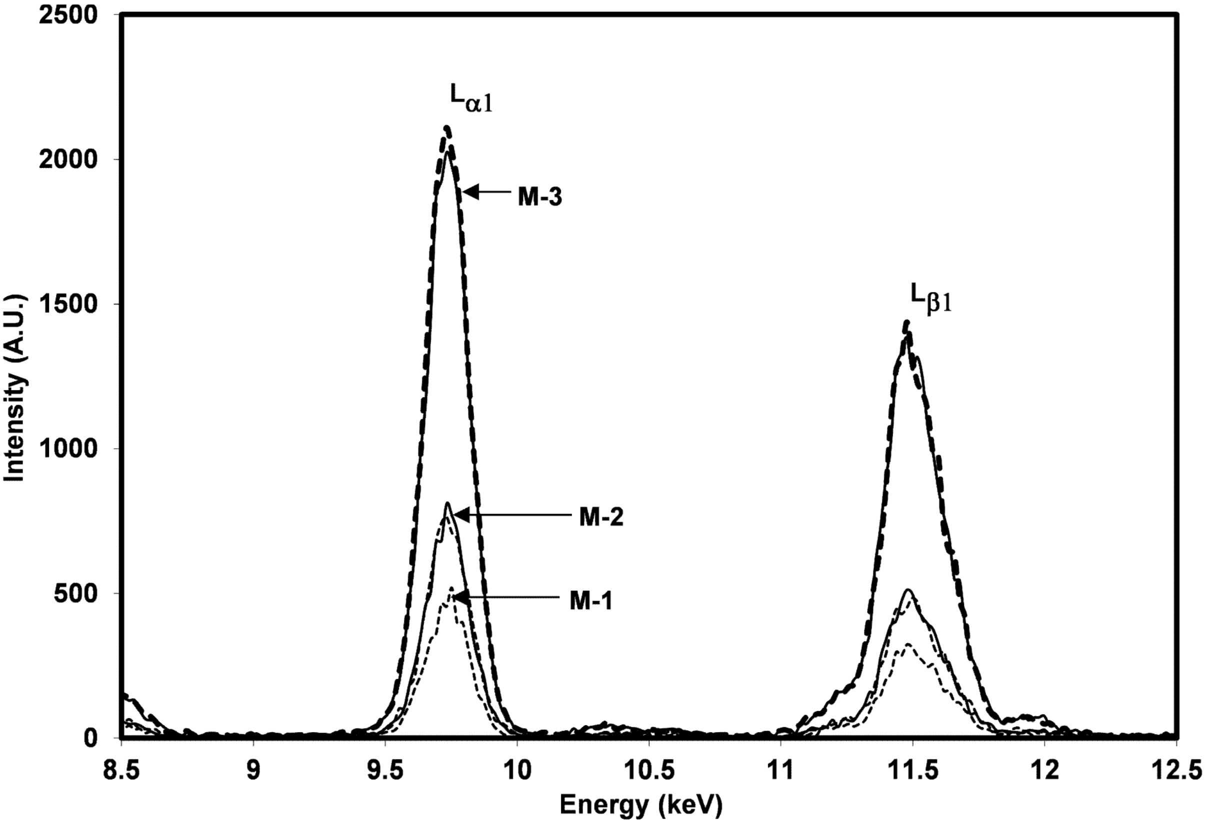

Fig. 5.1 *EDXRF spectra of the membrane samples equilibrated with 0.01 mol* L^{-1} $AuCl_4^-$ *ions. The solid and dash lines represent two surfaces of the membrane sample.*

Energy-dispersive X-ray fluorescence (EDXRF) analyses of both the surfaces of $AuCl_4^-$-loaded membrane samples are shown in Fig. 5.1. It is seen form this figure that Au contents in the membrane samples increased corresponding to increase in the ion-exchange capacity (Aliquat-336) of the membrane sample and $AuCl_4^-$ ions are uniformly distributed on both surfaces of the membrane sample.

The preparation of Au nanoparticles has also been carried out by reversing the processes involved in the formation of Au nanoparticles; i.e., the membrane sample has been first loaded with BH_4^-, and then placed in the solution containing $AuCl_4^-$. Au nanoparticles have been formed in the membrane, though the intensity of the surface plasmon band ($\lambda_{max} \approx 530$ nm) is significantly lower than the earlier case in which $AuCl_4^-$ –loaded membrane has been equilibrated with BH_4^-.

5.3.3. One side reduction in dead end cell

The effect of the plasticizer in the formation of Au nanoparticles has been studied by reducing the $AuCl_4^-$-loaded membrane with BH_4^- from one side in a dead end cell as shown in Fig.2.2. After reduction, the membrane samples have been equilibrated with the 0.1 mol L^{-1} NaCl solution to ensure the removal unreduced $AuCl_4^-$ ions from the membrane, if any. The EDXRF analyses of both the surfaces of BH_4^- equilibrated membrane samples are compared in Fig. 5.2. The penetration depth of X-ray photons in membrane may not be more than 8-10 μm which is lower than the thickness of the membrane samples (≈50 μm). Therefore, the

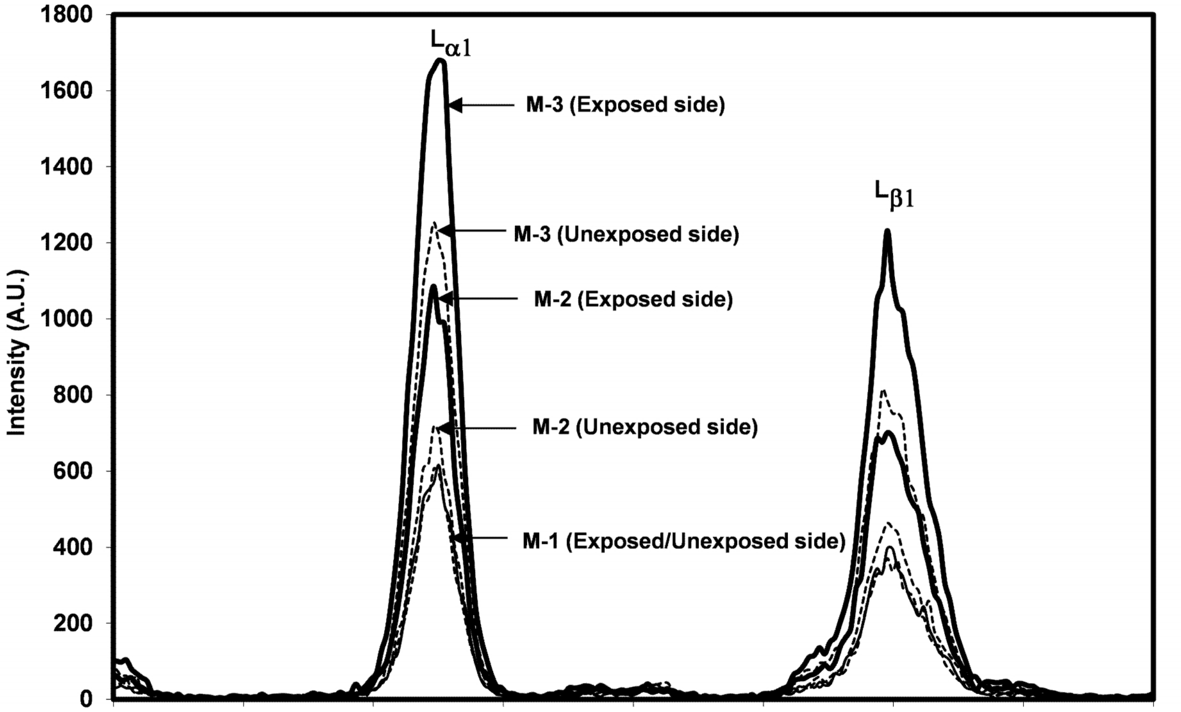

Fig. 5.2 *EDXRF spectra of the membrane samples after one side reduction with BH_4^- ions.*

significant difference in concentrations of Au nanoparticles on surface layers of membrane can be detected by the EDXRF analyses of reductant-exposed and unexposed surfaces of the membrane sample. It is seen from this figure that the Au concentration is significantly higher on the side exposed to BH_4^- ions than unexposed side in the membrane samples M-2 and M-3. However, there is no significant difference in Au concentrations on exposed and unexposed surfaces of M-1sample, which has lowest ion-exchange capacity among the membranes prepared in the present work. The presence of Au nanoparticles on both surfaces of one side reduced membrane samples indicates that BH_4^- invades the interior of the membrane and reduction occurs inside the matrix of membrane. In membrane with higher ion-exchange sites (M-3), the reduction is more on the side exposed to BH_4^- ions due to faster rate of transfer of $AuCl_4^-$ from interior to the exposed surface of the membrane. This would give rise to more Au nanoparticles concentration on the side exposed to BH_4^- ions.

5.3.4. Multiple cycles of loading and reduction

The ion-exchange capacity of the membrane sample has been measured after the formation of Au nanoparticles using radioactivity tagged I^- ions. The bulk of ion-exchange sites (≈80%) in the membrane sample have been found to be readily available for ion-exchange after the formation of Au nanoparticles in the membrane, see Table 5.4. This led to a possibility of increasing Au nanoparticles content in the membrane using the sequential cycles of loading of $AuCl_4^-$ ions followed by the reduction. A series of membrane samples have been prepared using varying concentration of aliquat -336 with different plasticizers (DOP, NPOE & TEHP). Compositions of these membranes are shown in Table 5.2. Multiple cycles of Au nanoparticles synthesis has been carried out in these membranes to increase Au nanoparticles content in the membrane matrix, which has been confirmed by EDXRF analyses. Thus, the amount of Au nanoparticles in the membrane matrix can be controlled either by concentration of the carrier (Aliquat-336) in the membrane or by keeping the fixed concentration of the carrier in membrane and repeating the cycles of loading and reduction.

5.3.5. Characterization of Au nanoparticles

As shown in Fig. 5.3, λ_{max} of surface plasmon band (SPB) of Au nanoparticles is at 530 nm and the intensity of SPB increases with equilibration time of the membrane samples with $NaBH_4$ solution. It is also seen from the Fig. 5.3 that width of SPB and λ_{max} has not changed with increase in its intensity as a function of reduction time. It indicates that Au nanoparticles have grown up to the finite size.

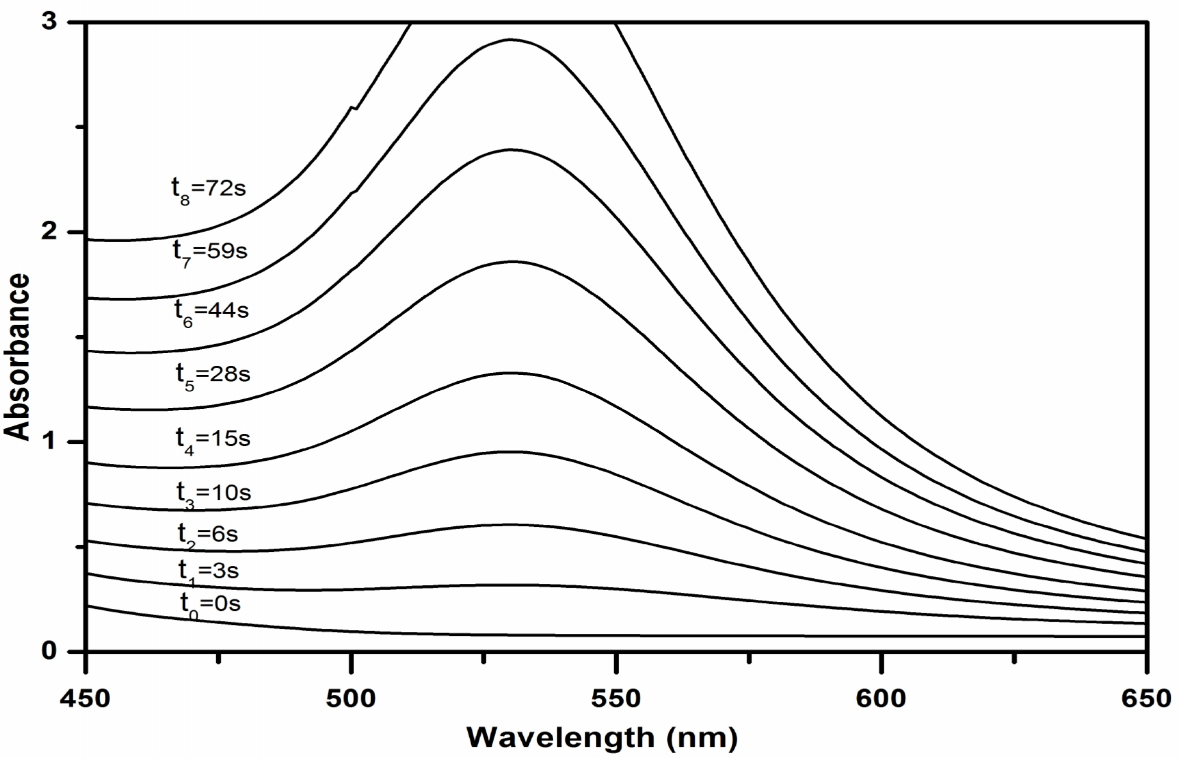

Fig. 5.3 *UV–Vis spectra of* $AuCl_4^-$*-loaded membrane sample (M-2) after equilibration in solution containing* BH_4^-.

In solid-phase immobilization, carrier-mediated agglomeration of nanoparticles and a coupling of the SPB due to inter-particles interactions lead to the emergence of another band, which is usually red-shifted as compared to the original feature. Therefore, absence of any change in SPB indicates that increase in Au nanoparticles in membrane has not led to agglomeration or inter-particles interactions. The λ_{max} and intensity of SPB of Au nanoparticles embedded in the matrix of membrane has been found to remain unaltered over a period of month for the samples kept in water as well as in air under ambient conditions. This indicated that Au nanoparticles are quite stable in the membrane. The high stability of Au nanoparticles in membrane can be attributed to steric stabilization of nanoparticles by the plasticized polymer matrix.

X-ray diffraction patterns of the membrane samples, after reduction with BH_4^- ions, contain broad peaks at scattering angles (2θ) corresponding to 111, 200, and 220 planes of the face centered cubic phase of Au as shown in Fig. 5.4. It indicates that Au nanoparticles formed in the membranes are nanocrystallites. Therefore, broadening of the diffraction peak width of Bragg reflection of 111 plane has been analyzed to estimate the average size of Au nanoparticles embedded in the membrane using Debye-Scherrer equation as explained in chapter 1, section 1.5.4 [196]. It is clear from the data given in Table 5.2 that the average size of Au nanoparticles formed in membranes having different plasticizers ranges from 7 to 13 nm. Also, the average size of Au nanoparticles has not increased significantly by increasing content of Au^0 in the membrane. The amount of Au^0 in the membrane matrix has been increased either by subjecting the membrane sample to multiple cycles of loading and reduction of $AuCl_4^-$ ions or in single cycle by increasing concentration of the carrier Aliquat-336 in the membrane matrix. The inability of Au nanoparticles to increase their sizes significantly indicates that the Au nanoparticles grow only up to certain size in the membrane due to steric hindrance caused by the polymer chains network in the membrane matrix. It is expected that membrane matrix would be more rigid in the absence of the plasticizer. It is evident from Table 5.2 that size of Au nanoparticles formed in membrane without plasticizer is smaller even though the carrier (Aliquat-336) concentration is quite high. It indicates that by increasing Au metal content in the membrane, the number density of Au nanoparticles has increased in the membrane rather than their sizes.

Table 5.2 *Size of Au nps formed in the polymer inclusion membranes as obtained from the analyses of XRD.*

S. ID	Plasticizer	Synthesis cycle	CTA (wt.%)	Plasticizer (wt.%)	Aliquat-336 (wt.%)	Particle size (A^{o})
M-4	DOP	1st	46.5	46.5	7	70
M-5	DOP	2nd	46.5	46.5	7	89
M-6	DOP	3rd	46.5	46.5	7	115
M-7	DOP	1st	38.5	38.5	23	93
M-8	DOP	2nd	38.5	38.5	23	108
M-9	DOP	3rd	38.5	38.5	23	128
M-10	DOP	4th	38.5	38.5	23	129
M-11	NPOE	1st	38.5	38.5	23	67
M-12	NPOE	2nd	38.5	38.5	23	103
M-13	TEHP	1st	38.5	38.5	23	103
M-14	TEHP	2nd	38.5	38.5	23	106
M-15	TEHP	3rd	38.5	38.5	23	76
M-16	TEHP	4th	38.5	38.5	23	146
M-17	No plasticizer	1st	62.5	0	37.5	76

The TEM images of membrane (M-2) (Fig.5.5) showed that the Au nanoparticles are nearly spherical and homogeneously dispersed in the matrix of membrane. The distribution of size of Au nanoparticles in membrane obtained from TEM images has been found to be narrow and the average size of Au nanoparticles is around 10 nm which is in close agreement with the size obtained from the analysis of broadening of the X-ray diffraction peak width. It is evident that Au nanoparticles are dispersed throughout the membrane matrix but excluded from the surface as shown in Fig. 5.5 (b). A possible mechanism involved in the formation of Au nanoparticles in plasticized anion-exchange membrane can be formulated as shown in Fig. 5.6. When plasticized membrane is equilibrated with $HAuCl_4$ solution, the $AuCl_4^-$ ions enter in the membrane by replacing Cl^- ions from quaternary ammonium cation (Aliquat-336). During reduction, the $AuCl_4^-$ ions present at the surface of membrane interact with BH_4^- ions and get reduced or exchanged with BH_4^- ions. The exclusion of Au nanoparticles from the surface may be due to exchange of $AuCl_4^-$ ions with BH_4^- ions or due to loss of Au nps from the surface during equilibration of the membrane sample in the reducing solution. This would result in loss of Au from the surface and invasion of BH_4^- ions (reductant) to interior of the membrane. After initial interaction at the surface, the BH_4^- may have invaded interior of membrane matrix leading to reduction of $AuCl_4^-$ in the bulk. The counterion-exchange process allows BH_4^- to enter in the membrane as an ion-pair with Aliquat-336.

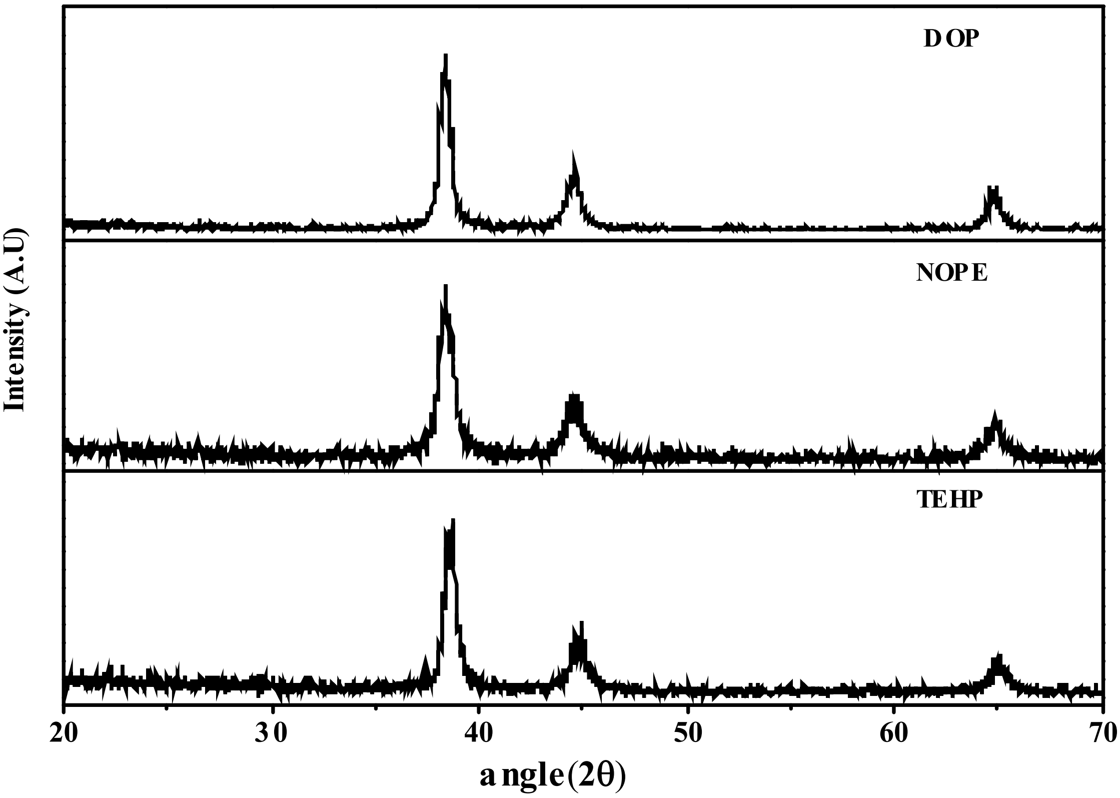

Fig. 5.4 *XRD of Au nps embedded PIMs having same compositions but different plasticizers.*

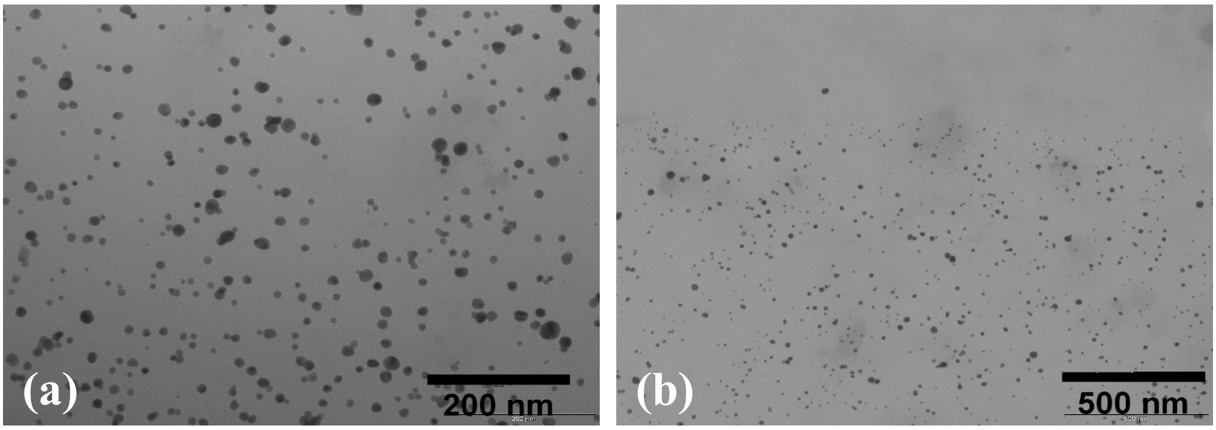

Fig. 5.5 *TEM image of cross-section of the membrane (M-2)showing distribution of Au nps (a) at the interior of the membrane and (b) near the surface of membrane.*

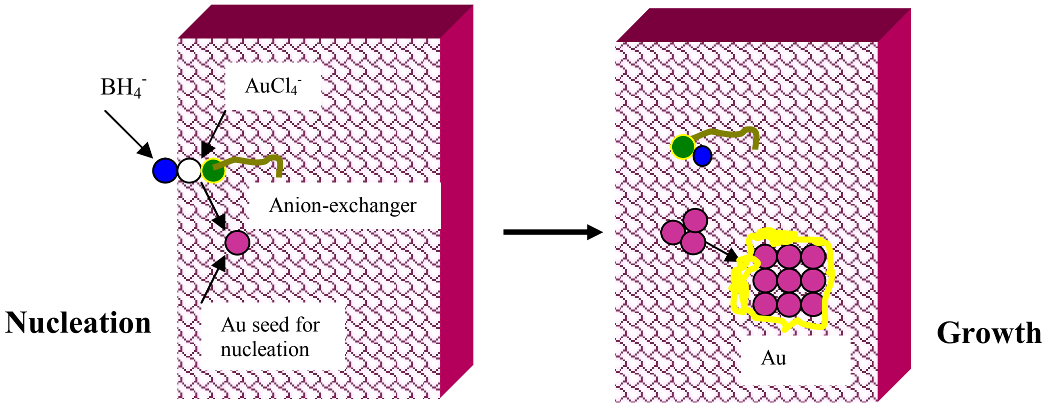

Fig. 5.6 *Schematic representation of formation of Au nps in the matrix of plasticized anion-exchange membrane.*

On increasing Au content in the membrane in second cycle of synthesis, the size dispersion range has broadened to 5-20 nm without changing the average sizes of nanoparticles see Fig. 5.7 (a). A few nanostructures (prism, rod, sphere, bipyramid, and cuboids), as shown in Fig. 5.7 (c), have been observed in the membrane matrix. However, the bulk of the Au remains as the spherical nanoparticles.

The nanostructures are mostly nanospheres of average size 72 nm and distribution from 43-107 nm. These are distributed throughout and corresponded to ≈ 5 % of total number of nanoparticles in the membrane matrix. The bands of high conc. of nanoparticles have also been observed inside the membrane, as shown in Fig. 5.7 (b). This may be due to formation of CTA strands entangled with Aliquat-336 at low plasticized zone at the interior of membrane.

5.3.6. Diffusional transport properties

In order to study the effects of Au nanoparticles on the diffusion mobility of the anions, the self-diffusion coefficients of I^- ions have been measured using the radiotracer method. The isotopic-exchange profiles of radioactivity tagged I^- ions diffusing out of the membrane samples, with and without Au nanoparticles, as a function of time have been analyzed by the method described in the chapter 1, section 1.5.1 . The ion-exchange capacity of the membrane sample has been measured before and after formation of the Au nanoparticles using radioactivity tagged I^- ions. The experimental and fitted data of the isotopic-exchange profiles of I^- ions in the membrane samples are shown in Fig.5.8, and values of self-diffusion coefficient (D) are given in Table 5.3. It is seen from Fig. 5.8 and Table 5.3 that the self-diffusion mobility of iodide ions has increased significantly after formation of the Au nanoparticles in membrane matrix.

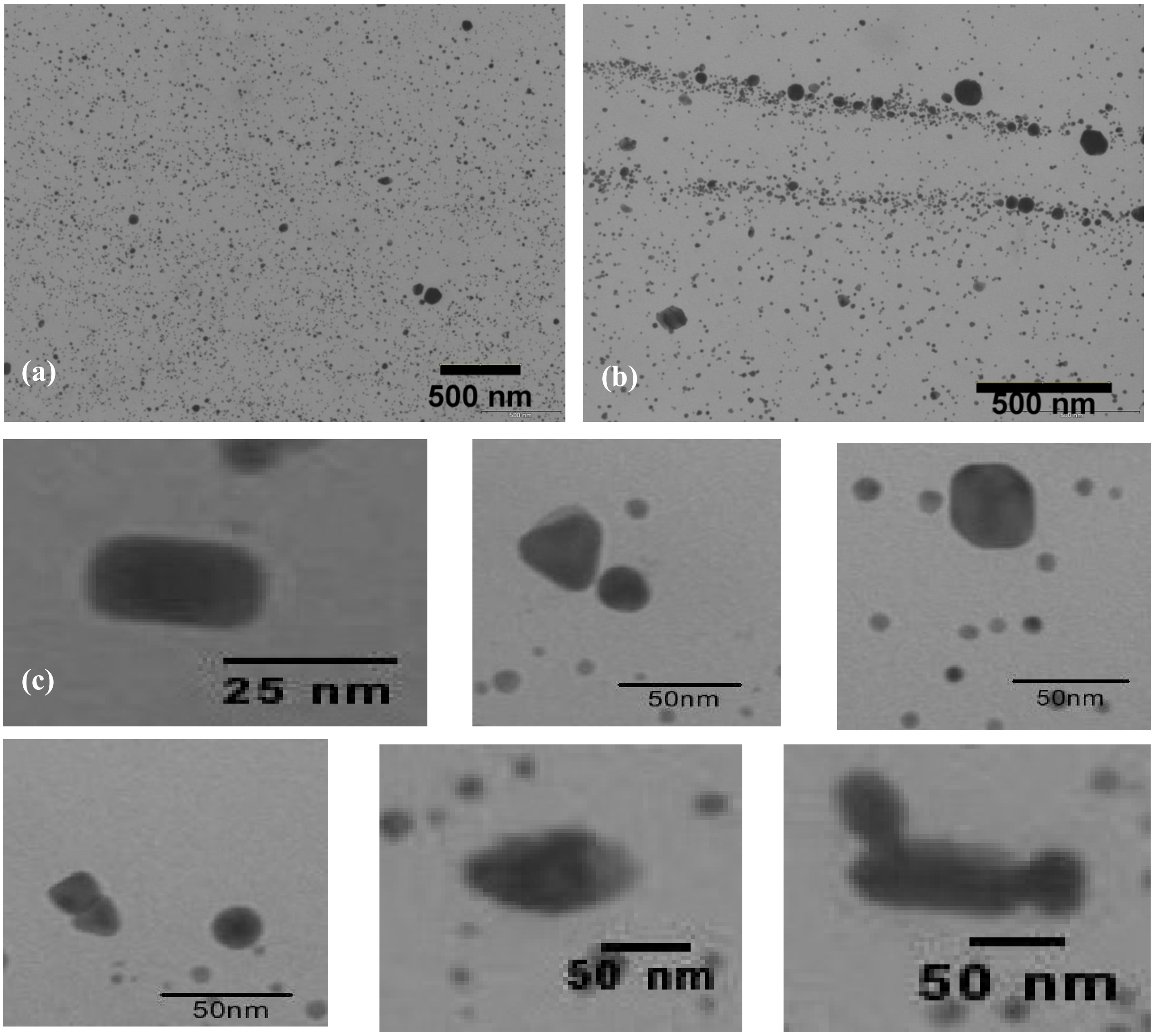

Fig. 5.7 *TEM images of cross-section of the membrane (M-2) after second cycle of loading and reduction. (a) bulk spatial distribution of Au nps (b) the bands of high concentration of Au nps formed at a few places in the interior of membrane (c) nanostructures formed in the membrane.*

Table 5.3 *Comparison of ion-exchange capacity and self-diffusion coefficients (D) of I^- ions in the membrane samples before and after formation of Au nanoparticles. Membrane composition was kept as a CTA = 45 %, DOP = 45 wt %, and Aliquat-336= 10 wt, %.*

Cycle of Au nps synthesis	Relative Ion-exchange capacity	D (I^-) (x 10^{-9} cm^2 s^{-1})
Nascent membrane	100 %	3.2 ± 0.2
After 1st cycle of synthesis	78.3 %	4.4 ± 0.4
After 2nd cycle of synthesis	76.3 %	7.0 ± 0.6
After 3rd cycle of synthesis	70.5 %	7.3 ± 0.6

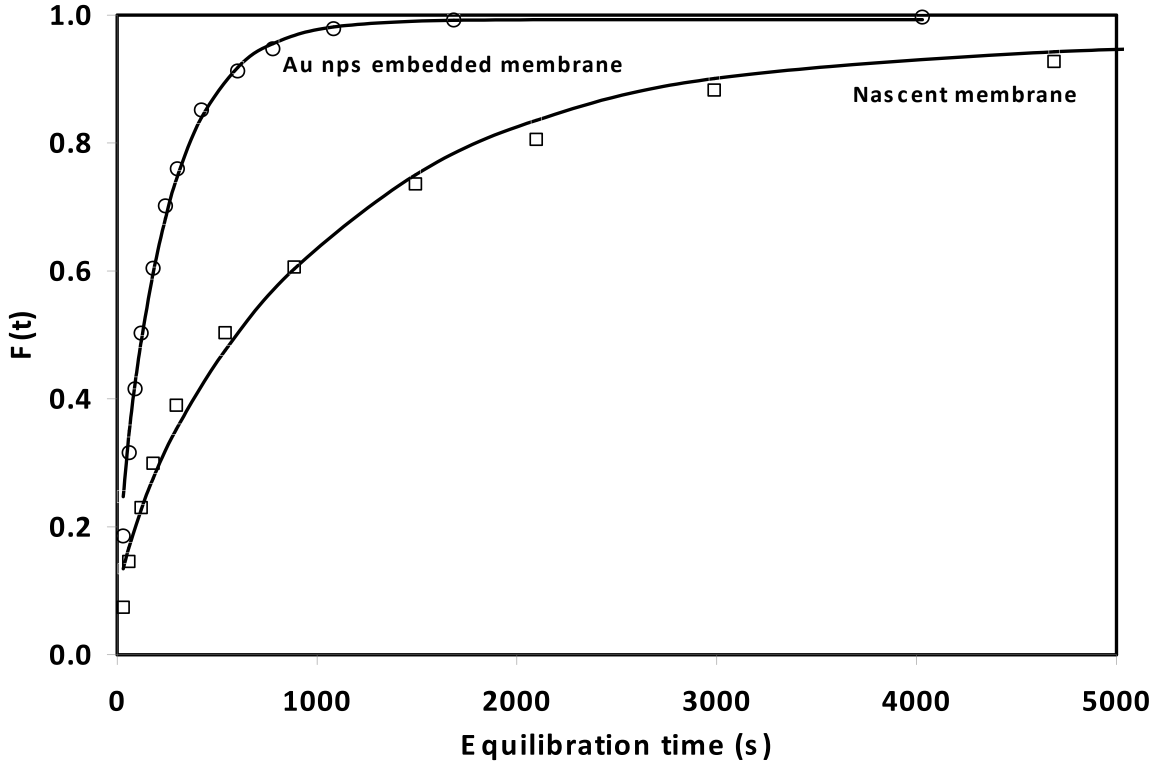

Fig. 5.8 *Variation of Isotopic-exchange rate $F(t_k)$ of I^- ions between the membrane and equilibrating aqueous salt solution as a function of time. Symbols and solid lines represent experimental and fitted data in equation 1.5, respectively.*

After second cycle of Au synthesis, the self-diffusion coefficient of I^- ions has increased 2 times of that in the membrane without nanoparticles. The higher diffusion mobility of I^- ions seems to indicate that tortuosity of the membrane diffusion channels might be reduced after the formation of the Au nanoparticles, which would decrease the effective diffusion path length of the anions. The inclusion of nanoparticles may create defects at the interfaces and in the matrix that will constitute preferential pathway for the ions.

The ion-exchange capacities of the membrane sample have been measured before and after formation of the Au nanoparticles using radioactivity tagged I^- ions. As can be seen from Table 5.3, (≈ 80% of the anion-exchange sites are readily available for exchange process after formation of the Au nanoparticles. The maximum loss of ion-exchange sites have been observed in the first cycle of synthesis, and thereafter it remains almost unaltered. The availability of bulk of Aliquat-336 (trioctylmethyl ammonium chloride) indicates that it has not capped the Au nanoparticles like cetyl trimethylammonium bromide (CTAB) reported in the literature [286], and its role is confined to transfer $AuCl_4^-$ ions in the membrane matrix. The reduction in the ion exchange capacity can be attributed to inaccessibility of ion exchange site due to formation of Au nanoparticles.

5.3.7. Interactions of Au nanoparticles with counterions

The surface plasmon band ($\lambda_{max} \approx 530$ nm) of Au nanoparticles has not changed on equilibration of the membrane samples with the solutions containing Cl^-, I^-, ClO_4^- and CH_3COO^- anions as shown in Fig. 5.9. This is contrary to the plasticized PVC membrane in which preformed Au nanoparticles were dispersed [287]. This Au nanoparticles embedded PVC membrane was found to change its color on equilibration with I^- ions. In present case, anions ions bind electrostatistically with Aliquat-336, which would minimize the interaction of anions with the Au nanoparticles in membrane matrix. It is seen from Fig. 5.9 that the characteristic surface plasmon band of Au nanoparticles has been completely disappeared in the membrane sample equilibrated with aqueous solution containing molecular iodine. Molecular iodine is soluble in the organic phase (plasticizer) present in membrane matrix. Molecular iodine would be able to interact with Au nanoparticles embedded in the plasticized CTA matrix. This indicated that Au nanoparticles are located in the transport channels formed by liquid fraction in the membrane. Hence, Au nanoparticles have been oxidized by I_2 in the membrane matrix.

$$Au + 2I_2 \rightarrow AuI_3 + I^-$$

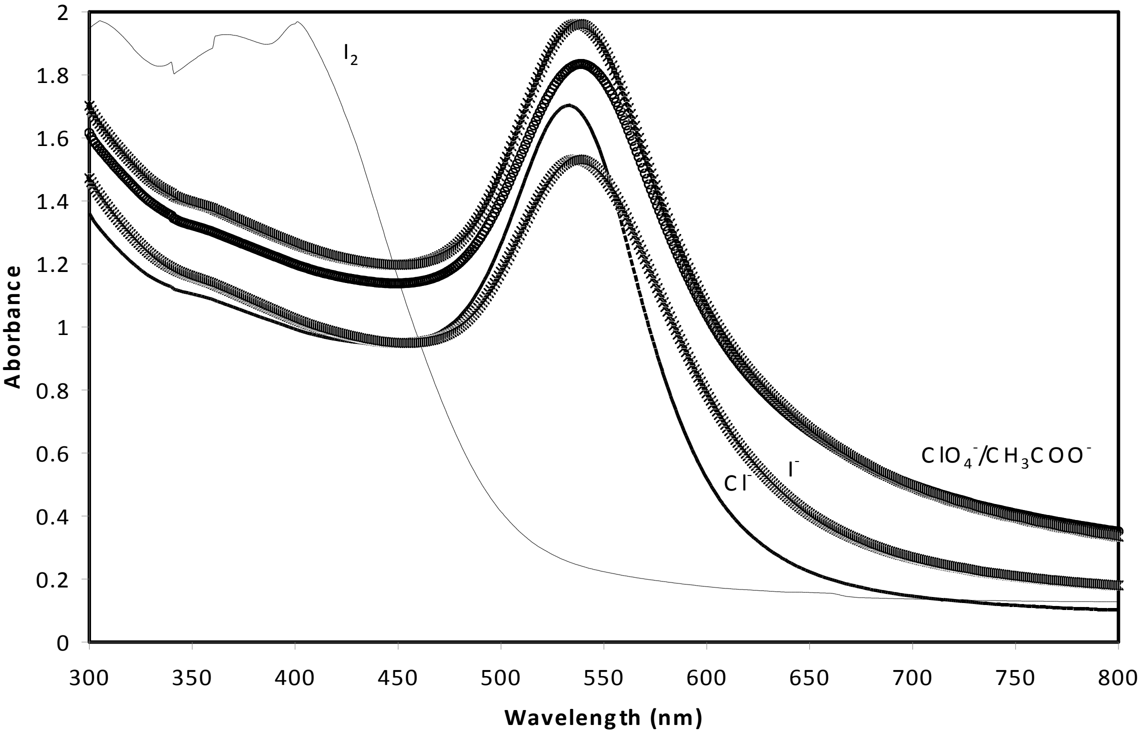

Fig. 5.9 *UV-Vis spectra of Au nanoparticles embedded in PIM after equilibration with the solutions containing different anions and molecular iodine.*

5.4. Conclusions

The present study demonstrates the possibility of using the polymer inclusion membrane as a stable host for metal nanoparticles. The metal nanoparticles can be prepared by the ion-exchange and reduction process involving the carrier that transfer desirable metal ions in the membrane. These homogeneous membranes are easy to construct, can be tailor made, and have good optical properties. Au content in the membrane can be increased by increasing the concentration of the carrier in the membrane as well as repeating the cycle of nanoparticles synthesis. The increase in Au^0 content in the membrane did not alter the average size of Au nanoparticles significantly, but slightly increased the size distribution. As seen in the present work, the ion-exchange sites are readily available after the formation of nanoparticles. This leads to the possibility of synthesizing the bimetallic or two different kinds of metal nanoparticles in same membrane matrix using sequential cycles of loading of relevant metal ions followed by the reduction. The formation of Au nanoparticles in the membrane improved its diffusional transport properties. This would significantly reduce the response time of the chemical sensor based on membrane as the permeation rates of the target ions across the membrane would be increased significantly. The presence of different anions did not affect the surface plasmon band of Au nanoparticles embedded in the membrane matrix. This was attributed to strong electrostatic binding of anions with the liquid anion-exchanger Aliquat-336 present in the membrane. However, molecular iodine could interact with Au nps as it is soluble in the plasticizer that protects the agglomeration of Au nps in the membrane matrix.

Chapter - 6

Summary and future outlook

6.1. Outcome of present work

Polymer nanocomposites contain nanoparticles of various types dispersed in polymer matrix, and are of immense technological importance because of their extensive use in homogeneous and heterogeneous catalysis, sensorics, electrochemical devices, optoelectronics, and artificial muscles. There are various ways of synthesizing metal−polymer nanocomposites. Ion-exchange membranes, because of having unique morphology in a combination of hydrophilic and hydrphobic domains, serve as a platform for in situ synthesis of nanoparticle using appropriate precursor metal ions. In the present thesis, different routes for synthesis of metal nanoparticles in the matrix of ion-exchange membranes have been studied. The ion-exchange membranes used for hosting metal nanoparticles are commercially available Nafion-117 membrane and home-made polymer inclusion membrane.

Nafion-117 membrane has been used for *in situ* synthesis of silver and rhodium nanoparticles from their cationic metal ion precursor. Ionic (BH_4^-) or non-ionic (formamide and dimethyl formamide) reductant have been used to preparer nanoparticles. BH_4^-, being anion, cannot enter in the membrane matrix due to "Donnan exclusion" and thus produced Ag nanoparticles near the surface of the membrane. Contrary to this, non-ionic (formamide and dimethyl formamide) reductant have invaded interior of the membrane matrix. This has been also confirmed by the EDXRF spectrum of membrane sample reduced by formamide in dead end cell. Formation of silver nanoparticles in the Nafion with non-ionic have been found to be quite slow. Mono dispersed silver nanoparticles throughout the bulk matrix of the Nafion-117 have been prepared by reducing silver loaded membrane by formamide at 65° C. Dimethyl formamide produced a bimodal distribution of nanoparticles throughout the membrane matrix. Thus the spatial distributions of silver nanoparticles in the ion-exchange membrane have been controlled by using ionic or non-ionic reducing agents. Reduction of Rh^{+3} loaded Nafion with formamide lead to formation fractal in the membrane matrix due to slow movement of Rh^{+3} in the membrane. The self-diffusion Cs^{+} and Eu^{3+} ions in the membrane have changed significantly after formation of uniformly dispersed nanoparticles dispersed in the membrane matrix.

Another method, involving the galvanic reactions of precursor ions with preformed Ag nanoparticles has been developed for synthesis of metal nanoparticles in the Nafion-117 membrane. The radiotracer tagged nanoparticles has been used to study the galvanic reactions of Ag nanoparticles with Hg^{2+}, Rh^{3+}, $PtCl_6^{2-}$, and $AuCl_4^{-}$ ions in the membrane matrix. Hg^{2+} oxidised silver nanoparticles in the membrane to form coalesced bigger size nanostructure. It can be used for developing a chemical sensor for Hg^{2+} ions. Contrary to direct reduction of Rh^{3+}loaded membrane, spherical nanoparticles have been observed when Rh^{3+} galvanic reacted with preformed silver nanoparticles in the Nafion. Galvanic reactions of anionic species of gold and platinum with sacrificial silver nanoparticles in the Nafion have produced gold and platinum nanoparticles. The spatial distributions of gold and platinum nanoparticles have been found to be dependent upon the spatial distribution of sacrificial silver nanoparticles in the Nafion matrix.

An anion exchanger polymer inclusion membrane has been synthesised for exploiting it as a host for the nanoparticles. The surface morphology of PIM samples with the varying amount of its constituent have been studied by AFM. The microscopy studies showed that PIMs are homogeneous gel-like membrane due to swelling of CTA with the plasticizer. The addition of plasticizers has changed the physical structure of the membranes, but it has not improved the ion-exchange capacities of PIMs significantly. The thermograms of DSC indicated that crystalline phases of CTA have been modified by addition of plasticizers in the membrane. The diffusion mobility of the ions in the membrane matrix has been found to be dependent on nature and amount of the plasticizer. The self-diffusion coefficient of I^{-} have been found maximum in the sample prepared with the plasticizer NPOE having highest ε_r and lowest viscosity. The variation of D (I^-) as a function of Aliquat-336 concentration has suggested the existence of threshold concentration carrier Aliquat-336. The self-diffusion coefficients of water in PIMs have been found to one magnitude higher than the self-diffusion coefficients of iodide ions. Self-diffusion mobility of various anions in the membrane have been investigated and found that they were in following order: $NO_3^- > Cl^- \approx I^- > SO_4^{2-}$. This class of membranes with embedded metal nanoparticles may be used for many applications by utilize the amazing properties of nanoparticles.

Au nanoparticles have been synthesized in the matrix of polymer inclusion membrane having anion exchange capacity by transferring anionic species of Au followed by reduction. The metal content in the membrane have been increased by increasing the concentration of the carrier in the membrane. About 80% of the ion-exchange sites have been found available after the formation of nanoparticles. These available ion-exchange sites have been used for multiple cycles of loading of relevant metal ions followed by the reduction. This method of increasing Au^0 content in the membrane matrix has increased the size distribution of Au nps without altering the average size of Au nanoparticles. This method of multiple cycles of loading and reduction may be utilized for the synthesis the bimetallic or two different kinds of metal nanoparticles in same membrane matrix. The diffusion mobility of I^- ions have increased after the formation of Au nanoparticles in the membrane matrix. The surface plasmon band of Au nanoparticles embedded in the membrane matrix did not change with presence of different counterions. However, molecular iodine could interact with Au nps as it is soluble in the plasticizer that protects the agglomeration of Au nps in the membrane matrix.

6.2. Future scope

These metal nanoparticles embedded membranes can be utilized for modifying the transport properties of the membrane and as a base material for developing the membrane based chemical sensors. For example, the sorption of Hg^{2+} ions in Ag nanoparticles embedded membrane sample was found to be quantitative (95±3%) from the well-stirred solution. The quantitative uptake of Hg^{2+} ions in cation-exchange membrane could be attributed to the concentration gradient of Hg^{2+} ions between aqueous solution and membrane maintained by the galvanic reaction that changes Hg^{2+} ions to Hg^0. The blue shift and decrease in the intensity of surface plasmon absorption band (SPB) of Ag nanoparticles can be used for generating the response signal for detection and quantification of Hg^{2+} ions by the using galvanic reaction.

Nafion-117 ionomer received much attention for its unique bicontinuous ionic cluster morphology in a combination of hydrophilic and hydrphobic domain, acting as a templates in synthesising metal nanoparticles. It is not clear how nanoparticles having different shapes and sizes were formed in 5 nm water clusters in Nafion-117 membrane. It is most likely that, the early growth of nanoparticles does occurs in the reverse miceller hydrophilic ionic clusters in Nafion. The formation of larger nanoparticles (with sizes greater than the average size of the ionic clusters) has been seen in this work. The growth mechanism of metal nanoparticles in reverse micelles of Nafion can be studied by small-angle X-ray scattering (SAXS) using synchrotron radiation. The understanding of mechanism of growth of nanoparticles would be useful for contolling shape, size and spatial distribution of metal nanoparticles in the ionomer matrix. This study would be important to use nanocomposite membrane for a desired application.

References

[1] W.W. Gerberich, W.M. Mook, C.R. Perrey, C.B. Carter, M.I. Baskes, R. Mukherjee, A. Gidwani, J. Heberlein, P.H. McMurry, S.L. Girshick, Journal of the Mechanics and Physics of Solids 51 (2003) 979.

[2] B.R. Cuenya, Thin Solid Films 518 (2010) 3127.

[3] T. David T, Nano Today 2 (2007) 40.

[4] G. Schmid, U. Simon, Chemical Communications (2005) 697.

[5] K.L. Kelly, E. Coronado, L.L. Zhao, G.C. Schatz, Journal of Physical Chemistry B 107 (2002) 668.

[6] Q. Wang, S. Wang, W. Hang, Q. Gong, Journal of Physics D: Applied Physics 38 (2005) 389.

[7] P. Chakraborty, Journal of Materials Science 33 (1998) 2235.

[8] R. Hao, R. Xing, Z. Xu, Y. Hou, S. Gao, S. Sun, Adv Mater 22 (2010) 2729.

[9] N.A. Frey, S. Peng, K. Cheng, S. Sun, Chemical Society Reviews 38 (2009) 2532.

[10] O.V. Yaroshchuk, L.O. Dolgov, A.D. Kiselev, Physical Review E - Statistical, Nonlinear, and Soft Matter Physics 72 (2005) 051715.

[11] A. Hinojosa, S.C. Sharma, Applied Physics Letters 97 (2010).

[12] D. Ortega, J.S. Garitaonandia, C. Barrera-Solano, M. Ramírez-del-Solar, E. Blanco, M. Domínguez, Journal of Non-Crystalline Solids 352 (2006) 2801.

[13] G. Schmid, Chemical Reviews 92 (1992) 1709.

[14] C.N.R. Rao, G.U. Kulkarni, P.J. Thomas, P.P. Edwards, Chemical Society Reviews 29 (2000) 27.

[15] E. Roduner, Chemical Society Reviews 35 (2006) 583.

[16] M.-C. Daniel, D. Astruc, Chemical Reviews 104 (2004) 293.

[17] Y. Ng Cheong Chan, G.S.W. Craig, R.R. Schrock, R.E. Cohen, Chemistry of Materials 4 (1992) 885.

[18] R.W. Baker, Membrane Technology and Applications, John Wiley & Sons Ltd, West Sussex, 2004.

[19] M.-S. Hu, H.-L. Chen, C.-H. Shen, L.-S. Hong, B.-R. Huang, K.-H. Chen, L.-C. Chen, Nat Mater 5 (2006) 102.

[20] S.B. Brijmohan, M.T. Shaw, Journal of Membrane Science 303 (2007) 64.

[21] J.P. Wilcoxon, J.E. Martin, F. Parsapour, B. Wiedenman, D.F. Kelley, Journal of Chemical Physics 108 (1998) 9137.

[22] S. Das, A.K. Pandey, A.A. Athawale, M. Subramanian, T.K. Seshagiri, P.K. Khanna, V.K. Manchanda, J Hazard Mater 186 (2011) 2051.

[23] C. Dong, G. He, H. Li, R. Zhao, Y. Han, Y. Deng, Journal of Membrane Science 387 (2012) 40.

[24] Y. Yang, H. Zhang, P. Wang, Q. Zheng, J. Li, Journal of Membrane Science 288 (2007) 231.

[25] F. Pirmoradi, L. Cheng, M. Chiao, Journal of Micromechanics and Microengineering 20 (2010) 015032.

[26] H.H. Himstedt, Q. Yang, L.P. Dasi, X. Qian, S.R. Wickramasinghe, M. Ulbricht, Langmuir 27 (2011) 5574.

[27] J. Dai, M.L. Bruening, Nano Letters 2 (2002) 497.

[28] R.D. Deshmukh, R.J. Composto, Chemistry of Materials 19 (2007) 745.

[29] Y. Ni, X. Ge, Z. Zhang, Q. Ye, Materials Letters 55 (2002) 171.

[30] Z. Zhang, L. Zhang, S. Wang, W. Chen, Y. Lei, Polymer 42 (2001) 8315.

[31] K.A. Mauritz, R.B. Moore, Chemical Reviews 104 (2004) 4535.

[32] R. Kumar, A.K. Pandey, S. Dhara, N.L. Misra, S.V. Ramagiri, J.R. Bellare, A. Goswami, Journal of Membrane Science 352 (2010) 247.

[33] A. Goswami, A. Acharya, A.K. Pandey, Journal of Physical Chemistry B 105 (2001) 9196.

[34] G. Suresh, Y.M. Scindia, A.K. Pandey, A. Goswami, Journal of Membrane Science 250 (2005) 39.

[35] G. Suresh, Y.M. Scindia, A.K. Pandey, A. Goswami, Journal of Physical Chemistry B 108 (2004) 4104.

[36] R. Kumar, A.K. Pandey, S. Das, S. Dhara, N.L. Misra, R. Shukla, A.K. Tyagi, S.V. Ramagiri, J.R. Bellare, A. Goswami, Chemical Communications 46 (2010) 6371.

[37] S.E. Skrabalak, J. Chen, Y. Sun, X. Lu, L. Au, C.M. Cobley, Y. Xia, Accounts of Chemical Research 41 (2008) 1587.

[38] C. Fontàs, R. Tayeb, M. Dhahbi, E. Gaudichet, F. Thominette, P. Roy, K. Steenkeste, M.-P. Fontaine-Aupart, S. Tingry, E. Tronel-Peyroz, P. Seta, Journal of Membrane Science 290 (2007) 62.

[39] R. Kumar, A.K. Pandey, M.K. Sharma, L.V. Panicker, S. Sodaye, G. Suresh, S.V. Ramagiri, J.R. Bellare, A. Goswami, Journal of physical chemistry B 115 (2011) 5856.

[40] R. Kumar, A.K. Pandey, A.K. Tyagi, G.K. Dey, S.V. Ramagiri, J.R. Bellare, A. Goswami, Journal of Colloid and Interface Science 337 (2009) 523.

[41] R. Kumar, A.K. Pandey, A. Goswami, R. Shukla, S.V. Ramagiri, J.R. Bellare, International Journal of Nanotechnology 7 (2010) 953.

[42] A.D. Pomogailo, V.N. Kestelman, Metallopolymer Nanocomposites, Springer Berlin Heidelberg, New York, 2005.

[43] L. Nicolais, G. Carotenuto, Metal-Polymer Nanocomposites, John Wiley & Sons, New Jersey, 2004.

[44] W. Caseri, Macromolecular Rapid Communications 21 (2000) 705.

[45] J.S. Taurozzi, in Environmental engineering, Michigan State University, Michigan, 2009.

[46] P. Vadgama, Journal of Membrane Science 50 (1990) 141.

[47] B. Adhikari, S. Majumdar, Progress in Polymer Science 29 (2004) 699.

[48] W.L. Chou, D.G. Yu, M.C. Yang, Polymers for Advanced Technologies 16 (2005) 600.

[49] L. Yan, Y.S. Li, C.B. Xiang, S. Xianda, Journal of Membrane Science 276 (2006) 162.

[50] E. Camponeschi, R. Vance, M. Al-Haik, H. Garmestani, R. Tannenbaum, Carbon 45 (2007) 2037.

[51] R.P. Feynman, Eng. Sci. 23 (1960) 22.

[52] C.J. Jones, S. Aizawa, in Advances in Microbial Physiology, Academic Press, 1991, p. 109.

[53] M.C. Daniel, D. Astruc, Chemical Reviews 104 (2004) 293.

[54] G. Schmid, U. Simon, ChemInform 36 (2005) no.

[55] A. Roucoux, J. Schulz, H. Patin, Chemical Reviews 102 (2002) 3757.

[56] J.M. Thomas, B.F.G. Johnson, R. Raja, G. Sankar, P.A. Midgley, Accounts of Chemical Research 36 (2003) 20.

[57] J. Schulz, A. Roucoux, H. Patin, Chemical Communications (1999) 535.

[58] A.C. Templeton, J.J. Pietron, R.W. Murray, P. Mulvaney, Journal of Physical Chemistry B 104 (2000) 564.

[59] C. Demaille, M. Brust, M. Tsionsky, A.J. Bard, Analytical Chemistry 69 (1997) 2323.

[60] G. Peto, G.L. Molnár, Z. Pászti, O. Geszti, A. Beck, L. Guczi, Materials Science and Engineering: C 19 (2002) 95.

[61] N. Chandrasekharan, P.V. Kamat, The Journal of Physical Chemistry B 104 (2000) 10851.

[62] P.V. Kamat, The Journal of Physical Chemistry B 106 (2002) 7729.

[63] O.V. Cherstiouk, P.A. Simonov, E.R. Savinova, Electrochimica Acta 48 (2003) 3851.

[64] T. Ishida, M. Haruta, Angewandte Chemie-International Edition 46 (2007) 7154.

[65] P. Jain, X. Huang, I. El-Sayed, M. El-Sayed, Plasmonics 2 (2007) 107.

[66] M. Pelton, M.Z. Liu, H.Y. Kim, G. Smith, P. Guyot-Sionnest, N.E. Scherer, Optics Letters 31 (2006) 2075.

[67] Y.T. Lim, M.Y. Cho, B.S. Choi, J.M. Lee, B.H. Chung, Chemical Communications (2008) 4930.

[68] P. Sharrna, S. Brown, G. Walter, S. Santra, B. Moudgil, Advances in Colloid and Interface Science 123 (2006) 471.

[69] X.G. Liu, C.L. Stern, C.A. Mirkin, Organometallics 21 (2002) 1017.

[70] S.J. Park, T.A. Taton, C.A. Mirkin, Science 295 (2002) 1503.

[71] X.M. Qian, S.M. Nie, Chemical Society Reviews 37 (2008) 912.

[72] C.A. Mirkin, R.L. Letsinger, R.C. Mucic, J.J. Storhoff, Nature 382 (1996) 607.

[73] H. Otsuka, Y. Akiyama, Y. Nagasaki, K. Kataoka, Journal of the American Chemical Society 123 (2001) 8226.

[74] N. Nath, A. Chilkoti, Journal of the American Chemical Society 123 (2001) 8197.

[75] A.K. Boal, V.M. Rotello, Journal of the American Chemical Society 121 (1999) 4914.

[76] A. Labande, J. Ruiz, D. Astruc, Journal of the American Chemical Society 124 (2002) 1782.

[77] S. Alayoglu, B. Eichhorn, Journal of the American Chemical Society 130 (2008) 17479.

[78] D. Astruc, F. Lu, J.R. Aranzaes, Angewandte Chemie-International Edition 44 (2005) 7852.

[79] H. Bonnemann, R.M. Richards, European Journal of Inorganic Chemistry (2001) 2455.

[80] G. Schmid, Clusters and Colloids: From Theory to Applications, Wiley-VCH Verlag GmbH, 2007.

[81] J. Turkevich, P.C. Stevenson, J. Hillier, Discussions of the Faraday Society (1951) 55.

[82] J.H. Fendler, Chemical Reviews 87 (1987) 877.

[83] J.C. Pivin, Materials Science and Engineering a-Structural Materials Properties Microstructure and Processing 293 (2000) 30.

[84] H.Y. Fan, Y.Q. Zhou, G.P. Lopez, Advanced Materials 9 (1997) 728.

[85] A. Brito, F.J. García, M.C. Alvarez-Galván, M.E. Borges, C. Díaz, V.A. de la Peña O'Shea, Catalysis Communications 8 (2007) 2081.

[86] R.M. Crooks, M. Zhao, L. Sun, V. Chechik, L.K. Yeung, Accounts of Chemical Research 34 (2000) 181.

[87] M.S. Islam, W.S. Choi, Y.B. Lee, H.-J. Lee, Journal of Materials Chemistry A 1 (2013) 3565.

[88] C.I. Contescu, K. Putyera, Dekker Encyclopedia of Nanoscience and Nanotechnology, CRC Press, New York, 2004.

[89] S.W. Lee, J.R. Kumpfer, P.A. Lin, G. Li, X.P.A. Gao, S.J. Rowan, R.M. Sankaran, Macromolecules 45 (2012) 8201.

[90] M. Mulder, Basic Principles of Membrane Technology, Kluwer Academic Publishers, Dordrecht, 1996.

[91] J.A. Nollet, Hippolyte-Louis Guerin and Louis-Francios Delatour (1748).

[92] C. Schonbein, in, British Patent, 1846.

[93] T. Graham, Philosophical Transactions of the Royal Society of London 151 (1861) 183.

[94] T. Graham, Philosophical Transactions of the Royal Society of London 156 (1866) 399.

[95] A. Fick, Annalen der Physik 170 (1855) 59.

[96] J.H. van 't Hoff, Z. Phys. Chem. 1 (1887) 481.

[97] W. Nernst, Z. Phys. Chem. 2 (1888) 613.

[98] M. Planck, Ann. Physik u. Chem., N. F. 39 (1890) 161.

[99] F.G. Donnan, Zeitschrift für Elektrochemie und angewandte physikalische Chemie 17 (1911) 572.

[100] H.S. Thompson, J. Roy. Agri. Soc. Engl. 11 (1850) 68.

[101] J.T. Way, J. Roy. Agri. Soc. Engl. 11 (1850) 313.

[102] L. Michaelis, A. Fujita, Biochemische Zeitschrift 158 (1925) 28.

[103] M.R.J. Wyllie, H.W. Patnode, Journal of Physical and Colloid Chemistry 54 (1950) 204.

[104] W. Juda, W.A. Mcrae, Journal of the American Chemical Society 72 (1950) 1043.

[105] T. Sata, Ion exchange membranes: preparation, characterization Modification and Application, The Royal Society of Chemistry, Cambridge, 2004.

[106] H. Strathmann, Ion-exchange membrane separation processes, Elsevier, 2004.

[107] C. Heitner-Wirguin, Journal of Membrane Science 120 (1996) 1.

[108] H.L. Yeager, A. Eisenberg, Perfluorinated Ionomer Membranes, American Chemical Society: Washington, DC, 1982, p. 1.

[109] W.Y. Hsu, T.D. Gierke, Journal of Membrane Science 13 (1983) 307.

[110] J. Chou, E.W. McFarland, H. Metiu, The journal of physical chemistry. B 109 (2005) 3252.

[111] P.J. James, T.J. McMaster, J.M. Newton, M.J. Miles, Polymer 41 (2000) 4223.

[112] T.D. Gierke, G.E. Munn, F.C. Wilson, Perfluorinated Ionomer Membranes, American Chemical Society, 1982, p. 195.

[113] T.D. Gierke, G.E. Munn, F.C. Wilson, Journal of polymer science. Part A-2, Polymer physics 19 (1981) 1687.

[114] L. Rubatat, G. Gebel, O. Diat, Macromolecules 37 (2004) 7772.

[115] L. Rubatat, A.L. Rollet, G. Gebel, O. Diat, Macromolecules 35 (2002) 4050.

[116] M. Fujimura, T. Hashimoto, H. Kawai, Macromolecules 14 (1981) 1309.

[117] M. Fujimura, T. Hashimoto, H. Kawai, Macromolecules 15 (1982) 136.

[118] H.G. Haubold, T. Vad, H. Jungbluth, P. Hiller, Electrochimica Acta 46 (2001) 1559.

[119] M.H. Litt, in B.M. Culbertson (Editor), ACS, San Francisco, CA, USA, 1997, p. 80.

[120] Y.Q. Wang, Y. Kawano, S.R. Aubuchon, R.A. Palmer, Macromolecules 36 (2003) 1138.

[121] W.Y. Hsu, T.D. Gierke, Macromolecules 15 (1982) 101.

[122] A. Gruger, A. Régis, T. Schmatko, P. Colomban, Vibrational Spectroscopy 26 (2001) 215.

[123] S.J. Paddison, J.A. Elliott, Solid State Ionics 177 (2006) 2385.

[124] S.J. Paddison, J.A. Elliott, Physical Chemistry Chemical Physics 8 (2006) 2193.

[125] J.A. Elliott, D. Wu, S.J. Paddison, R.B. Moore, Soft Matter 7 (2011) 6820.

[126] G. Gebel, Polymer 41 (2000) 5829.

[127] G. Gebel, J. Lambard, Macromolecules 30 (1997) 7914.

[128] G. Gebel, R.B. Moore, Macromolecules 33 (2000) 4850.

[129] F. Kubota, M. Goto, Solvent Extraction Research and Development 12 (2005) 11.

[130] W. Walkowiak, C.A. Kozlowski, Desalination 240 (2009) 186.

[131] X.J. Yang, A.G. Fane, K. Soldenhoff, Industrial and Engineering Chemistry Research 42 (2003) 392.

[132] M. Barboiu, A. Cazacu, M. Michau, R. Caraballo, C. Arnal-Herault, A. Pasc-Banu, Chemical Engineering and Processing 47 (2008) 1044.

[133] J.D. Lamb, C.A. Morris, J.N. West, K.T. Morris, R.G. Harrison, Journal of Membrane Science 321 (2008) 15.

[134] N.M. Kocherginsky, Q. Yang, L. Seelam, Separation and Purification Technology 53 (2007) 171.

[135] M.E. Vilt, W.S.W. Ho, Journal of Membrane Science 342 (2009) 80.

[136] F.J. Hernández-Fernández, A.P. de los Ríos, F. Tomás-Alonso, J.M. Palacios, G. Víllora, Journal of Membrane Science 341 (2009) 172.

[137] J. De Gyves, E.R. De San Miguel, Industrial and Engineering Chemistry Research 38 (1999) 2182.

[138] L. Canet, P. Vanel, N. Aouad, E. Tronel-Peyroz, J. Palmeri, P. Seta, Journal of Membrane Science 163 (1999) 109.

[139] J. Lee, H.K. Lee, K.E. Rasmussen, S. Pedersen-Bjergaard, Analytica Chimica Acta 624 (2008) 253.

[140] L. Arce, L. Nozal, B.M. Simonet, M. Valcárcel, A. Ríos, TrAC - Trends in Analytical Chemistry 28 (2009) 842.

[141] Z. Zhang, J. Buffle, H.P. Van Leeuwen, K. Wojciechowski, Analytical Chemistry 78 (2006) 5693.

[142] A.J.B. Kemperman, D. Bargeman, T. Van Den Boomgaard, H. Strathmann, Separation Science and Technology 31 (1996) 2733.

[143] X.J. Yang, A.G. Fane, J. Bi, H.J. Griesser, Journal of Membrane Science 168 (2000) 29.

[144] H.D. Zheng, B.Y. Wang, Y.X. Wu, Q.L. Ren, Colloids and Surfaces A: Physicochemical and Engineering Aspects 351 (2009) 38.

[145] R. Fortunato, C.A.M. Afonso, J. Benavente, E. Rodriguez-Castellón, J.G. Crespo, Journal of Membrane Science 256 (2005) 216.

[146] M.G. Dastgir, L.G. Peeva, A.G. Livingston, T.A. Morley, J.H.G. Steinke, Industrial and Engineering Chemistry Research 44 (2005) 7659.

[147] M. Ulbricht, Polymer 47 (2006) 2217.

[148] K.L. Thunhorst, R.D. Noble, C.N. Bowman, Journal of Membrane Science 156 (1999) 293.

[149] B.J. Elliott, W.B. Willis, C.N. Bowman, Journal of Membrane Science 168 (2000) 109.

[150] A. Duhart, J.F. Dozol, H. Rouquette, A. Deratani, Journal of Membrane Science 185 (2001) 145.

[151] T. Vasudevan, S. Das, A.K. Debnath, A.K. Pandey, Journal of Membrane Science 342 (2009) 113.

[152] L.D. Nghiem, P. Mornane, I.D. Potter, J.M. Perera, R.W. Cattrall, S.D. Kolev, Journal of Membrane Science 281 (2006) 7.

[153] W. Walkowiak, R.A. Bartsch, C. Kozlowski, J. Gega, W.A. Charewicz, B. Amiri-Eliasi, Journal of Radioanalytical and Nuclear Chemistry 246 (2000) 643.

[154] M. Sugiura, Separation Science and Technology 28 (1993) 1453.

[155] E.R. de San Miguel, A.M. Hernandez-Andaluz, J.G. Banuelos, J.M. Saniger, J.C. Aguilar, J. de Gyves, Materials Science and Engineering a-Structural Materials Properties Microstructure and Processing 434 (2006) 30.

[156] J.S. Kim, S.K. Kim, J.W. Ko, E.T. Kim, S.H. Yu, M.H. Cho, S.G. Kwon, E.H. Lee, Talanta 52 (2000) 1143.

[157] Y.M. Scindia, A.K. Pandey, A.V.R. Reddy, Journal of Membrane Science 249 (2005) 143.

[158] C. Fontàs, R. Tayeb, S. Tingry, M. Hidalgo, P. Seta, Journal of Membrane Science 263 (2005) 96.

[159] J.C. Aguilar, M. Sánchez-Castellanos, E. Rodríguez De San Miguel, J. De Gyves, Journal of Membrane Science 190 (2001) 107.

[160] E. Bakker, P. Bühlmann, E. Pretsch, Chemical Reviews 97 (1997) 3083.

[161] P. Buhlmann, E. Pretsch, E. Bakker, Chemical Reviews 98 (1998) 1593.

[162] B. Adhikari, S. Majumdar, Progress in Polymer Science (Oxford) 29 (2004) 699.

[163] R. Eugster, T. Rosatzin, B. Rusterholz, B. Aebersold, U. Pedrazza, D. Ruegg, A. Schmid, U.E. Spichiger, W. Simon, Analytica Chimica Acta 289 (1994) 1.

[164] M.I.G.S. Almeida, R.W. Cattrall, S.D. Kolev, Journal of Membrane Science 415 (2012) 9.

[165] Y. Sakai, K. Kadota, T. Hayashita, R.W. Cattrall, S.D. Kolev, Journal of Membrane Science 346 (2010) 250.

[166] J.S. Gardner, J.O. Walker, J.D. Lamb, Journal of Membrane Science 229 (2004) 87.

[167] J.K. Sears, J.R. Darby, The Technology of Plasticizers, John Wiley & Sons, New York, 1982.

[168] L. Canet, M. Ilpide, P. Seta, Separation Science and Technology 37 (2002) 1851.

[169] Z.H. Mbhele, M.G. Salemane, C.G.C.E. van Sittert, J.M. Nedeljkovic, V. Djokovic, A.S. Luyt, Chemistry of Materials 15 (2003) 5019.

[170] J.Y. Kim, D.H. Shin, K.J. Ihn, Macromolecular Chemistry and Physics 206 (2005) 794.

[171] M. Sangermano, Y. Yagci, G. Rizza, Macromolecules 40 (2007) 8827.

[172] T.Yu. Ryabova, A.S.Chirkov, L.S. Radkevich, N.V. Evtushok, Ukr. Chem. J. 59 (1993) 1329.

[173] Y. Nakao, Journal of Colloid and Interface Science 171 (1995) 386.

[174] A. Matsubayashi, K. Fukunaga, T. Tsuji, K. Ataka, H. Ohsaki, Langmuir 27 (2011) 733.

[175] T.C. Wang, M.F. Rubner, R.E. Cohen, Langmuir 18 (2002) 3370.

[176] M. Watanabe, H. Uchida, M. Emori, Journal of Physical Chemistry B 102 (1998) 3129.

[177] M. Watanabe, H. Uchida, M. Emori, Journal of the Electrochemical Society 145 (1998) 1137.

[178] A.W.H. Mau, C.B. Huang, N. Kakuta, A.J. Bard, A. Campion, M.A. Fox, J.M. White, S.E. Webber, Journal of the American Chemical Society 106 (1984) 6537.

[179] M. Yoon, Y. Kim, Y.M. Kim, V. Volkov, H.J. Song, Y.J. Park, I.W. Park, Materials Chemistry and Physics 91 (2005) 104.

[180] I.W. Park, M. Yoon, Y.M. Kim, Y. Kim, J.H. Kim, S. Kim, V. Volkov, Journal of Magnetism and Magnetic Materials 272–276, Part 2 (2004) 1413.

[181] I.W. Park, M. Yoon, Y.M. Kim, Y. Kim, H. Yoon, H.J. Song, V. Volkov, A. Avilov, Y.J. Park, Solid State Communications 126 (2003) 385.

[182] C. Burato, P. Centomo, G. Pace, M. Favaro, L. Prati, B. Corain, Journal of Molecular Catalysis a-Chemical 238 (2005) 26.

[183] B. Corain, C. Burato, P. Centomo, S. Lora, W. Meyer-Zaika, G. Schmid, Journal of Molecular Catalysis a-Chemical 225 (2005) 189.

[184] Y.-P. Sun, P. Atorngitjawat, Y. Lin, P. Liu, P. Pathak, J. Bandara, D. Elgin, M. Zhang, Journal of Membrane Science 245 (2004) 211.

[185] S. Wang, P. Liu, X. Wang, X. Fu, Langmuir 21 (2005) 11969.

[186] H.W. Rollins, F. Lin, J. Johnson, J.-J. Ma, J.-T. Liu, M.-H. Tu, D.D. DesMarteau, Y.-P. Sun, Langmuir 16 (2000) 8031.

[187] J. Xu, D. Bhattacharyya, Industrial & Engineering Chemistry Research 46 (2007) 2348.

[188] X. Zan, Z. Su, Langmuir 25 (2009) 12355.

[189] A. Sachdeva, S. Sodaye, A.K. Pandey, A. Goswami, Anal. Chem. 78 (2006) 7169.

[190] J. Crank, The Mathematics Diffusion, Oxford University Press, New York, 1979.

[191] F. Helfferich, Ion exchange, McGraw Hill, New York, 1962.

[192] E. Brown, Introduction to Thermal Analysis, Kluwer Academic Publishers, Dordrecht, 2001.

[193] D.A. Skoog, D.M. West, Principles of instrumental analysis, Saunders College, Philadelphia, 1980.

[194] J.I. Langford, L. Daniel, Reports on Progress in Physics 59 (1996) 131.

[195] R. Jenkins, Methods and Practices in X-ray Powder Diffraction, JCPDS, International Centre for Diffraction Data, Swarthmore, 1986.

[196] H.P. Klug, L.E. Alexander, X-Ray Diffraction Procedures: For Polycrystalline and Amorphous Materials, Wiley-Interscience, New York, 1974.

[197] P. Scherrer, Göttinger Nachrichten Math. Phys. 2 (1918) 98.

[198] J.I. Langford, A.J.C. Wilson, Journal of Applied Crystallography 11 (1978) 102.

[199] M. Knoll, E. Ruska, Zeitschrift Fur Physik 78 (1932) 318.

[200] D.B. Williams, C.B. Carter, Transmission Electron Microscopy: A Textbook for Materials Science Springer Limited, New York, 2009.

[201] G. Binnig, C.F. Quate, C. Gerber, Physical Review Letters 56 (1986) 930.

[202] Sheng, Czajkowsky, Shao, Journal of Microscopy 196 (1999) 1.

[203] N.H. Jalani, K. Dunn, R. Datta, Electrochimica Acta 51 (2005) 553.

[204] X. Teng, Y. Zhao, J. Xi, Z. Wu, X. Qiu, L. Chen, Journal of Membrane Science 341 (2009) 149.

[205] P. Liu, J. Bandara, Y. Lin, D. Elgin, L.F. Allard, Y.-P. Sun, Langmuir 18 (2002) 10398.

[206] R.A. Alvarez-Puebla, G.A. Nazri, R.F. Aroca, Journal of Materials Chemistry 16 (2006) 2921.

[207] R. Knake, P. Jacquinot, P.C. Hauser, Analyst 127 (2002) 114.

[208] M. Watanabe, H. Uchida, Y. Seki, M. Emori, P. Stonehart, Journal of the Electrochemical Society 143 (1996) 3847.

[209] T.M. Thampan, N.H. Jalani, P. Choi, R. Datta, Journal of the Electrochemical Society 152 (2005) A316.

[210] S. Malhotra, R. Datta, Journal of the Electrochemical Society 144 (1997) L23.

[211] K.T. Adjemian, S.J. Lee, S. Srinivasan, J. Benziger, A.B. Bocarsly, Journal of the Electrochemical Society 149 (2002) A256.

[212] K.A. Mauritz, I.D. Stefanithis, S.V. Davis, R.W. Scheetz, R.K. Pope, G.L. Wilkes, H.H. Huang, Journal of Applied Polymer Science 55 (1995) 181.

[213] M. Krishnan, J.R. White, M.A. Fox, A.J. Bard, Journal of the American Chemical Society 105 (1983) 7002.

[214] Q. Zhang, C.Z. Huang, J. Ling, Y.F. Li, The Journal of Physical Chemistry B 112 (2008) 16990.

[215] M.P. Rodgers, Z. Shi, S. Holdcroft, Journal of Membrane Science 325 (2008) 346.

[216] I. Pastoriza-Santos, L.M. Liz-Marzán, Nano Letters 2 (2002) 903.

[217] I. Pastoriza-Santos, L.M. Liz-Marzán, Langmuir 18 (2002) 2888.

[218] I. Pastoriza-Santos, L.M. Liz-Marzán, Langmuir 15 (1999) 948.

[219] M.Y. Han, C.H. Quek, W. Huang, C.H. Chew, L.M. Gan, Chemistry of Materials 11 (1999) 1144.

[220] H.S. Sodaye, P.K. Pujari, A. Goswami, S.B. Manohar, Journal of Radioanalytical and Nuclear Chemistry 214 (1996) 399.

[221] A. Herrera, H.L. Yeager, Journal of the Electrochemical Society 134 (1987) 2446.

[222] E.W. Schneider, M.W. Verbrugge, Applied Radiation and Isotopes 44 IN11.

[223] M.W. Verbrugge, R.F. Hill, Journal of the Electrochemical Society 137 (1990) 893.

[224] D. Gierke T, E. Munn G, C. Wilson F, Perfluorinated Ionomer Membranes, American Chemical Society, 1982, p. 195.

[225] G. Suresh, S. Sodaye, Y.M. Scindia, A.K. Pandey, A. Goswami, Electrochimica Acta 52 (2007) 5968.

[226] I. Yoon, A.M. Zimmerman, C.C. Tester, A.M. DiCiccio, Y. Jiang, W. Chen, Chemistry of Materials 21 (2009) 3924.

[227] L.M. Sander, Contemporary Physics 41 (2000) 203.

[228] T.A. Witten, Jr., L.M. Sander, Physical Review Letters 47 (1981) 1400.

[229] T.A. Witten, L.M. Sander, Physical Review B 27 (1983) 5686.

[230] Y.G. Sun, B. Mayers, Y.N. Xia, Advanced Materials 15 (2003) 641.

[231] Y. Sun, Y. Xia, Journal of the American Chemical Society 126 (2004) 3892.

[232] Y.G. Sun, B. Wiley, Z.Y. Li, Y.N. Xia, Journal of the American Chemical Society 126 (2004) 9399.

[233] D. Wu, X. Xu, X. Liu, The Journal of Chemical Physics 129 (2008) 074711.

[234] M. Hu, J.Y. Chen, M. Marquez, Y.N. Xia, G.V. Hartland, Journal of Physical Chemistry C 111 (2007) 12558.

[235] W.Y. Dong, Y.J. Sun, C.W. Lee, W.M. Hua, X.C. Lu, Y.F. Shi, S.C. Zhang, J.M. Chen, D.Y. Zhao, Journal of the American Chemical Society 129 (2007) 13894.

[236] Y. Sun, B.T. Mayers, Y. Xia, Nano Letters 2 (2002) 481.

[237] Y. Sun, Y. Xia, Science 298 (2002) 2176.

[238] J. Chen, B. Wiley, J. McLellan, Y. Xiong, Z.-Y. Li, Y. Xia, Nano Letters 5 (2005) 2058.

[239] M. Mohl, A. Kumar, A.L.M. Reddy, A. Kukovecz, Z. Konya, I. Kiricsi, R. Vajtai, P.M. Ajayan, The Journal of Physical Chemistry C 114 (2009) 389.

[240] Q. Li, C. Wang, Chemical Physics Letters 375 (2003) 525.

[241] K.W. Kim, S.M. Kim, S. Choi, J. Kim, I.S. Lee, ACS Nano 6 (2012) 5122.

[242] S. Koh, P. Strasser, Journal of the American Chemical Society 129 (2007) 12624.

[243] P. Mani, R. Srivastava, P. Strasser, The Journal of Physical Chemistry C 112 (2008) 2770.

[244] Y. Khalavka, J. Becker, C. Sonnichsen, Journal of the American Chemical Society 131 (2009) 1871.

[245] C.R. Martin, M. Nishizawa, K. Jirage, M. Kang, S.B. Lee, Advanced Materials 13 (2001) 1351.

[246] G.A. Somorjai, H. Frei, J.Y. Park, Journal of the American Chemical Society 131 (2009) 16589.

[247] A. Henglein, C. Brancewicz, Chemistry of Materials 9 (1997) 2164.

[248] A. Henglein, The Journal of Physical Chemistry 97 (1993) 5457.

[249] T. Morris, H. Copeland, E. McLinden, S. Wilson, G. Szulczewski, Langmuir 18 (2002) 7261.

[250] Y. Bi, G. Lu, Chemical Communications (2008) 6402.

[251] R.W. Drier, H.L. Walker, Philosophical Magazine Series 7 16 (1933) 294.

[252] A.A. Rudnitskii, A.N. Khotinskaya, Russ. J. Inorg. Chem. 4 (1959) 1053.

[253] G.V. Ramesh, T.P. Radhakrishnan, ACS Applied Materials & Interfaces 3 (2011) 988.

[254] S. Sodaye, R. Tripathi, A.K. Pandey, A.V.R. Reddy, Analytica Chimica Acta 514 (2004) 159.

[255] P. Bühlmann, E. Pretsch, E. Bakker, Chemical Reviews 98 (1998) 1593.

[256] M. Sugiura, M. Kikkawa, S. Urita, Separation Science and Technology 22 (1987) 2263.

[257] M. Sugiura, M. Kikkawa, S. Urita, A. Ueyama, Separation Science and Technology 24 (1989) 685.

[258] C. Sgarlata, G. Arena, E. Longo, D. Zhang, Y. Yang, R.A. Bartsch, Journal of Membrane Science 323 (2008) 444.

[259] S.P. Kusumocahyo, T. Kanamori, K. Sumaru, S. Aomatsu, H. Matsuyama, M. Teramoto, T. Shinbo, Journal of Membrane Science 244 (2004) 251.

[260] Q. Ye, S. Borbély, G. Horvai, Analytical Chemistry 71 (1999) 4313.

[261] R. Tripathi, A.K. Pandey, S. Sodaye, B.S. Tomar, S.B. Manohar, S. Santra, K. Mahata, P. Singh, S. Kailas, Nuclear Instruments and Methods in Physics Research, Section B: Beam Interactions with Materials and Atoms 211 (2003) 138.

[262] E. Rodríguez de San Miguel, J.C. Aguilar, J. de Gyves, Journal of Membrane Science 307 (2008) 105.

[263] U. Fiedler, Analytica Chimica Acta 89 (1977) 111.

[264] S. Sodaye, G. Suresh, A.K. Pandey, A. Goswami, Radiochimica Acta 94 (2006) 347.

[265] S. Sodaye, G. Suresh, A.K. Pandey, A. Goswami, Journal of Membrane Science 295 (2007) 108.

[266] T.G. Levitskaia, D.M. Macdonald, J.D. Lamb, B.A. Moyer, Physical Chemistry Chemical Physics 2 (2000) 1481.

[267] J.A. Riggs, B.D. Smith, Journal of the American Chemical Society 119 (1997) 2765.

[268] T.A. Munro, B.D. Smith, Chemical Communications (1997) 2167.

[269] M.F. Paugam, J. Buffle, Journal of Membrane Science 147 (1998) 207.

[270] K.M. White, B.D. Smith, P.J. Duggan, S.L. Sheahan, E.M. Tyndall, Journal of Membrane Science 194 (2001) 165.

[271] T. Malewitz, P.N. Pintauro, D. Rear, Journal of Membrane Science 301 (2007) 171.

[272] J.S. Gardner, Q.P. Peterson, J.O. Walker, B.D. Jensen, B. Adhikary, R.G. Harrison, J.D. Lamb, Journal of Membrane Science 277 (2006) 165.

[273] R.D. Armstrong, A.K. Covington, W.G. Proud, Journal of Electroanalytical Chemistry 257 (1988) 155.

[274] P. Millet, Journal of Membrane Science 50 (1990) 325.

[275] J.H. Daane, R.E. Barker, Journal of Polymer Science Part B-Polymer Letters 2 (1964) 343.

[276] O. Arous, M. Amara, H. Kerdjoudj, Journal of Applied Polymer Science 93 (2004) 1401.

[277] F.J. Keplinger, A. Jachimowicz, F. Kohl, Analytical Chemistry 70 (1998) 4271.

[278] R.A. Robinson, R.H. Stokes, Electrolyte Solutions, Butterworths Scientific Publication, London, 1959.

[279] A.K. Pandey, A. Goswami, D. Sen, S. Mazumder, R.F. Childs, Journal of Membrane Science 217 (2003) 117.

[280] G. Thau-Alexandrowicz, Journal of Membrane Science 4 (1978) 151.

[281] A.J. Easteal, A.V.J. Edge, L.A. Woolf, Journal of Physical Chemistry 88 (1984) 6060.

[282] T. Zwickl, B. Schneider, E. Lindner, T. Sokalski, U. Schaller, E. Pretsch, Analytical Sciences 14 (1998) 57.

[283] A.D.C. Chan, X. Li, D.J. Harrison, Analytical Chemistry 64 (1992) 2512.

[284] S. Sodaye, G. Suresh, A.K. Pandey, A. Goswami, Journal of Physical Chemistry B 113 (2009) 12482.

[285] S.A. Piletsky, T.L. Panasyuk, E.V. Piletskaya, I.A. Nicholls, M. Ulbricht, Journal of Membrane Science 157 (1999) 263.

[286] M. Grzelczak, J. Pérez-Juste, P. Mulvaney, L.M. Liz-Marzán, Chemical Society Reviews 37 (2008) 1783.

[287] K.Y. Lee, D.W. Kim, J. Heo, J.S. Kim, J.K. Yang, G.W. Cheong, S.W. Han, Bulletin of the Korean Chemical Society 27 (2006) 2081.

List of Publications

[1] ***R. Kumar***, A.K. Pandey, M.K. Sharma, L.V. Panicker, S. Sodaye, G. Suresh, S.V. Ramagiri, J.R. Bellare, A. Goswami, Diffusional transport of ions in plasticized anion-exchange membranes, **Journal of physical chemistry B**, 115 (2011) 5856-5867.

[2] ***R. Kumar***, A.K. Pandey, S. Das, S. Dhara, N.L. Misra, R. Shukla, A.K. Tyagi, S.V. Ramagiri, J.R. Bellare, A. Goswami, Galvanic reactions involving silver nanoparticles embedded in cation-exchange membrane, **Chemical Communications**, 46 (2010) 6371-6373.

[3] ***R. Kumar***, A.K. Pandey, S. Dhara, N.L. Misra, S.V. Ramagiri, J.R. Bellare, A. Goswami, Inclusion of silver nanoparticles in host poly(perfluorosulfonic) acid membrane using ionic and non-ionic reductants, **Journal of Membrane Science**, 352 (2010) 247-254.

[4] ***R. Kumar***, A.K. Pandey, A. Goswami, R. Shukla, S.V. Ramagiri, J.R. Bellare, Plasticised polymer inclusion membrane as tunable host for stable gold nanoparticles, **International Journal of Nanotechnology**, 7 (2010) 953-966.

[5] ***R. Kumar***, A.K. Pandey, S.V. Ramagiri, J.R. Bellare, A. Goswami, Positioning of platinum nanoparticles in cation-exchange membrane by galvanic reaction, **AIP Conference Proceedings**, 1313, 2010, pp. 143-145.

[6] ***R. Kumar***, A.K. Pandey, A.K. Tyagi, G.K. Dey, S.V. Ramagiri, J.R. Bellare, A. Goswami, In situ formation of stable gold nanoparticles in polymer inclusion membranes, **Journal of Colloid and Interface Science**, 337 (2009) 523-530.